Regulation of glucose transporter trafficking in response to changing glucose availability

By

Susan Jo Qualls-Histed

Dissertation

Submitted to the Faculty of the

Graduate School of Vanderbilt University

in partial fulfillment of the requirements

for the degree of

DOCTOR OF PHILOSOPHY

In

Cell and Developmental Biology

May 12, 2023

Nashville, TN

Approved:

William Tansey, Ph. D.

Walter Chazin, Ph.D.

Chin Chiang, Ph.D.

Todd Graham, Ph.D.

Jason MacGurn, Ph.D.

This work is dedicated to my boys, Stephen and Adrian

Acknowledgements

I am grateful to my advisor, Jason MacGurn, for being a great mentor throughout my time in his lab. He has been incredibly supportive through all the ups and downs I have encountered in my graduate school career. I can always count on him to give me enthusiastic input and plenty of ideas. I truly appreciate everything he has taught me. I am also very thankful for my lab mates. They always provide valuable scientific input and keep the lab a supportive and enjoyable space. I also want to thank my committee members, Dr. Bill Tansey, Dr. Todd Graham, Dr. Chin Chiang, and Dr. Dr. Walter Chazin. They have always provided me with crucial feedback and kept me on track through this long process.

I want to thank my family for all their support. Especially my mom, Lucy, and my sister, Anna, for always believing in me and being a phone call away when I needed you. And thank you to my dad, who is the source of my scientific mind and loved to learn about what it is that I do in that lab all day. I miss him immensely and very much wish he could be here for the end of this journey.

Finally, I want to thank my husband, Stephen. I never could have finished this degree without his unwavering support. He has taken on so much so that I can focus on my studies and has never once complained. Instead he has cheered me on through every victory and comforted me through the failures. He is the most selfless person I know and I can't imagine my life without him at the center. And, of course, I have to thank my little grad school baby, Adrian. Nothing has brought me more joy than welcoming him into my life. He has spent countless evenings and weekends with me in the lab and he's happy to do it (as long as there's Pocoyo on the computer and "snacks from my boss"). He may have stalled things a bit, but I'd say he's worth it.

Table of Contents

List of Tables

Table **Page**

List of Figures

Figure **Page**

Chapter 1

Introduction

Glucose is an essential nutrient for all living organisms, serving as an important metabolic substrate. As such, glucose homeostasis is highly regulated and dysregulation is connected to major diseases such as diabetes, cancer, and a variety of neurological disorders (*1*). In mammals, blood glucose levels are tightly regulated and there are several glucose-sensing mechanisms in place to maintain normal glucose metabolism. For example, the pancreas and liver work together to maintain this balance in the blood. High blood glucose levels prompt the pancreas to release the hormone insulin, which signals for glucose uptake by cells in adipose and muscle tissue, while low blood glucose leads the pancreas to release the hormone, glucagon, which signals for the liver to release glucose into the blood **(Figure 1.1A)**. Without this system of checks and balances functioning properly, blood glucose levels cannot be properly maintained, resulting in diabetes mellitus.

The facilitative glucose transporter (GLUT) family is largely responsible for maintaining glucose homeostasis in mammalian cells. Most cells in the human body express multiple GLUT family transporters. They are tightly regulated both transcriptionally and post-translationally (*2*-*7*). The first GLUT to be discovered and one of the most extensively studied, GLUT1, can be found on the surface of virtually every cell type. The structure and transport kinetics of GLUT1 are well characterized, though there is still more to learn, particularly with regards to how GLUT1 is regulated. The work presented in this thesis details my efforts to understand how cells regulate the subcellular localization of GLUT1 in response to changes in glucose availability. In **Chapter 3,** I report the characterization of GLUT1 trafficking to lysosomes in response to glucose transport and examine vital roles played by the functional domains of ARRDC protein, TXNIP, and the regulatory post-translational modifier ubiquitin. In **Chapter 4,** I share additional experiments characterizing the biochemical features of TXNIP and ubiquitylation of GLUT1. Overall, this thesis uncovers important mechanisms of GLUT1 regulation. These findings broaden our understanding of GLUT1 and can inform ongoing efforts to develop therapeutics that strategically target GLUT1.

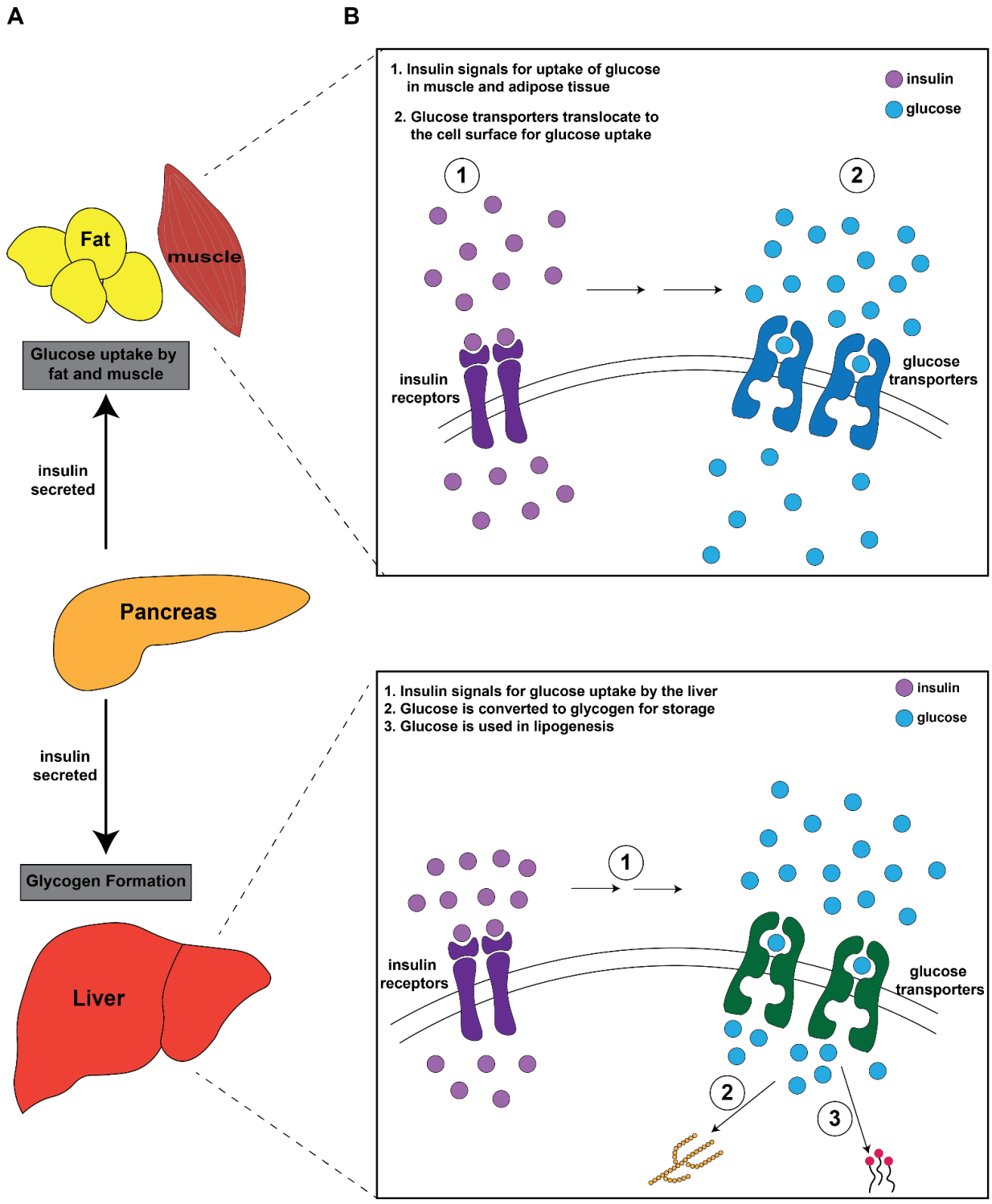

Figure 1.1: Glucose regulation on the organismal (A) and molecular (B) level in response to high blood glucose.

1.1 Glucose homeostasis at different scales in biology and physiology

To achieve glucose homeostasis at an organismal level, our bodies have evolved strategies to regulate the transport of glucose at multiple scales. Crosstalk between

organs ensures that glucose is transported to tissues where it is needed. For instance, glucose-excited (GE) neurons in the ventromedial nucleus of the hypothalamus (VMH) promote the lowering of glucose levels. When the glucose load increases, the VMH neurons activate a signal cascade leading to an increase in insulin sensitivity in peripheral tissues and therefore a decrease in blood glucose (*8*). This cascade starts when glucose enters the extracellular space of the brain via glucose transporters in the blood brain barrier (BBB). It is then transported into glial cells and metabolized to lactate. The lactate is then further metabolized to pyruvate and that pyruvate is taken up by the mitochondria to produce energy in the form of ATP. This decreases the AMP: ATP ratio causing the ATP-dependent K^+ channels to close and depolarization of the membrane. The resulting increase in action potential frequency and neurotransmitter release signals for the increase of peripheral glucose uptake and decrease of hepatic glucose production (*9*).

The brain has a high energy demand, so improper regulation of glucose leads to several neurological diseases. One example is the neurodevelopmental syndrome GLUT1 deficiency syndrome (GLUT1-DS), caused by a lack of the major glucose transporter at the BBB. It is characterized by developmental delay, mental retardation, and drug-resistant seizures in infancy (*1*). There is also growing evidence that type 2 diabetes mellitus does not just damage peripheral nerves but is also associated with increased risk of neurodegenerative disease (*10*). Studies have shown that individuals with type 2 diabetes mellitus have a 60% greater risk of developing dementia than those without diabetes. Fluctuations in blood glucose levels are common in diabetes patients. Unsteady glucose levels can affect glucose availability to the brain by modifying glucose transporter expression and kinetics as well as permeability at the BBB (*11*).

At a cellular level, glucose homeostasis relies on regulation of glucose uptake from the extracellular environment. Because glucose molecules are large in size and polar molecules, they are not able to cross the membrane via simple diffusion and need a transporter protein in order to enter the cell via either facilitated diffusion or active transport **(Figure 1.1B)**. Normal blood glucose levels are ~5.5 mM while the normal glucose concentration in the brain is ~2 mM. When blood glucose drops to hypoglycemic levels (~2.8 mM and ~0.16 mM in the brain), pancreatic alpha cells release glucagon. Glucagon binds to G protein-coupled receptors (GPCRs) on the liver,

which activates G proteins and continues the signaling cascade by activating adenylate cyclase. Adenylate cyclase produces cAMP, which goes on to activate protein kinase A. The cascade continues until glycogen phosphorylase activates glycogen breakdown to glucose, so that glucose can be released into the blood via glucose transporters (*12*). When the body is experiencing hyperglycemia (~20 mM in the body and ~5 mM in the brain), pancreatic beta cells release insulin. After insulin is secreted, it binds to insulin receptors on fat and muscle cells to initiate a signaling cascade that leads to fusion of vesicles containing glucose transporters to the PM. Once the glucose transporters are at the plasma membrane, fat and muscle cells uptake glucose and bring down the blood glucose concentration to normal levels (*13*). As these transporters largely control glucose homeostasis, it is vital that they are properly regulated.

1.2 Glucose transporter families in mammalian cells

There are two major families of glucose transporters encoded in mammalian genomes-sodium-glucose linked transporters (SGLTs) and facilitative glucose transporters (GLUTs). The SGLTs are sodium-glucose cotransporters that utilize sodium gradients generated by PM sodium-potassium ATPase pumps to drive glucose import against its concentration gradient. There are six SGLTs but SGLT1 and SGLT2 are the most well characterized. They are primarily expressed on the lining of the small intestine to absorb glucose from ingested food and in renal tubules to re-absorb glucose filtered by the kidneys (*14*). SLGT2 inhibitors have been FDA-approved to treat hyperglycemia. These drugs inhibit reabsorption of glucose by SGLT2 in the renal tubule, which reduces blood glucose levels without relying on insulin release (*15*).

The GLUT family is part of the solute carrier (SLC) gene family with over 65 subgroups and are specifically called *SLC2* genes. There are 14 GLUTs divided into three classes **(Table 1.1)** based on sequence similarity (**Figure 1.2).** All members of the SLC2 family have 12 membrane-spanning helices with intracellular N- and C- termini and a large cytoplasmic loop between the sixth and seventh transmembrane domains. They also contain at least one N-glycosylation site. Despite their name, not all GLUT members have been clearly established to facilitate glucose transport. Twelve of the fourteen GLUTs can transport glucose in experimental conditions; however, glucose is not

necessarily the primary substrate under physiological conditions. Individual GLUT family members can exhibit specific transport substrates, kinetic properties, and tissue expression and this variation allows the GLUT family to cover the diverse needs of the human body. Virtually every tissue in the human body expresses at least one of these glucose transporters, often multiple (*16*). The importance of glucose as a cellular energy source explains the ubiquity of GLUTs in humans and other eukaryotes.(*2, 16, 17*)

Class	GLUT	Tissue Localization (humans)	Substrates	Post-translational modifications			Associated genetic diseases
				Glycosylation	Phosphorylation	Other	
1	GLUT1	Ubiquitous, expressed at high levels in brain, erythrocytes	glucose, galactose, glucosamine, mannose, ascorbate	N45	S226[109]	Acetylation (1M)	GLUT1-deficiency syndrome[113]
	GLUT2	Liver, pancreatic β-cells, intestine, kidney	glucose, frustose, galactose	N62	T523[7]		Fanconi-Bickel syndrome[18,24]
	GLUT3	Brain, white blood cells	glucose, galactose, mannose, xylose	N43			Glioblastoma[27]
	GLUT4	Skeletal & cardiac muscle, adipose tissue (white and brown)	glucose	N57	S274[62]	S-palmitoyl C223[61] Ubiquitylation[72]	Type 2 diabetes[76]
	GLUT14	Testis	glucose	N67			
2	GLUT5	Small instestine, kidney, testis, adipose, skeletal muscle	fructose	N51		Acetylation (1M)[4]	Long QT Syndrome[34]
	GLUT7	Small intestine, colon, testis, prostate	glucose and fructose	N57			
	GLUT9	Liver, kidney, small intestine, placenta, lung, white blood cells	urate, glucose & fructose (low affinity)	N90	S9[7] , S515[7]		Renal hypouricemia[18]
	GLUT11	Skeletal muscle, heart	glucose, fructose	N47			
3	GLUT6	Spleen, brain, lymphocytes	low affinity for glucose & fructose	N370	S23[6]		
	GLUT8	Testis, brain, mammary tissue, adrenal gland, liver, spleen, lung, brown adipose tissue	glucose, fructose,	N349			
	GLUT10	Liver, vascular smooth muscle, pancreas	dehydro-ascorbate, glucose	N334			Arterial tortuosity syndrome[18]
	GLUT12	Adipose tissue, heart, skeletal muscle, mammary tissue, prostate	glucose	unknown			
	GLUT13/ HMIT	Brain	myo-inositol	unknown	S640[8], S645[8]		

Table 1.1: GLUT family members. Summary of GLUT transporters characteristics including tissue localization, substrate specificity, PTMs, and genetic diseases associated with the protein.

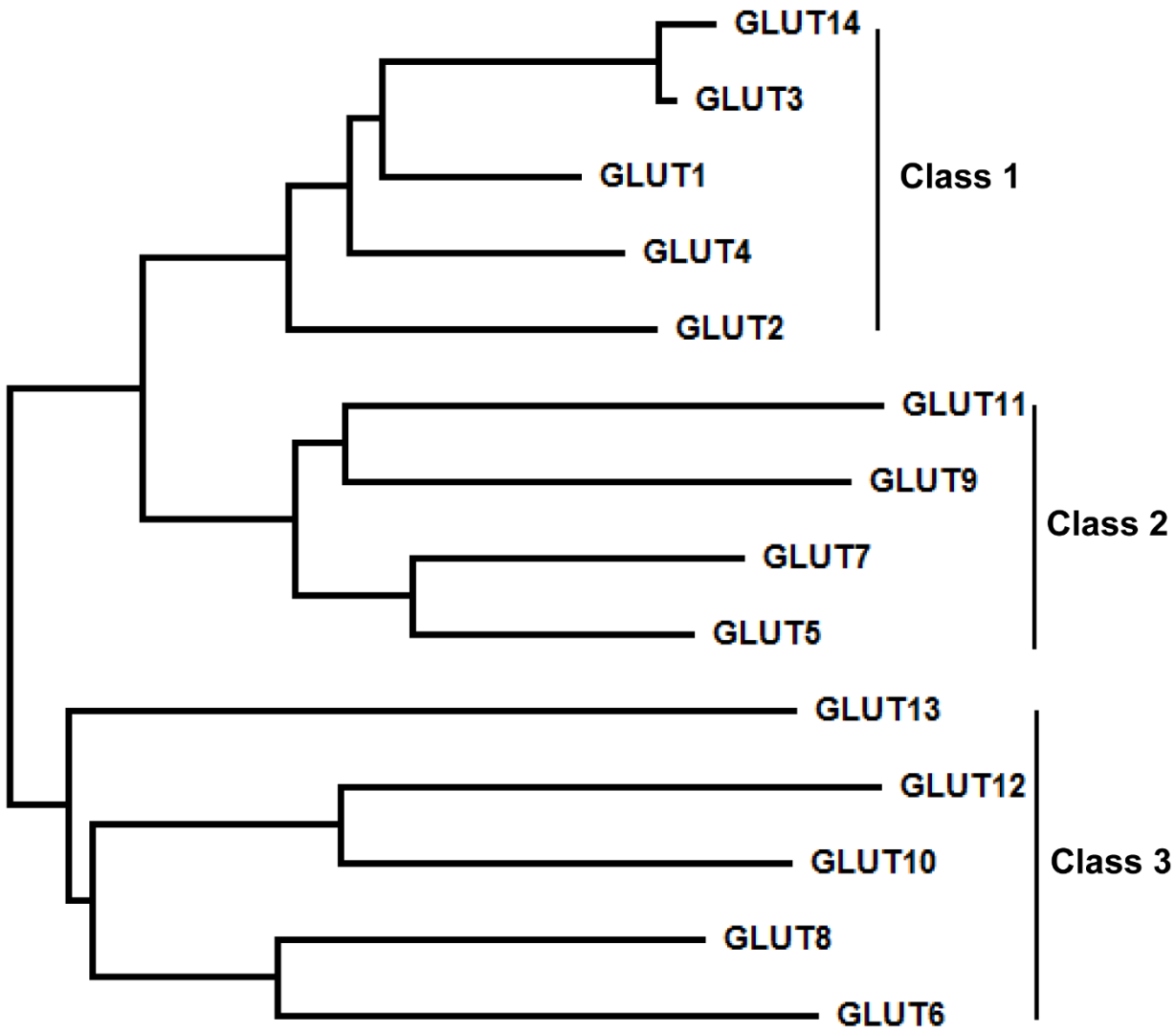

Figure 1.2: Phylogeny tree for facilitative glucose transporter (GLUT1) family. Family members are divided into 3 classes based on sequence similarity. Tree generated using Molecular Evolutionary Genetics Analysis (MEGA).

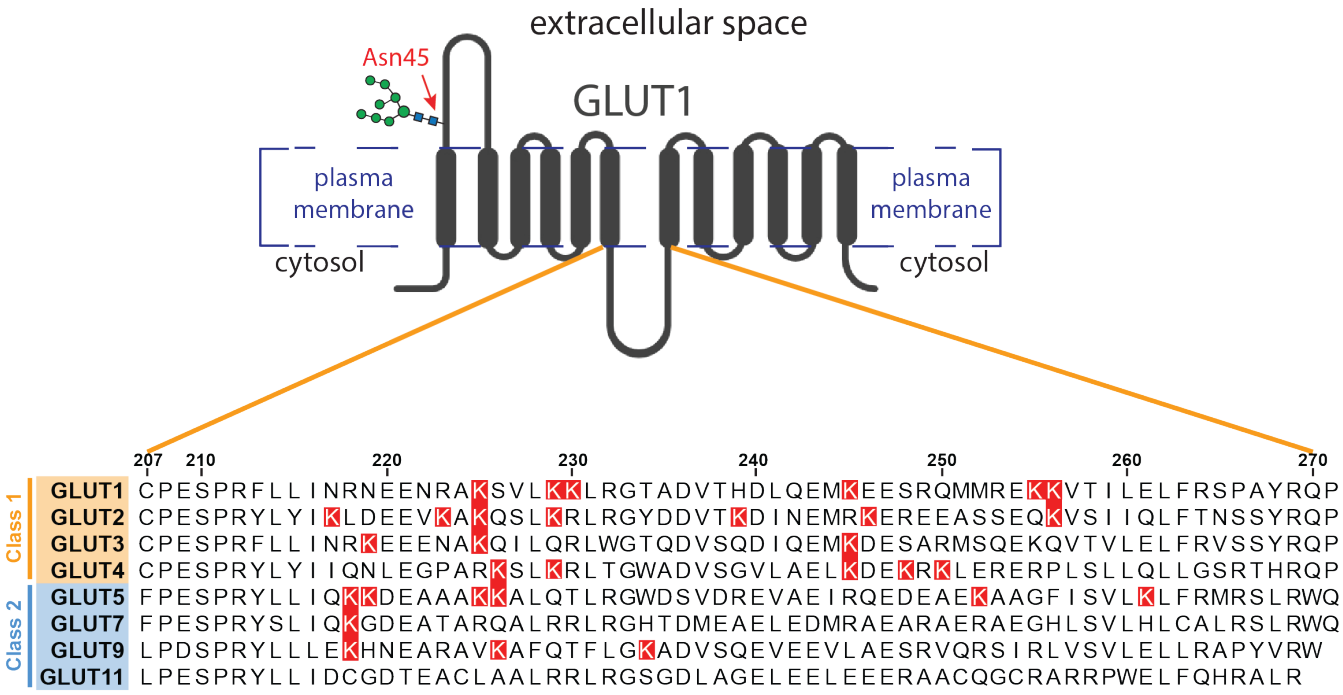

Figure 1.3: Topology of GLUT1 and sequence alignment of the major cytoplasmic loops for Class 1 and Class 2 GLUTs.

1.2.1 Class 1 GLUTs

Class 1 GLUTs (1-4) are the most studied members of the GLUT family and it is well established that they transport glucose *in vivo.* Class 1 GLUTs have an N-linked glycosylation site on a conserved asparagine residue in the first exofacial loop **(Figure 3)**. GLUT1, GLUT3, and GLUT4 have determined protein structures (*18-20*). GLUT1 is ubiquitously expressed but highly expressed in erythrocytes and the blood brain barrier. GLUT1, which is the main focus of this thesis dissertation, is discussed in greater detail in the following section.

GLUT2 is highly expressed in the liver, pancreatic beta cells, kidney, intestine, and other endodermal cells. Unlike GLUT1, GLUT2 also has a high for fructose with a K_M of ~20 mM and a K_M of ~67 mM for glucose. GLUT2 is the primary transporter for both sugars from the intestines to the liver blood supply (portal circulation). GLUT2 in the liver removes fructose from the portal vein in order to maintain low levels in the circulating blood (*2*). It is required in rodent but redundant in human β cells due to the presence of GLUT1 and GLUT3 (*21*). In liver cells, GLUT2 takes in glucose resulting from nutrient intake and releases glucose in times of fasting. When glucose needs to be released from hepatocytes via GLUT2, it is supplied by either degradation of glycogen or gluconeogenesis. GLUT2 is required for glucose uptake in the liver but the release of glucose can utilize an alternate pathway in its absence involving a plasma membrane transport system that has yet to be identified (*22, 23*).

GLUT3 is mainly expressed in the brain and has a low K_M of 1-2 mM. Since normal fasting blood glucose levels range from ~5.5 mM – 7.7 mM, GLUT3 facilitates rapid uptake of glucose from blood into neurons to meet the metabolic demands of the brain (*2, 24*). GLUT14 was discovered to be a duplicon of GLUT3, found just 10Mb upstream of the *SLC2A3* gene. But while GLUT3 is primarily expressed in the brain and can also be found in ovary and testis, GLUT14 is expressed specifically in the testis (*25*). GLUT14 substrate specificity has not been characterized yet, but it is assumed to be similar to GLUT3 based on their sequence similarity.

GLUT4 is the primary GLUT expressed in adipose tissue, heart and skeletal muscle. It is the main insulin-responsive transporter, which means it is integrally involved in regulating the uptake of glucose into fat and muscle to maintain glucose homeostasis.

GLUT4 is unique among the GLUTs in that it is kept in an intracellular reservoir of vesicles termed GLUT4 storage vesicles (GSVs) that are rapidly translocated to the cell surface upon insulin stimulation. The K_M for GLUT4 is about the same as the fasting blood glucose concentration (~5 mM) and stays the same even in the presence of insulin. Hence, the V_{MAX} of GLUT4 increases dramatically and glucose is very quickly taken up by the cells upon insulin release (*26, 27*). GLUT4 is of great medical interest as understanding its function and regulation could aid in developing therapeutics for metabolic disease.

1.2.2 Class 2 GLUTs

Class 2 GLUTs (GLUT5, GLUT7, GLUT9, and GLUT11) are not primarily glucose transporters, often preferring fructose. GLUT5 is highly expressed in the small intestine, kidney, and sperm as well as fat and skeletal muscle at lower levels. It has a higher affinity for fructose than glucose and its expression in the small intestine actually regulated by fructose levels (*28*). GLUT5 is responsive to insulin in fat and muscle cells and has been shown to be overexpressed in diabetic muscle (*29, 30*). It has also been shown to be mutated in the arrhythmogenic disorder, long QT syndrome, in which exercise triggers arrhythmia (*31*). GLUT7 is highly expressed in the small intestine, colon, testis, and prostate (*32*). Despite being the closest relative to GLUT5, the substrate for GLUT7 is not the same and is still disputed. Fructose was reported to be a substrate for human GLUT7 expressed in Xenopus oocytes (*32*); however, when the Xenopus experiment was repeated, in addition to expression in NIH-3T3, GLUT7 did not show fructose or glucose transport activity in Xenopus nor NIH-3T3 cells (*33*).

GLUT9 has two splice variants in humans with differing tissue expression and subcellular localization. The longer isoform is most strongly expressed in the basolateral membrane of renal tubular cells, liver, and placenta. The short isoform is only expressed in the apical membrane of renal tubular cells and placenta. Interestingly, the substrate for GLUT9 was discovered to be urate. GLUT9 is an efflux transporter of urate from tubular cells. While GLUT9 strays from transporting hexoses, it is still Na^+-independent and facilitates diffusion. However, in this case it is sensitive to membrane potential. The increase of K^+ outside of the cell facilitates the efflux of urate, moving from negative to positive potential (*34, 35*).

The last member of the class 2 GLUTs is GLUT11. GLUT11 has been shown to transport both fructose and glucose (*36*). There are three splice variants (A,B,C) of GLUT11 that each show unique tissue distribution, but all appear to have the same function. GLUT11-A is found in heart, skeletal muscle, and kidney, GLUT11-B is found in kidney, adipose tissue, and placenta, and GLUT11-C is expressed in adipose tissue, heart, skeletal muscle, and pancreas (*37*). GLUT11 is one of the least studied GLUTs so not much is known about the transporter past its substrate and expression pattern.

1.2.3 Class 3 GLUTs

Class 3 GLUTs are distinguished from other classes by an N-linked glycosylation on the fifth exofacial loop. GLUT6 (called GLUT9 when it was first discovered) is expressed in the spleen, lymphocytes, and brain. Substrate specificity for GLUT6 is unknown, however it does have a very low affinity for glucose and fructose (*38, 39*). GLUT6 was localized to lysosomal membranes in inflammatory macrophages and is reported to regulate glycolysis (*40*). Like GLUT6, GLUT8 also localizes to lysosomes and late endosomes and transports both glucose and fructose (*41, 42*). It is found at high levels in testis, spermatozoa, and mammary gland alveolar cells (*2*). There are several proposed functions for GLUT8. It was found to be involved in hexose transport across intracellular membranes and was also shown to regulate fructose transport in enterocytes (*41, 42*). In mammary cells, it plays a role, alongside GLUT1, in glucose uptake to support lactose synthesis (*43*).

GLUT10 is found in a wide array of tissues including pancreas, placenta, heart, lung, liver, brain, fat, muscle, and kidney. It has a low K_M (0.3 mM) for 2-deoxyglucose when exogenously expressed in Xenopus oocytes but has very low *in vivo* activity (*16, 44*). The main substrate appears to be dehydro-ascorbate. On a subcellular level, GLUT10 can be found in mitochondria of artery cells where it plays a role in redox control by accumulating dehydro-ascorbate (*45*).

GLUT12 is mostly found in insulin-responsive tissues (fat, heart, skeletal muscle) but also in mammary gland alveolar cells. Upon insulin stimulation, GLUT12 in skeletal muscles moves from an intracellular location to the plasma membrane. It is suspected that GLUT12 preceded GLUT4 evolutionarily and became redundant (*46, 47*). GLUT13 (also known as H(+)-myo-inositol transporter or HMIT) is the last member of the class 3

GLUTs, localized primarily to neuronal tissue. The substrate for HMIT is myo-inositol and transport is coupled to proton movement (*48*).

GLUT1 and GLUT4 have been extensively studied because of their prevalence in glucose regulation and human disease; therefore, the next two sections will summarize current understanding of these transporters regarding structure and transport activity, cellular function and regulation, and pathophysiology.

1.3 Regulation of glucose homeostasis by GLUT4

It has been known since 1980 that insulin stimulates the translocation of a glucose transporter inside the cell to the plasma membrane in both adipocytes (*49, 50*) and muscle cells (*51, 52*). But scientists were not able to isolate and clone the particular protein, GLUT4, until 1989 (*53-57*). Since its discovery, researchers have been interested in understanding the regulation GLUT4.

1.3.1 Structure and transport activity

The structure of GLUT4 bound to small molecule inhibitor cytochalasin B (CCB) was determined by cryo-EM in 2022 with resolution of 3.3 Å (*20*) **(Figure 1.4)**. When bound to CCB, the glucose transporter has an “inward open” conformation. GLUT1 and GLUT4 have 65% sequence identity and 79% sequence similarity, so it is not surprising that GLUT1, whose structure was determined by the same group in 2014 (*18*), is structurally very similar. In order to crystallize GLUT1 and GLUT3 (*19*), the glycosylation site was either mutated or the protein was deglycosylated prior to crystallization. One of the advantages of cryo-EM is the ability to resolve post-translational modifications and Yuan et. al. was therefore able to resolve glycosylation on Asn57 of GLUT4. The other major difference seen between the GLUT1 and GLUT4 structures was the intracellular helical (ICH) domain. ICH5 was not visible in the GLUT1 structure, but the GLUT4 ICH5 is fully resolved (*20*).

GLUTs in general undergo conformational changes to catalyze hexose transport. The GLUT4 structure revealed that ICH5 has an important role in this conformational change, serving as a latch that is open when the protein is inward facing and closed in the outward facing conformation (based on the outward facing crystal structure of

GLUT3, where ICH5 is conserved between the two transporters) (*19, 20*). Single point mutations of residues within this “latch” of ICH5 caused the transport activity of GLUT4 to decrease by as much as 70%, demonstrating the importance of ICH5 in the glucose transport activity of GLUT4 (*20*). Class I GLUTs also have a conserved Ser-Thr-Ser motif on extracellular loop 7 that is important for conformational change. If any of these three residues are mutated, the protein is locked in the outward-facing conformation (*58*). Unique to the GLUT transporters with the highest affnty for glucose (GLUT1, GLUT3, GLUT4) is a Gln-Leu-Ser motif in the seventh transmembrane helix, whereas GLUT transporters with a higher affinity for fructose (GLUT2) have a His-Val-Ala motif in TM7 (*59*).

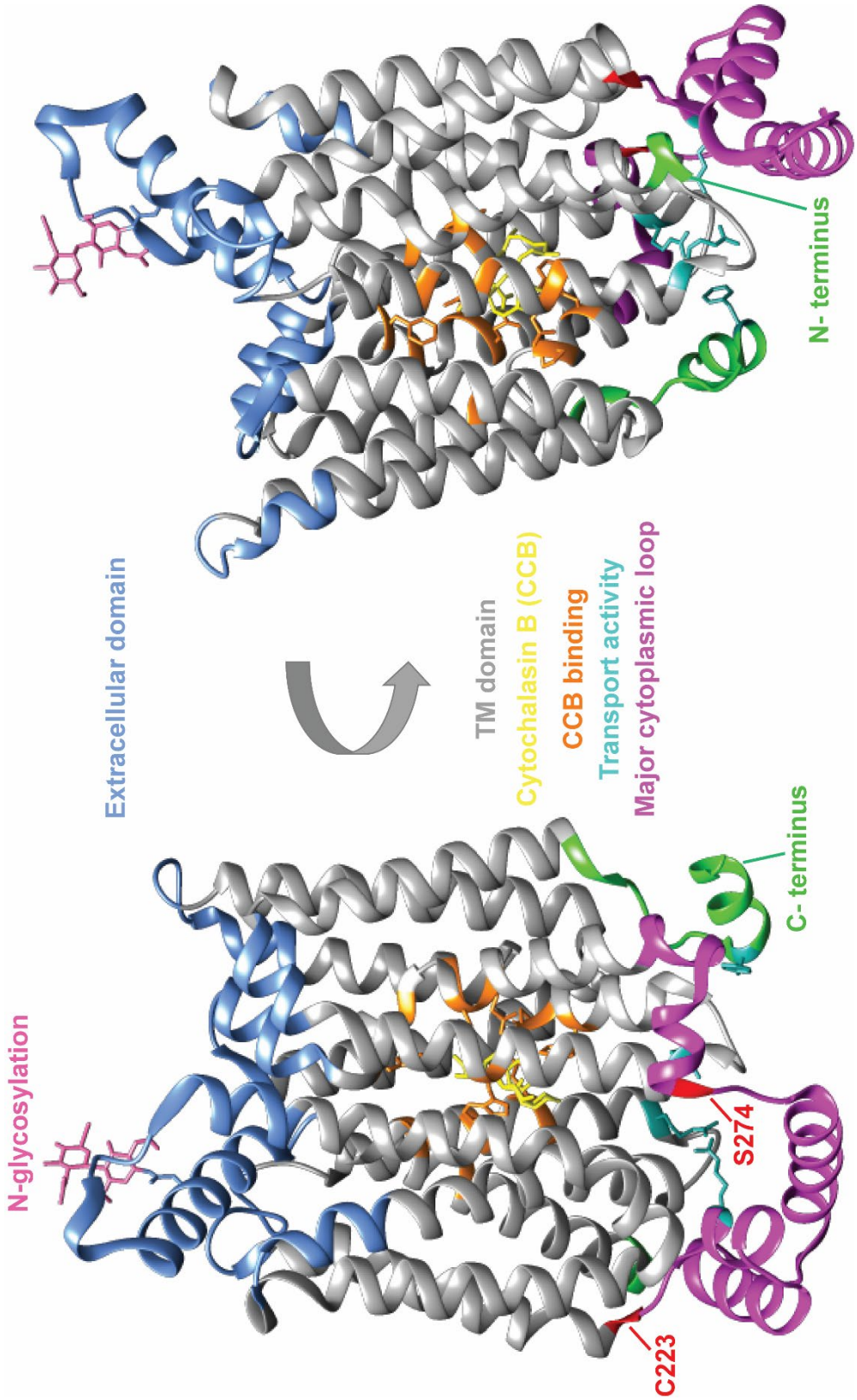

Figure 1.4: Structure of GLUT4 bound to inhibitor cytochalasin (CCB). Determined by cryo-EM at 3.3 Å resolution (*20*). Residues and regions of note labeled. Cys223 is palmitoylated and plays a role in translocation of GLUT4 to the PM (*60*). Ser274 is phosphorylated by SGK1 (*61*) and promotes glucose uptake by increase of GLUT4 at the PM.

1.3.2 Cellular function and regulation

Under basal conditions, GLUT4 is virtually absent from the surface of adipocytes and muscle cells. The glucose transporter is sequestered inside the cell on endosomes and, predominantly (85-90%), on *trans*-golgi network (TGN) membranes and the specialized GSVs (*62*). Upon glucose stimulation, the exocytosis rate of GLUT4 is drastically increased and approximately 50% of this intracellular GLUT4 is redistributed to the cell surface. Rather than GLUT4 remaining static at the PM, the cell is continuously recycling it. When insulin is removed, surface GLUT4 rapidly returns to basal levels along with the exocytosis and endocytosis rates (*13*). While GLUT4 does have a specialized trafficking pathway, it also utilizes the canonical endosomal and recycling pathways (*63*). It undergoes clathrin-mediated endocytosis along with other common recycling cargo like the transferrin receptor (TfR) but then diverges from the other cargo and is transported to the TGN and GSVs. Use of multiple trafficking routes makes it difficult to distinguish the GSV compartments from typical endosomal compartments (*13*).

Post-translational modifications, including phosphorylation, ubiquitylation, and palmitoylation play an important role in the regulation of GLUT4. The insulin receptor itself is a tyrosine kinase and upon ligand-binding, a complex signal transduction network is initiated. The two canonical insulin receptor signaling cascades are the extracellular signal regulated kinase (ERK) pathway and the phosphatidylinositol 3-kinase (PI3K) pathway. The ERK pathway is involved in regulation of gene expression and regulation of cell growth and differentiation, while the PI3K pathway is responsible for most of the metabolic effects of insulin that are of interest here (*64*). The insulin receptor kinase activity on insulin receptor substrate-1 (IRS-1) leads to recruitment of PI3K to the plasma membrane. PI3K activity increases phosphatidylinositol 3,4,5-trisphosphate (PIP_3), which in turn activates the Akt kinase. One of Akt's targets is the Rab GTPase-activating protein (RabGAP), TBC1D4 (also known as AS160). TBC1D4 is a key component in regulation of insulin-dependent glucose transport, serving as a negative regulator of the insulin-initiated GLUT4 translocation to the PM (*13*). When an Akt phosphorylation site on TBC1D4 (Thr 642) is mutated to alanine, insulin-stimulated GLUT4 translocation decreases. When the GAP function of this Thr642A mutant is inactivated, GLUT4 translocation is no longer blocked (*13, 65*). This suggests that Akt

phosphorylation of Thr642 on TBC1D4 inhibits its GAP activity, and it is this GAP activity that is responsible for inhibiting GLUT4 translocation. TBC1D4 phosphorylation promotes binding with a 14-3-3 protein, which results in an increase of insulin-stimulated GLUT4 translocation (*66*). All these findings suggest that phosphorylation of, and subsequent 14-3-3 protein binding to TBC1D4, block its GAP activity and allow GLUT4 translocation to the cell surface.

While there are many kinases involved in the GLUT4 translocation pathway, there is only one reported phosphorylation site on human GLUT4 at Ser274 (*61*) **(Figure 3)**. Ser274 is phosphorylated by the kinase SGK1 (serum- and glucocorticoid-inducible kinase). Jeyaraj et. al. co-expressed GLUT4 and SGK1 in *Xenopus* oocytes and observed an increase in GLUT4 at the cell surface (*61*). There is also one confirmed site of palmitoylation at Cys223 (*60*). Knockout of the palmitoyl transferase (PAT) DHHC7 in adipose tissue and muscle led to a decrease in palmitoylation of GLUT4 and suppressed insulin-dependent GLUT4 translocation to the membrane. Also, DHHC7 KO mice experienced hyperglycemia and glucose intolerance, suggesting palmitoylation is a vital component of insulin-regulated glucose homeostasis.

Evidence of GLUT4 ubiquitylation is limited to one study in human adipocytes (*67*). Lamb et. al. were not able to detect GLUT4 ubiquitylation in adipocytes directly by immunoprecipitation (coIP), presumably due to low protein levels of ubiquitin on GLUT4; however, they provided the following evidence supporting ubiquitylation of GLUT4. Because they could not coIP ubiquitin with GLUT4 pull-down, they instead GST-tagged the UBA (ubiquitin-associated) domain of Dsk2p, a protein known to bind polyubiquitin (*68*). They showed that GLUT4 pulled down with the UBA construct. IRS-1, which has been reported to be ubiquitylated in adipocytes (*69*), was used as a positive control and was shown to co-precipitate with GST-UBA. However, some limitations should be pointed out. There is no evidence in the literature that IRS-1 interacts the UBA domain of Dsk2p and no ubiquitin immunoblot was included with this coIP experiment to confirm ubiquitylation of IRS-1. When the UBA was mutated, IRS-1 and GLUT4 no longer co-precipitated. Also, a mutant of GLUT4 with all cytoplasmic lysine residues mutated to alanine (GLUT4-7K/R) did not pull down with the GST-UBA (*67*). They also demonstrated a decreased presence of GLUT4-7K/R at the surface of adipocytes after insulin treatment in comparison with WT GLUT4. This decreased presence of GLUT4-

7K/R at the cell surface indicates that the GLUT4 lysine residues are required for its insulin-stimulated translocation (*67*). Additional studies will be needed to confirm the ubiquitylation of GLUT4 and further investigate its role in regulating GLUT4 translocation.

1.3.3 Pathophysiology

Type 2 diabetes (T2D) is largely characterized by the inability of muscle and fat cells to effectively take up glucose from the blood in response to insulin. As discussed above, GLUT4 is trafficked to the cell surface from intracellular GSVs in response to insulin and glucose transport is considered a rate limiting step in glucose homeostasis processes (*70*). So, it follows that GLUT4 plays a significant role in T2D pathophysiology. There have been many studies over the years demonstrating that defective translocation of GLUT4 to the cell surface is a major contributor to insulin resistance typically seen in T2D(*71-73*). However, it is still not clear at what stage in GLUT4 translocation the defect is occurring. It could be missorting of GSVs, inability to fuse with the plasma membrane, or defective mobilization of GSVs (*13*). This has yet to be elucidated, but it is a very active area of research.

There are efforts to translate knowledge of GLUT4 to clinical treatment of T2D. Overexpression of GLUT4 in mice has positive effects on glucose metabolism, but exceeding physiological levels led to hypoglycemia, hypoinsulinemia (low blood levels of insulin), and lactacidemia (high levels of lactic acid in the blood) (*74*). In order to increase GLUT4 levels in a more physiologically appropriate manner, some groups are attempting to elucidate the mechanism of action behind the increase of GLUT4 in response to exercise. Exercise-induced increases in glucose uptake and GLUT4 cell surface expression are not affected by insulin resistance, which suggests that there is a pathway separate from insulin induction that leads to GLUT4 at the cell surface (*75, 76*). If this alternate pathway to increased GLUT4 could be illuminated, it could be a promising therapeutic target for T2D.

1.4 Regulation of glucose homeostasis by GLUT1

In 1976, glucose transport was reconstituted with a protein fraction partially purified from erythrocytes (*77, 78*). The protein responsible for this glucose transport was later purified, cloned and termed GLUT1 (*79-81*). While it is ubiquitously expressed and present in virtually all tissues, it is highly expressed in endothelial cells at the blood brain barrier and in the brain, in erythrocytes, and in the placenta (*16*). Its involvement in a variety of cancers and other diseases has made GLUT1 a major focus of research since it was first discovered. A great deal has been elucidated about the structure, transport kinetics, function, regulation, and pathophysiology of GLUT1. But there is still more to be discovered, particularly in regard to how its transport of glucose and presence at the cell surface is regulated.

1.4.1 Structure and transport activity

The crystal structure of human GLUT1 was determined in 2014 at 3.2Å resolution (*18*) **(Figure 1.5)**. In order to obtain crystals, a N45T mutation was made at the glycosylation site to eliminate heterogeneity. Also, a E329Q mutation was made to lock the transporter in the inward facing conformation (*82*). An intracellular helical bundle (ICH) comprised of 4 short α-helices (ICH1-4) connected the N and C domains of the protein, which enclosed a cavity on the intracellular side in the inward facing conformation. As mentioned above, ICH5, the helix after TM12, could not be resolved presumably because of its flexibility in the inward conformation (*18*). Deng et. al. also used the N and C domains of *Escherichia coli* GLUT1 homologue XylE, to solve the structure by molecular replacement. By comparing the inward-facing GLUT1 and outward-facing XylE structures, the researchers suggested that both transporters have a single substrate-binding site that is alternately accessed by the inside and outside of the PM. The C-terminal domain of GLUT1 is proposed to be involved in substrate binding while the N-terminal domain coordinates the alternating access to each side of the PM and the ICH domains are critical to “latch” intracellular substrate access while the transporter is in the outward-facing conformation (*18*).

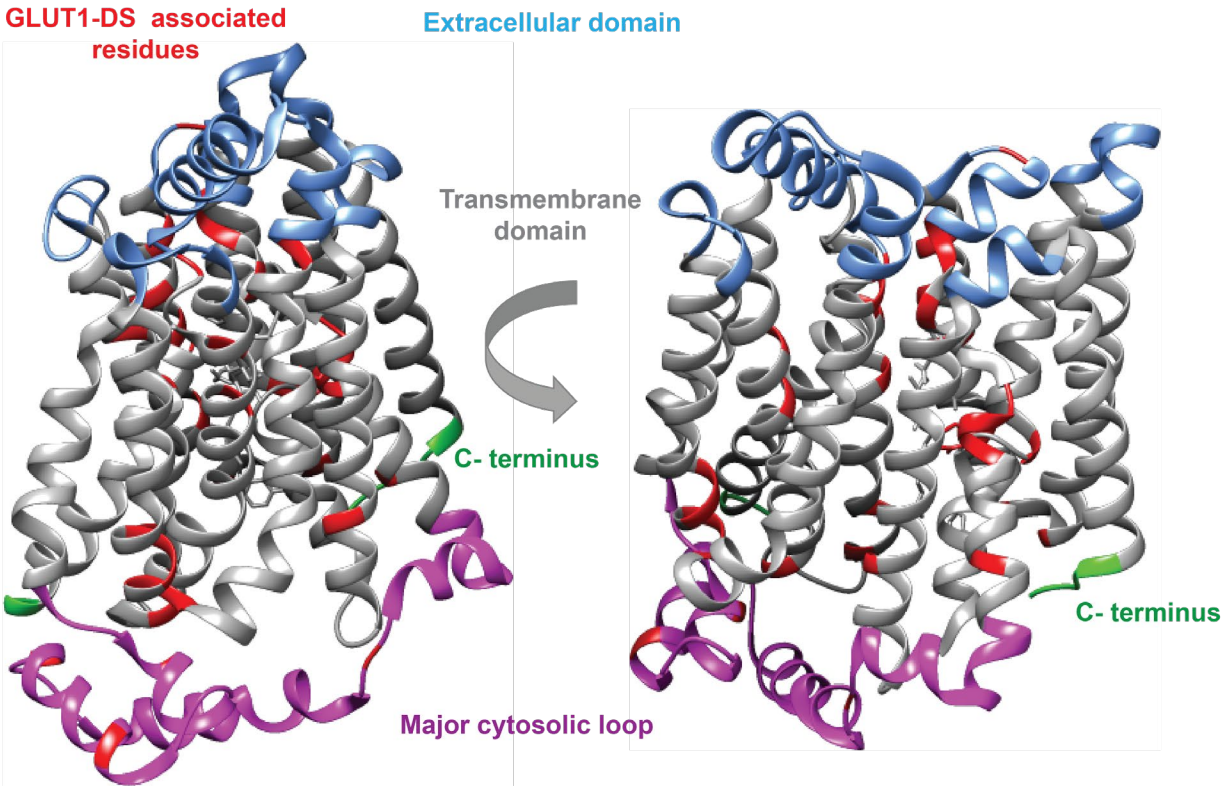

Figure 1.5: GLUT1 x-ray crystallography structure at 3.2 Å resolution (*18*). Residues that have been linked to GLUT1 deficiency syndrome (GLUT1-DS) are highlights in red.

On the extracellular side of GLUT1, there is a glutamine in TM5 (Gln161) that is known to be important for recognition of extracellular glucose(*83*) .TM1 and TM7 come into contact when the protein in in the inward-facing conformation, which suggests these two domains are largely responsible for outward gating. Asn34 on TM1 coordinates hydrogen bonds with Ser294 and Thr295 on TM7 and Thr310 on TM8. This network of hydrogen bonding serves to block substrate binding on the extracellular side when the transporter is in the inward-facing conformation (*18*). There is also Arg126 in TM4 that presumably interacts with Tyr292 on TM7 via a cation-pi interaction between the guanidinium group of Arg126 and the benzene ring of Tyr292 to strengthen the extracellular gate closure in the inward-facing conformation (*18*). All of these residues will be relevant when discussing the pathophysiology of GLUT1 in section 1.4.3.

Most GLUT1 kinetic experiments have been performed in erythrocytes because GLUT1 is abundant in these cells, making up as much as 10% of all integral membrane proteins (*16*). The K_M for GLUT1 influx (~2 mM) is significantly lower than the fasting blood glucose concentrations of ~5.5 mM. This means that there is typically an influx of glucose from the blood to the cell and availability of transporter at the cell surface is a rate limiting step for substrate influx. GLUT1 has a higher affinity for glucose on the outward-facing binding site than the inward-facing binding site (*84*), meaning the V_{max} and K_m for net sugar influx are lower than for sugar efflux by as much as 10-fold (*85*). Also, GLUT1 exhibits trans-acceleration, in which the presence of glucose on one side of the membrane increases the initial rate of transport from the opposite side. This suggests that a conformational change involving the empty transporter is rate limiting for glucose transport (*16*).

There are currently two popular models for glucose transport by GLUT1. The two site/fixed site transport model proposes that multiple binding sites are simultaneously accessible on both sides of the membrane. Proponents of this model argue that it accounts for the complex kinetics of GLUT1. The second model is alternating access transport in which there are mutually exclusive substrate binding sites on each side of the membrane and only one substrate can be transported at a time (*2*). Crystal structures for GLUT1 and other GLUTs strongly support the alternating access model. As described above, in both the GLUT1 and GLUT4 structures, there is an “inward open” conformation where the outward facing binding site it blocked by a “latch”. They

also show that the transporter is sterically crowded in the channel which suggests two molecules of glucose could not pass through at once as is suggested with the fixed sites model. In regards to the complex kinetics of GLUT1, there is data suggesting GLUT1 forms oligomers (*86*). In this case, a dimer of GLUT1 could have two substrates simultaneously bound on opposite sides of the membrane. As we learn more about the precise transport kinetics and structure of GLUT1, we will be more capable of pinpointing the exact cause of diseases associated with defective glucose transport.

1.4.2 Function and regulation

GLUT1 is responsive to many growth factors including IL-3, IGF-1, TGF-β, and HIF-1 (*87-91*) and several major pathways are involved in GLUT1 expression. The glycogen synthase kinase-3/tuberous sclerosis complex/ mammalian target of rapamycin (GSK3/TSC/mTOR) pathway is one example. GSK3 was originally found to be a key regulator of glycogen synthase but is now known to play roles in several other pathways and processes such as transcription, translation, apoptosis, and glucose metabolism (*92*). In the case of glucose metabolism, GSK3 negatively regulates glucose uptake and GLUT1 expression via TSC/ mTOR (*93, 94*). The signaling cascade starts with GSK3 activating the TSC2 subunit of TSC. TSC2 has GAP activity and interacts directly with the GTPase, Rheb (*95*). When TSC2 is inactivated, Rheb-GTP accumulates and promotes the kinase activity of mTOR towards S6 kinase. When S6K is phosphorylated by mTOR, S6K promotes protein translational in the cell. Conversely, when TSC2 is active, Rheb-GTP is decreased leading to reduced mTOR and S6K activation and thus decrease glucose uptake and GLUT1 expression (*96*). When TSC2 was deleted or the GSK3 phosphorylation sites on TSC2 were mutated, GLUT1 expression and glucose uptake were increased. When the mTOR inhibitor, rapamycin, was introduced to cells lacking TSC2, there was no longer an increase in glucose uptake nor GLUT1 expression. These results suggest that the GSK3 effect on GLUT1 is TSC2 dependent and mTOR mediates the TSC2 effects (*96*).

Regulation of trafficking is another method of GLUT1 regulation. The retromer recycling pathway has been shown to play a role in regulating GLUT1 levels at the cell surface (*97*). Steinberg et. al. found via a SILAC proteomics approach that GLUT1 interacts with the PDZ-domain-containing sorting nexin 27 (SNX27). SNX27 is an early

endosome-associated protein involved in sorting specific endosomal cargo proteins that have a PDZ ligand at the C terminus. SNX27 promotes retrieval and recycling of this cargo back to the PM by interaction with the retromer recycling complex, which is a heterotrimer composed of VPS26, VPS29, and VPS35. SNX27 interacts with the retromer-associated Wiskott-Aldrich syndrome protein and SCAR homologue (WASH) complex and serves as an adaptor between the PDZ ligand-containing cargo and the retromer/WASH complex to aid in recycling to the PM (*98, 99*). After looking at the SNX27 interactome, Steinberg et. al. used SILAC proteomics again to compare the biotinylated surface proteome in control, SNX27 siRNA knock down (KD), and VPS35 siRNA KD cells. Subsequently, they looked for proteins that were enriched in the SNX27 interactome but lost from the cell surface in SNX27- and VPS35-depleted cells. GLUT1 fell into this category and therefore was concluded to be a SNX27-retromer recycling cargo protein. They also found that GLUT1 was trafficked to the lysosome when SNX27 and/or VPS35 were knocked down or when the PDZ ligand of GLUT1 was deleted (*97*). This work reveals that the SNX27-retromer pathway plays an important role in endosome-to-PM recycling of GLUT1.

In relation to the role of retromer complex in GLUT1 regulation, autophagy was found to promote glucose uptake in times of metabolic or oncogenic stress via retromer-dependent GLUT1 trafficking to the cell surface. TBC1D5 functions as a RabGAP for Rab7, which is a critical protein for recruiting the retromer complex to the endosomal membrane, and therefore TBC1D5 is a key regulator of retromer activity. When cells are in full nutrient media, TBC1D5 interacts with the retromer complex, inhibiting its function. Under glucose starvation conditions, TBC1D5 dissociates from the retromer complex and instead associates with $LC3^{+}$ autophagosomes leading to increases GLUT1 recycling to the PM. Hence, autophagy promotes GLUT1 at the cell surface and glucose uptake (*100*).

Another active area of research concerns the negative regulation of GLUT1 by the arrest domain-containing (ARRDC) protein, thioredoxin interacting protein (TXNIP). In 2007, Parikh et. al. reported that *txnip* gene expression was a strongly suppressed by insulin but stimulated by glucose. Overexpression of TXNIP protein decreased cellular glucose while RNA interference knockdown in adipocytes and skeletal muscle increased glucose uptake. (*101*). It was not until 2013 that this negative regulation of

glucose uptake by TXNIP was linked to GLUT1. Wu et. al. showed that TXNIP suppressed glucose uptake by binding to GLUT1 and promoting GLUT1 endocytosis. They found that GFP-TXNIP colocalized with clathrin-coated pits and Myc-GLUT1 co-immunoprecipitated with HA-TXNIP, suggesting TXNIP is directly involved in GLUT1 endocytosis. They also showed that GLUT1 steady state protein levels as well as glucose uptake increased with TXNIP knockdown, and both phenotypes could be complemented by reintroduction of TXNIP. Finally, they demonstrated that endocytosis of HA-GLUT1 was much faster when WT TXNIP was co-expressed in comparison to a TXNIP variant that cannot interact with clathrin (*102*).

GLUT1 is also regulated by post-translational modifications. N-glycosylation is a conserved post-translational modification among all GLUTs and it has been shown that mutating the glycosylation site of GLUT1 results in a significantly shorter half-life and localization to intracellular compartments rather than the PM (*103*). GLUT1 was found to be phosphorylated by protein kinase C in 1985 (*104*); however, the connection to regulation of GLUT1 was not made until 2015 (*105*). It was known that the phorbol ester, 12-O-tetradecanoylphorbol-13-acetate (TPA) increased glucose uptake in a biphasic manner, with a faster and slower component (*106*) and that phorbol esters act on diacylglycerol (DAG)-dependent forms of PKC to exert tumor promoter behaviors on cells (*107*). While the slow surge in glucose uptake can be explained by transcriptional upregulation of GLUT1 (*108*) the faster increase was discovered to be the result of phosphorylation of Ser226 by PKC (*105*). Interestingly, the response to GLUT1 phosphorylation differed in different cell types. *Xenopus* oocytes, rat fibroblasts, primary human endothelial cells increased glucose uptake upon TPA-induced phosphorylation by increasing GLUT1 at the PM, hence increasing the V_{MAX}. On the other hand, GLUT1 in primary human erythrocytes was phosphorylated in response to TPA treatment but there was no increase in glucose uptake, which the authors speculate may be due to the lack of trafficking machinery in these cells. The PKC motif surrounding Ser226 in GLUT1 was found to be mutated in some cases of GLUT1 deficiency syndrome (*105*), which is described further in the following section.

Aside from Ser226 phosphorylation, little is known about post-translational modifications of GLUT1. The phosphorylation site and several known GLUT1-DS mutations are located on the major cytosolic loop. Similarly, GLUT4 has residues

associated with its regulation in the major cytoplasmic loop (**Figure 4).** This thesis will detail the discovery of a ubiquitylation site on GLUT1 and the role ubiquitylation plays in regulation of GLUT1 trafficking.

1.4.3 Pathophysiology

When glucose transport to the brain is impaired, the lack of fuel for the brain has serious health consequences. GLUT1 is a major contributor to glucose transport at the blood brain barrier and a defect in GLUT1 can lead to GLUT1 deficiency syndrome (GLUT1-DS). GLUT1-DS is characterized by infant on-set drug-resistant seizures, developmental delay, and microcephaly (small head). As they move into adolescent-adulthood, patients experience different movement disorders like dystonia (involuntary muscle contraction) and paroxysmal exertional dyskinesias (involuntary movement disorders following exercise). Most patients have autosomal dominant *de novo* heterozygous mutations in the GLUT1 gene *SLC2A1*. There have been dozens of mutations in the *SLC2A1* gene identified that lead to GLUT1-DS, including defects in transcription of the gene, translation of the GLUT1 protein, processing, and trafficking of the protein (*109-111*). GLUT1 can function as a tetramer to facilitate glucose transport (*112*), so mutations in the protein could lead to GLUT1-DS in a variety of ways to disrupt this oligomer: protein misfolding, destabilization of the interaction between GLUT1 molecules needed for glucose transport, unwanted interaction with other proteins, or protein aggregation. The type of genetic mutation is also often correlated to disease severity. For example, missense mutations generally have a milder phenotype while deletions or truncations (nonsense mutations) tend to have more severe disease phenotypes (*109, 113, 114*).

GLUT1-DS patients with mutations on a disordered cytosolic region at the C-terminus were found to have a missense mutation that introduced a dileucine motif (*111*). Dileucine motifs are known to bind either clathrin or AP-2 (*115*) so Meyer et. al. investigated the trafficking of a disease-associated GLUT1 mutant, Pro485Leu. A SILAC interactome comparing WT GLUT1 to the dileucine mutant showed an increased interaction with clathrin in the mutant. When they observed localization of the two GLUT1 constructs expressed in HEK cells by immunofluorescence, the WT GLUT1 was localized to the PM while the Pro485L GLUT1 was localizing to internal endocytic compartments. GLUT1 Pro485Leu had significantly increased colocalization with

markers of early, late, and recycling endocytic compartments as well as the TGN (*111*). They also generated patient-derived induced pluripotent stem cells (iPSCs) using a skin punch from a GLUT1-DS patient with the GLUT1 Pro485Leu mutation. The iPSCs were similarly mislocalized to compartments along the endocytic pathway. When the Pro485Leu mutation was introduced into mice via CRISPR/Cas9 gene editing, Meyer et. al. found that homozygous GLUT1 mutant mice die shortly after birth and had mislocalized GLUT1 at the endothelial cells of the blood brain barrier (*111*).

There are several GLUT1-DS patient mutations within the highly conserved PKC motif of the protein (*105*). Three of these are missense mutations that replace R223 with a nonconserved residue. Another mutation causes the insertion of residues PPV between V227 and K228, again disrupting the PKC motif. When Lee et. al. performed *in vitro* assays with these four GLUT1 mutants, they were no longer efficiently phosphorylated in comparison to a control GLUT1 protein construct. While the mutants still exhibited transport levels similar to WT GLUT1, they did not have the TPA-induced increase in 2DG seen by WT GLUT1. This could possibly account for the glucose transport defects seen in patients with the PKC motif mutations (*105*).

Solving the structure of GLUT1 was an opportunity to learn more about the functional implications of the GLUT1-DS mutations seen in patients. Dong et. al. observed that the mutations tended to be concentrated in three clusters of the protein. Cluster 1 consists of mutations involved in substrate binding, which possibly lead to an inability to recognize glucose and, therefore, a decrease in transport (*116, 117*). Cluster 2 contains mutations at the interface of the protein's transmembrane domain and ICH domain. As discussed in section 1.4.1, the ICH domain of GLUT1 appears to serve as a latch to close off the inward-facing binding site and allow alternating access to substrate on the outward-facing binding site. Indicative of the importance of this TM-ICH domain interaction, nearly half of the GLUT1-DS mutations map to cluster 2. Mutations in the third cluster line the substrate transport path. As mentioned above, there is a hydrogen-bonding network between TM1, TM7, and TM8 that occludes the outward-facing binding site when GLUT1 is in the inward-open conformation. A number of patient mutations that affect four residues vital for this network: Asn34Ile, Asn34Ser, Asn34Tyr, Ser294Pro, Thr295Met, and Thr310Ile. There are also 3 patient mutations to Arg126,

which is important for the cation-pi interaction with Tyr292 that keeps the outward-facing binding site occluded in the inward-open conformation (*18*).

Currently, the most common treatment for GLUT1-DS is a ketogenic diet in order to raise the number of ketone bodies in the blood and provide the brain with an alternative fuel source. Ketones cross the BBB via monocarboxylate transporter 1 (MCT1) and provide a source of acetyl CoA that can be fed into the tricarboxylic acid (TCA) cycle. (*118*) While a ketogenic diet helps prevent seizures early on, the effectiveness of this diet for other disease characteristics varies from patient to patient. For this reason, other therapeutic options are being explored such as gene therapy. Researchers have shown in mice that using adeno-associated virus serotype 9 (AAV9) to deliver GLUT1 to the mouse (either systemically or directly to the brain) can be effective. GLUT1-DS model mice treated with AAV9-GLUT1 had increased cerebral GLUT1 expression, improved motor function, increased cerebrospinal fluid glucose levels, brain growth, and increased glucose uptake into the brain. These results were promising enough that several groups are working to translate this to human treatment of GLUT1-DS (*119, 120*).

GLUT1 is ubiquitously expressed and it is overexpressed in many cancers, including breast, brain, ovarian, lung, and pancreatic (*121-125*). Tumors rely heavily on a constant supply of glucose for metabolism and growth; therefore, the cell needs glucose transporters at the surface to outcompete normal cells for access to extracellular glucose. This increased glucose uptake by cancer cells is useful for imaging and staging tumors with positron emission tomography (PET). Using ^{18}F-labeled glucose (2-[^{18}F]-2-deoxy-D-glucose or 2FDG) as a substrate for GLUT1, doctors can visualize where 2FDG accumulates in the body in real time as an indication of where tumors are located (*126, 127*). Elevated expression of GLUT1 correlates with poor survival in most solid tumors (*128*). Paired with the fact that transport of glucose is a rate limiting step for cancer cells to consume glucose, the association of GLUT1 expression levels with poor prognosis make the protein an attractive drug target for solid tumors. Studies have looked at several ways of inhibiting GLUT1 including decreasing mRNA and/or protein and inhibiting or altering its transporter function (*129*). While GLUT1 inhibition methods have been researched extensively *in silico* and *in vitro*, there have been far fewer *in vivo* studies. The small molecule inhibitor WZB117 was shown to suppress tumor growth

and inhibit the tumor-initiating capacity of cancer stem cells in mice transplanted with human tumor cells. Another GLUT1 inhibitor, STF-31, delayed tumor growth in renal cell carcinoma xenografts (*130-132*). Overall, targeting GLUT1 for cancer therapeutic purposes is promising, but translation to the clinic is not imminent.

1.5 TXNIP and the ARRDC family in trafficking regulation

TXNIP is one of six members of the mammalian arrestin-domain-containing (ARRDC) or α-arrestin family of proteins, which were identified as part of the larger arrestin family of proteins in 2008 when Alvarez et. al. re-evaluated the phylogeny of the arrestins and identified new additions to the family. The α-arrestins are more ancient in comparison to the visual/β-arrestins and can be found in fungi, worms, budding yeast, and protists (*133*). β-arrestins are more studied than the ARRDCs and are known to act as trafficking adaptors that bind to cargo proteins and interact with AP-2 and clathrin in order to promote cargo turnover (*134*). In contrast, cellular functions for ARRDCs are still being discovered.

1.5.1 Structure and function of TXNIP

The defining structural features of the arrestin family are N- and C-terminal arrestin-fold domains, each of which contains seven anti-parallel beta sheets (*135*). TXNIP is a 391-residue protein and has an arrestin domain spanning from residues 7-301. The C-terminal end of TXNIP has two PY motifs at Pro331 and Pro375 and a clathrin-binding motif at Pro350. The crystal structure of TXNIP has been determined in pieces, each revealing more about the structure-function relationship of TXNIP. The first structure determined showed the N-terminal domain of TXNIP. This structure revealed that TXNIP has the β-arrestin folds characteristic of the family, but is structurally more similar to the VPS26 branch of the arrestin family as opposed to the β-arrestins (*136*). Next, the N- and C-terminal arrestin domains were determined in complex with thioredoxin (TRX). This structure revealed that TXNIP binding to TRX requires a structural rearrangement in which a disulphide bond within the protein changes from Cys63-Cys247 to Cys63-Cys190. There is also a new disulphide bond formed with TRX between TXNIP Cys247 and TRX Cys32 (*137*). Hwang et. al. also demonstrated that the TXNIP-TRX disulphide bond is dissolved in the presence of high concentrations of

reactive oxygen species (ROS), which is consistent with the role TXNIP plays as a negative regulator of the antioxidative activity of TRX. Finally, the two PY motifs on the C-terminal tail were shown in complex with the WW domains of the E3 ubiquitin ligase Itch (*136-138*) **(Figure 1.6)**. This study revealed that the four WW domains of Itch each have different binding affinities for TXNIP but there was strong binding avidity when all the WW domains had multivalent interactions with the two PY motifs of TXNIP (*138*).

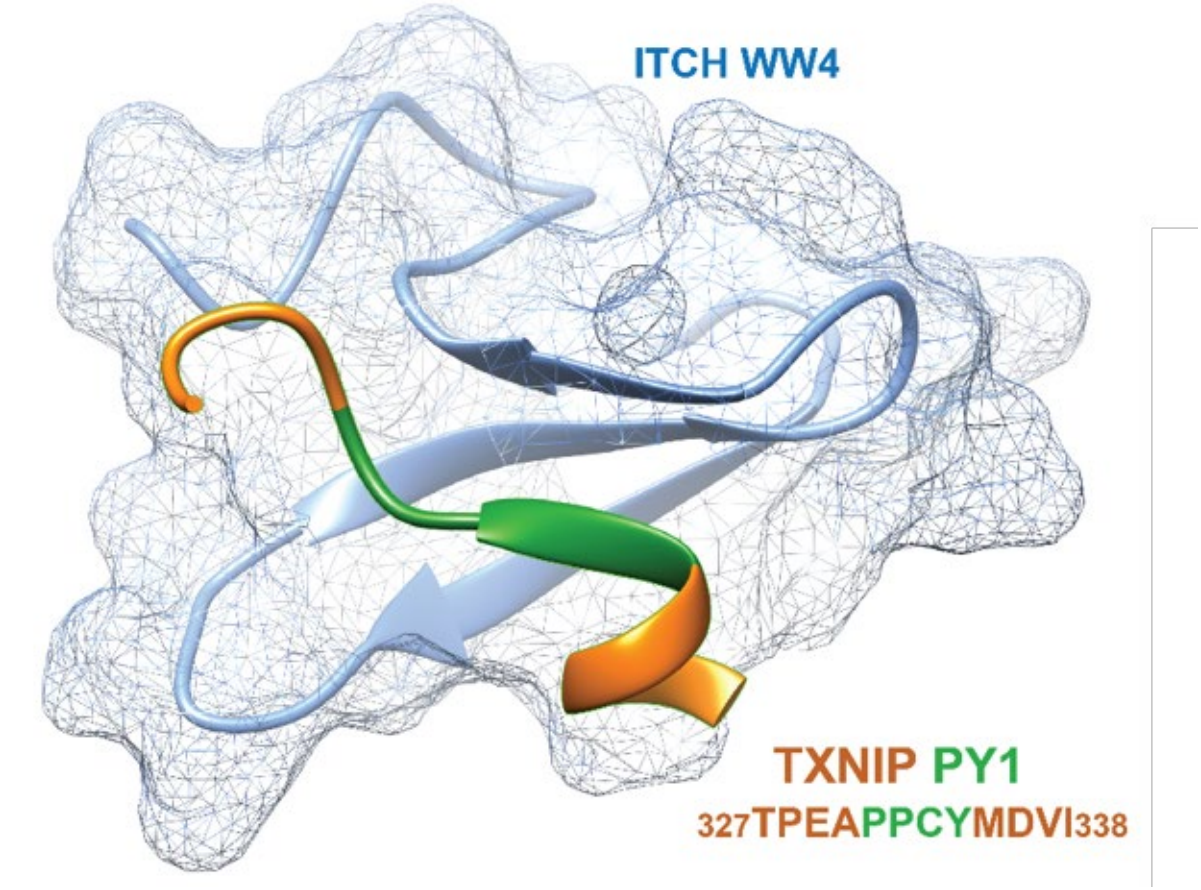

Figure1.6: Structure of a PY motif motif of TXNIP interacting with the WW domains of E3 ubiquitin ligase, Itch.

TXNIP was first discovered to regulate the redox system by inhibiting the antioxidative activity of TRX (*139*), but observations of its increased expression stimulated by glucose suggested a role in metabolism (*140, 141*). It was subsequently found that TXNIP can inhibit glucose uptake independent of TRX binding and many metabolic functions were due to the arrestin domains rather than its redox function (*142*). After finding that TXNIP expression was strongly induced in pancreatic islet cells in response to increased glucose (*143*), it was discovered that TXNIP plays a key part in regulation of pancreatic β-cells. Elevated levels of glucose have damaging effects on the pancreas, leading to β-cells becoming dysfunctional (*144, 145*). Under these hyperglycemic conditions, TXNIP induces β-cell apoptosis by activating the mitochondrial death pathway via activation of apoptosis signal-regulating kinase 1 (ASK1) (*146*). Under oxidative stress, TXNIP is shuttled from the cytosol and nucleus to the mitochondria where ASK1 kinase activity is inhibited by mitochondrial thioredoxin (Trx2). When TXNIP is shuttled in, it competes with ASK1 for binding to Trx2. This releases ASK1 and allows the β-cell apoptosis signaling cascade to be initiated (*146-148*).

Other major functions of TXNIP include regulating glucose and reducing insulin sensitivity in peripheral tissues(*101, 149, 150*). When overexpressed in mice, TXNIP suppresses glucose-induced insulin secretion, suggesting it may serve as a negative feedback regulator to prevent excess glucose uptake into cells (*151*). TXNIP's regulation of glucose transport is a major topic in this dissertation.

1.5.2 TXNIP in trafficking regulation

TXNIP exerts its control over glucose uptake by regulating glucose transporters GLUT1 and GLUT4. In 2013, it was found that TXNIP negatively regulates GLUT1 both directly and indirectly (*102*). Indirectly, Wu et. al. observed that TXNIP shRNA knockdown in human liver cell line, HepG2, resulted in increased levels of GLUT1 mRNA. This increase in GLUT1 mRNA could be suppressed by reintroducing TXNIP. While this affects GLUT1 protein levels on a longer time scale, TXNIP was found to directly regulate GLUT1 by promoting its endocytosis to suppress glucose uptake. These two modes of regulation are part of a negative feedback loop in which increased glucose uptake leads to inhibition of further glucose uptake. Due to high levels of glucose metabolites in the cell, transcription factors ChREBP and Mlx are activated and drive the transcription of TXNIP (*152*). The increase in TXNIP in turn downregulates

GLUT1 at the cell surface, and therefore decreases glucose uptake. Wu et. al. used total internal reflection fluorescence (TIRF) to show GFP-TXNIP localize at the PM as “dynamic speckles”, appearing and then disappearing from the cell surface. They postulate that this, in combination with TXNIP’s colocalization with clathrin-coated pit marker, clathrin light chain (CLC), and an endocytic marker, transferrin, indicates TXNIP is involved in endocytosis of PM proteins. They also mutated a di-leucine motif (Leu351 and Leu352) on TXNIP that likely serves as a clathrin binding site and observed a loss of colocalization with CCP markers (*102*). shRNA knockdown of TXNIP caused an increase in GLUT1 protein levels and TXNIP coprecipitated GLUT1 (and vice versa). TXNIP has a phosphorylation site at Ser308 that promotes its degradation. This degradation is coordinated via the PY motifs of TXNIP binding to the WW domains of E3 ligase Itch (*153*). When the PY motifs on TXNIP were mutated, the degradation of TXNIP was blocked. They also showed that overexpression of TXNIP led to a faster rate of GLUT1 endocytosis in comparison to control or the clathrin-binding mutant TXNIP (*102*). This study demonstrated a clear role for TXNIP in negative regulation of GLUT1, likely by promoting endocytosis of GLUT1 from the PM.

GLUT4 is also regulated by TXNIP. When various cell lines are induced with growth factors, TXNIP is phosphorylated by protein kinase B (Akt) (*154*). In a mouse adipocyte cell line (3T3-L1), insulin stimulation led to phosphorylation of TXNIP and a subsequent increase in glucose uptake. This glucose uptake could be suppressed with an AKT inhibitor or mutation of the phosphorylation site on TXNIP (Ser308Ala) (*154*). Waldhart et. al. showed an increased rate of GLUT4 endocytosis in 3T3-L1 cells when TXNIP was expressed. They also showed that TXNIP KO mice had higher levels of adipose tissue and skeletal muscle ^{18}FDG absorption in comparison to WT animals, despite having the same level of GLUT4 expression. The TXNIP KO mice were hypoglycemic with decreased glucose uptake in the liver to leave more glucose available for other organs (*154*). The lack of TXNIP results in higher basal levels of GLUT4 and therefore excessive glucose uptake that leads to hypoglycemia.

1.6 Summary of thesis

The work presented in this thesis outlines the response of GLUT1 to shifts in glucose availability and how the lysosomal trafficking of GLUT1 is regulated by ubiquitin and TXNIP. In **Chapter 3** I establish that GLUT1 localizes to late endocytic and lysosomal compartments in response to increased glucose. I also show that the clathrin-binding and E3 ligase-binding PY motifs on TXNIP play a vital role in the trafficking of GLUT1. Further, I demonstrate that GLUT1 is ubiquitylated on its major cytoplasmic loop, and loss of the cytoplasmic lysine residues interferes with proper trafficking of GLUT1. In **Chapter 4,** I present a SILAC-based TXNIP interaction profile, demonstrate additional post-translational modifications on GLUT1, and further characterize the factors involved in negative regulation of GLUT1. In **Chapter 5,** I provide insight and discussion of the vital role GLUT1 trafficking regulation plays in maintaining glucose homeostasis, the necessary components required to maintain proper regulation of GLUT1 that remain unidentified, and how targeting the machinery involved in this GLUT1 trafficking may lead to therapeutic progress for GLUT1-associated diseases such as GLUT1-DS and cancer.

Chapter 2

Materials and Methods

2.1 Experimental model and subject details

HeLa cells (Female), MDA-MB-231 cells (Female), and HEK293T (Female) cells were purchased from American Type Culture Collection (ATCC). HeLa and HEK293T cell lines were cultured in DMEM with 10% FBS and 1% penicillin/streptomycin at 37^{o}C in 5% CO_2. MDA-MB-231 cells were cultured in RPMI with 10% FBS and 1% penicillin/streptomycin at 37^{o}C in 5% CO_2. Cells stably expressing GLUT1-GFP (WT, $1K_{245}$-->R,$11K_{cyto}$-->R, $6K_{loop}$-->R, $5K_{tails}$-->R, 1K245), GLUT1-FLAG, FLAG-Ub, $FLAG_{EXOFACIAL}$-GLUT1, and GFP-GLUT1 were generated using the Retro-X vectors pQCXIP and pQCXIN (Clontech) retroviral vector system. Cells stably expressing TXNIP (WT, cb, py) and DN VPS4-HA were generated using lentiviral packaging plasmids pMD2 and Pax2 along with the pInducer20 vector. The HeLa *txnip* knockout cells were generated using the CRISPR/Cas-9 editing system.

2.2 Methods details

2.2.1 Assays for visualizing GLUT1

GLUT1 trafficking colocalization imaging assays: Cells were split onto 25 mm glass coverslips (or glass bottom dishes for live imaging in regular) high glucose media. Cells were switched to no glucose media for 24 hours and then switched to the appropriate glucose concentration. At the indicated time point, cells were fixed in 4% PFA for 10 minutes or washed with PBS and prepared for live imaging

Cell surface protein biotinylation: Biotinylation protocol was adapted from Singh et. al. (*155*). HeLa cells were washed twice with cold $DPBS^{+}$ then incubated with gentle rocking at 4^{o}C with 0.5 mg/ml EZ-Link NHS-SS-Biotin (Thermo Scientific) twice for 20 minutes. Biotin was quenched with five 5-minute washes with cold 100 mM glycine, 0.2% BSA in PBS. Cells were washed twice with cold $DPBS^{+}$ and then lysed with lysis buffer (50 mM Tris/HCl pH7.4, 150 mM NaCl, 1 mM EDTA, 1% Triton X-100, protease

inhibitor tablet). Lysates were rotated at 4^{O}C for an hour and then centrifuged for 15 minutes at 4^{o}C, 16,000 x g. 1 mg of protein lysate was incubated overnight with NeutrAvidin UltraLink beads (Thermo Scientific) at 4^{o}C. Beads were washed once with cold lysis buffer, three times with cold lysis buffer without Triton X-100 and once with cold 0.1% Triton X-100, 350 mM NaCl, 5 mM EDTA. Biotinylated proteins were eluted from the beads by heating for 10 minutes at 70^{o}C in Laemmli sample buffer (Bio-Rad). Input samples and eluates were analyzed by immunoblot.

2.2.2 Transfections

Plasmid transfections were performed using Lipojet (SignaGen, SL100468) and Lipofectamine LTX with PLUS reagent (Thermo Fisher, 15338100) according to manufacturer's protocol.

2.2.3 Cloning

All GLUT1 plasmids were subcloned into modified pQCXIP vectors from glut1 cDNA (Transomic). Mutations were introduced via geneblocks (IDT) or primer amplification. The inducible TXNIP vector was generated using Gateway cloning with the pENTR1A donor vector and the pInducer20 destination vector. The txnip cDNA was purchased from Transomic. The E228Q VPS4 was constructed with geneblocks (IDT) cloned into the pINDUCER20, using the same Gateway method as described for TXNIP vectors.

2.2.4 CRISPR/Cas9 gene deletion of txnip

CRISPR/Cas9 txnip knockout plasmids were purchased from Santa Cruz Biotechnologies. HeLa cells were electroporated with the KO plasmids and a Cas9-NLS plasmid twice then single cells were sorted into 96 well plates. KO clones were screened by Western blot and PCR. The diagnostic primers used were: 5'GGAGGGTGAAAGCTGATTAG and 5'CACATGCTCACTGCACATTG.

2.2.5 Fluorescence Microscopy

All microscopy images were acquired using the DeltaVison Elite System (GE Healthcare) and processed using SoftWoRx software. Pearson Correlation Coefficient was measured using SoftWorx or the JACoP (BIOP version) FIJI plugin. Alternate colocalization for data in **Fig1G** was determined using a FIJI macro (https://github.com/dsrichardson/fiji_macros/blob/master/2D_object_colocalization). The

macro identifies the center of mass of each vesicle (6 pixels in size) in the GFP channel then determines the nearest neighbor in the AF-594 channel. Centers of mass less that the average diameter were considered colocalized.

Live Cell Imaging: When doing live cell imaging, cells were plated onto glass bottom dishes and switched to media without phenol red for imaging. For FM4-64 staining of the plasma membrane, cells were washed with ice cold PBS and kept on ice. 8 mM FM4-64 was diluted 1:1000 in ice cold HBSS and added to cells 5 minutes before imaging. For LysoTracker imaging, LysoTracker Deep Red (Thermo Fisher) was diluted to 50nM in culture media and cells were incubated with the dye for 2 hours at 37^{o}C. Cells were then washed with PBS and switched to phenol red-free DMEM media for imaging.

Fixed cell immunofluorescence: Cells were seeded on glass coverslips and fixed when they reached ~50% confluency with 4% paraformaldehyde for 10 minutes at room temperature and washed with PBS three times. Cells were permeabilized and blocked with 10% Normal Donkey Serum (Jackson Immunoresearch), 0.1% saponin in PBS then incubated with primary antibody for 1-2 hours at room temperature in 1% NGS, 0.05% Tween-20, PBS. Cells were then washed 3 times with1% NDS 0.05% Tween-20 in PBS and incubated with Alexa Fluor- conjugated secondary antibody at room temperature for 1 hour. After washing, coverslips were mounted with ProLong Diamond mountant with DAPI (ThermoFisher).

2.2.6 Immunoblots and co-immunoprecipitation

Cells were collected in lysis buffer (50 mM Tris-HCl, 150 mM NaCl, 5 mM EDTA, 1% NP-40, 20 mM MG132, 1 mM PMSF, 10 mM Iodoacetamide, 1 mM 1,10-Phenanthroline monohydrate, Roche Complete protease Inhibitor tablets, Roche Phos-Stop phosphatase inhibitor tablets) and centrifuged to isolate protein. Protein concentration was measured using Bradford Assay and a 1 mg/ml protein solution was made. For Ub co-immunoprecipitation experiments, cells were transiently transfected with HA-Ub plasmid 24hours before lysing. 1 ml of 1 mg/ml solution was added to a-FLAG magnetic beads (Sigma). For whole cell lysates, Laemmli buffer was added and samples were put at 65^{o}C for 10 minutes. Co-IPs were incubated at 4^{o}C for 1 hour with rotation, washed 3 times with wash buffer (25 mM Tris pH 7.5, 2.5% glycerol, 150 mM NaCl), and eluted by

incubation with FLAG peptide for 30 minutes at 4°C twice. Protein samples were run on 12% polyacrylamide gels, transferred onto PVDF membrane, and imaged after antibody incubation on the LiCor Odyssey CLx Infrared imager.

2.2.7 SILAC-based quantitative proteomic analysis

Quantitative mass spectrometry analysis by SILAC was performed on MDA-MB-231 cells stably expressing the indicated FLAG-tagged substrate. These cells were cultured in the presence of either heavy or light isotypes (lysine and arginine, Sigma-Aldrich) for at least 6 doublings to ensure incorporation of these isotopes into 100% of the proteome. Affinity purification was performed as previously described (*156*). Eluted proteins were digested with 1 μg Trypsin Gold (Promega) at 37°C overnight. Digested peptides were cleaned up on a Sep-Pak C18 column. Purified peptides were then dried, reconstituted in 0.1% trifluoroacetic acid, and analyzed by LC-MS/MS using an Orbitrap XL mass spectrometer. Database search and SILAC quantitation were performed using MaxQuant software.

2.3. Quantification and statistical analysis

2.3.1 Quantification

Pearson's Coefficient of Correlation measurements: When determining the colocalization, at least 20 cells from 3 different images were measured for each condition using either Softworx software or the JACoP (BIOP version) plugin for FIJI. The mean Pearson's coefficient and standard deviation are represented in the quantifications shown.

Immunoblot quantification of GLUT1 biotinylation: Details of the quantification and normalization can be found in the statistical reporting document for Fig 1SD. For each time point, FIJI was used to quantify the whole lane for both the input and IP samples. Next, the IP measurement was divided by the input measurement. To normalize, the [IP/input] values for each time point were divided by the T=0 [IP/ input] value. This was done for at least 3 biological replicates and presented in Figures 1B and 1SD with means and standard deviations.

Quantification of FLAG co-immunoprecipitations (GLUT1-FLAG and FLAG-Ub): Details of the quantification and normalization can be found in the statistical reporting document for Figures 5E-I. The entirety of each input and eluate/IP lane was measured for all a-FLAG, α-Ubiquitun, and α-GLUT1 immunoblots using FIJI. The measurement for the protein of interest (POI) (GLUT1 or HA-Ub) was then divided by the corresponding FLAG measurement. To normalize, each "Eluate POI/FLAG" was divided by the "POI/FLAG" of the control condition (e.g.in Fig5e, all eluate conditions are divided by the no glucose "GLUT1/FLAG-Ub" measurement). This was done for at least 3 biological replicates and presented in Figures 3.5E,G,I with means and standard deviations.

2.3.2 Statistical Analysis

Detailed statistical analysis can be found in the accompanying Statistical Reporting Document. For each statistical analysis, a Student's t test was used to test for a statistically significant difference between the means of the two variables of interest. The alpha value for each experiment was set at 0.05 and a *p* value was calculated using the Student's t test function in Microsoft Excel to determine statistical significance. All quantified western blot and colocalization data are the mean of the indicated number of independent experiments. Each coIP and biotinylation figure with statistical analysis represents n ≥ 3 where n represents biological replicates. For quantification of all microscopy-based experiments, n ≥ 20 where n represents single cells. For all figures with statistics, error bars represent standard deviation from the mean. Details of statistical analysis for specific experiments can be found in the figure legends.

For statistical analysis in Chapter 4, the spreadsheet can be found here: https://docs.google.com/spreadsheets/d/e/2PACX-1vRhGSQFGiSTDTjkaicBMotSwIoXVnKSiaT49r_qY0Sh8VOghMnUcRadnIzvFNaQZ-86BATz-PZRsMzD/pubhtml

2.4 Key resources table

REAGENT or RESOURCE	SOURCE	IDENTIFIER
Antibodies		
CD63 antibody [MEM-259]	abcam	Abcam Cat# ab8219, RRID:AB_306364
VPS35 antibody	abcam	Abcam Cat# ab10099, RRID:AB_296841
Glucose Transporter GLUT1 antibody [EPR3915]	abcam	Abcam Cat# ab115730, RRID:AB_10903230
Rabbit Anti-Sodium Potassium ATPase Monoclonal Antibody, Unconjugated, Clone EP1845Y	abcam	Abcam Cat# ab76020, RRID:AB_1310695
EEA1	BD Biosciences	BD Biosciences Cat# 610457, RRID:AB_397830
VPS4A Antibody (A-11)	Santa Cruz Biotechnology	Santa Cruz Biotechnology Cat# sc-393428, RRID:AB_2773025
WWP1 monoclonal antibody (M01A), clone 1A7	Abnova	Abnova Cat# H00011059-M01A, RRID:AB_1717151
GLUT1 antibody	Proteintech	Proteintech Cat# 21829-1-AP, RRID:AB_10837075
Rabbit Anti-NEDD4L Polyclonal Antibody, Unconjugated	Cell Signaling Technology	Cell Signaling Technology Cat# 4013, RRID:AB_1904063
EEA1 (C45B10) Rabbit mAb	Cell Signaling Technology	Cell Signaling Technology Cat# 3288, RRID:AB_2096811
Purified Mouse Anti-LBPA (BMP)	Echelon Biosciences	Echelon Biosciences Cat# Z-PLBPA, RRID:AB_11129226
Rabbit Anti-GAPDH Monoclonal Antibody, Unconjugated, Clone 14C10	Cell Signaling Technology	Cell Signaling Technology Cat# 2118, RRID:AB_561053
Monoclonal ANTI-FLAG® M2 antibody produced in mouse	Millipore	Cat #: F1804; RRID:AB_262044
Mouse anti-Tubulin	Vanderbilt Antibody and Protein Resource Core	N/A
Mouse anti-HA	Vanderbilt Antibody and Protein Resource Core	N/A

DYKDDDDK Tag Polyclonal Antibody	ThermoScientific	Cat #: PA1-984B RRID: AB_347227
Chemicals, Peptides, and Recombinant Proteins		
MG-132	APExBIO	Cat# A2585
3-O-methyl-d-glucopyranose	Millipore Sigma	Cat# M4879
EZ-Link NHS-SS-Biotin	Thermo Fisher	Cat# 21331
Phenanthroline	Sigma-Aldrich	Cat# P9375
Iodoacetamide	Sigma-Aldrich	I1149
WWP1 Active human recombinant, expressed in baculovirus infected insect cells	Sigma-Aldrich	Cat# SRP0229
Recombinant Human Usp2 Catalytic Domain	Boston Biochem	Cat# E-504
PNGase F	Promega	V483A
recombinant Shrimp Alkaline Phosphatase	New England BioLabs	Cat# M0371S
Experimental Models: Cell Lines		
Human cells: MDA-MB-231 cells	ATCC	Cat #: MDA-MB-231 (ATCC® HTB-26); RRID:CVCL_0062
Human cells: HEK293T cells	ATCC	Cat# CRL-3216 RRID: CVCL_0063
Human cells: HeLa cells	ATCC	Cat# CCL-2 RRID: CVCL_0030
Human cells: MDA-MB-231 cells stably expressing GLUT1-GFP	This study	N/A
Human cells: HEK293T cells stably expressing FLAG-Ub	This study	N/A
Human cells: HeLa cells stably expressing GLUT1-GFP (WT, $1K_{245}$-->R,$11K_{cyto}$-->R, $6K_{loop}$-->R, $5K_{tails}$-->R, 1K245)	This study	N/A
Human cells: HeLa cells stably expressing GLUT1-FLAG	This study	N/A
Human cells: HeLa cells stably expressing $FLAG_{exofacial}$-GLUT1	This study	N/A
Human cells: HeLa cells stably expressing GFP-GLUT1	This study	N/A

Human cells: HeLa cells stably expressing GLUT1-GFP + TXNIP (WT, cb, py)	This study	N/A
Human cells: HeLa cells stably expressing GLUT1-FLAG + TXNIP (WT, cb, py)		N/A
Oligonucleotides		
ojam5373- txnip KO diagnostic primer (F), GGAGGGTGAAAGCTGATTAG	This study	N/A
ojam5374- txnip KO diagnostic primer (R), CACATGCTCACTGCACATTG	This study	N/A
Recombinant DNA		
pQCXIN	ClonTech	Cat# 631514
pENTR1A	addgene	Cat# 17398 RRID: Addgene_17398
pInducer20	addgene	Cat# 44012 RRID: Addgene_4401
pRK5-HA-Ubiquitin-WT	addgene	Cat# 17608 RRID: Addgene_17608
WT FLAG-WWP1	Neilsen, C.P. et. al.	
4ww FLAG-WWP1 (W377F, P380A, W409F, P412A, W484F, P487A, F524A, P527A)	Neilsen, C.P. et. al.	N/A
WT WWP1	this study	N/A
WT Nedd4L	this study	N/A
WT TXNIP	this study	N/A
$TXNIP_{cb}$	this study	N/A
$TXNIP_{py}$	this study	N/A
WT TXNIP-FLAG	this study	N/A
$TXNIP_{py}$-FLAG	this study	N/A
WT GLUT1-GFP	this study	N/A
WT GLUT1-FLAG	this study	N/A
WT $FLAG_{exofacial}$-GLUT1	this study	N/A
HA-VPS4A-E228Q	this study	N/A
$1K_{245}$-->R GLUT1-GFP	this study	N/A
$11K_{cyto}$-->R GLUT1-GFP	this study	N/A
1K245 GLUT1-GFP	this study	N/A
$6K_{loop}$-->R GLUT1-GFP	this study	N/A
$5K_{tails}$-->R GLUT1-GFP	this study	N/A
VDUP1 CRISPR/Cas9 KO plasmid (h)	Santa Cruz Biotechnology	Cat# sc-400664
Software and Algorithms		

Softworx	GE	SCR_019157
MaxQuant	Max Planck Institute of Biochemistry	SCR_014485
FIJI	NIH	SCR_002285
Image Studio Lite software	LICORE	SCR_013715

2.5 Plasmid used in the study

Designation	Backbone	Description	Source
pQCXIP	--	Retroviral vector for constitutive ORF expression in mammalian cells with puromycin resistance gene	ClonTech
pQCXIN	--	Retroviral vector for constitutive ORF expression in mammalian cells with neomycin resistance gene	ClonTech
pENTR1A	--	Gateway entry vector	addgene
pInducer20	--	Gateway destination vector.Tet-inducible lentiviral vector for ORF expression in mammalian cells	addgene
pRK5-HA	--	Mammalian expression plasmid	addgene
WT TXNIP	pInducer20	Inducible WT TXNIP	This study
$TXNIP_{cb}$	pInducer20	Inducible TXNIP clathrin-binding mutant	This study
$TXNIP_{py}$	pInducer20	Inducible TXNIP PY motif mutant	This study
WT TXNIP-FLAG	pQCXIN	WT TXNIP with C-terminal 3xFLAG tag	This study
$TXNIP_{py}$-FLAG	pQCXIN	TXNIP PY motif mutant with C-terminal 3xFLAG tag	This study
WT GLUT1-GFP	pQCXIP	WT GLUT1 with a C-terminal GFP tag	This study
WT GLUT1-FLAG	pQCXIP	WT GLUT1 with a C-terminal 3xFLAG tag	This study
WT FLAG-GLUT1	pQCXIP	WT GLUT1 with a FLAG tag on the first exofacial loop	This study
$1K_{245}$→R GLUT1-GFP	pQCXIP	$1K_{245}$→R GLUT1 mutant with C-terminal GFP tag	This study
$11K_{cyto}$→R GLUT1-GFP	pQCXIP	$11K_{cyto}$→R GLUT1 mutant with C-terminal GFP tag	This study
1K245 GLUT1-GFP	pQCXIP	1K245 GLUT1 mutant with C-terminal GFP tag	This study
$6K_{loop}$→R GLUT1-GFP	pQCXIP	$6K_{loop}$→R GLUT1 mutant with C-terminal GFP tag	This study
$5K_{tails}$→R GLUT1-GFP	pQCXIP	$5K_{tails}$→R GLUT1 mutant with C-terminal GFP tag	This study
HA-Ub	pRK5-HA	Ubiquitin with an N-terminal HA tag	addgene
WT FLAG-WWP1	pQCXIP	WT WWP1 with an N-terminal 3xFLAG tag	Neilsen, C.P. et. al.
4ww FLAG-WWP1	pQCXIP	WWP1 with all 4 WW domains mutated, with a N-terminal 3xFLAG tag	Neilsen, C.P. et. al.
WT WWP1	pQCXIN	WT untagged WWP1	This study
WT Nedd4L	pQCXIN	WT untagged Nedd4L	This study
$Vps4A^{E228Q}$-HA	pInducer20	3xHA-VPS4A with E228Q DN mutation in dox-inducible vector	This study

Chapter 3

Lysosomal trafficking of the glucose transporter GLUT1 requires sequential regulation by TXNIP and ubiquitin

A paper published in *iScience* (2023)

Susan J. Qualls-Histed [1], Casey P. Nielsen[1] and Jason A. MacGurn [1] *

[1] Department of Cell and Developmental Biology, Vanderbilt University, Nashville, TN, 37240, United States

*Address correspondence to Jason A. MacGurn; email: jason.a.macgurn@vanderbilt.edu

3.1 Abstract

Glucose transporters are principal gatekeepers of cellular glucose metabolism. Understanding mechanisms that regulate their activity, trafficking, and degradation can provide insight into physiological regulation of glucose homeostasis and diseases that arise from dysregulation of glucose transport. Glucose is known to stimulate endocytic clearance of the human glucose transporter GLUT1, but once internalized the mechanisms that regulate its trafficking itineraries are not well understood. Here, we report that increased glucose availability triggers lysosomal trafficking of GLUT1 in HeLa cells, with a subpopulation of GLUT1 routed through ESCRT-associated late endosomal compartments. This itinerary requires the arrestin-like protein TXNIP, which interacts with both clathrin and E3 ubiquitin ligases to promote GLUT1 lysosomal trafficking. We also find that glucose stimulates GLUT1 ubiquitylation, which in turn promotes GLUT1 lysosomal trafficking. Our results suggest excess glucose first stimulates TXNIP-mediated endocytosis of GLUT1 and, subsequently, ubiquitylation to promote trafficking to the lysosome. Our findings underscore how complex coordination of multiple regulators is required for fine tuning of GLUT1 stability at the cell surface.

3.2 Introduction

Glucose transporters at the plasma membrane (PM) regulate the uptake of extracellular glucose and thus can be regarded as principal gatekeepers of cellular metabolism. In mammalian cells, two transporter families are responsible for glucose uptake: the facilitative glucose transporters, or GLUTs, and the sodium-glucose co-transporters, or SGLTs. SGLTs couple glucose uptake with sodium transport in order to drive import against a concentration gradient. Whereas SGLTs primarily function in absorption and resorption of glucose in specific tissues (*157*), GLUTs are widely expressed in diverse cell types where they facilitate diffusion of glucose into cells down a concentration gradient (*2*). The human genome encodes 14 GLUTs, which are part of the major facilitator superfamily (*16, 158*) and have a conserved topology consisting of 12 transmembrane domains, short N- and C-terminal cytosolic tails, and a large cytosolic loop between TM6 and TM7 (which we refer to as the “major cytosolic loop”). Some GLUT family members exhibit tissue-specific expression (e.g., GLUT2 in the liver and intestinal epithelia) while some are broadly expressed (e.g., GLUT1) (*16, 159*). While structures and transport mechanisms have been well-characterized for a few GLUTs (*18, 19*) very little is known about their regulation in a cellular context. One exception is GLUT4, the primary insulin-responsive glucose transporter operating in peripheral tissues, which undergoes regulated trafficking and secretion in response to insulin signaling by well-characterized mechanisms (*13, 160*). By contrast, far less is known about regulation of other GLUT family members. For example, GLUT1 is broadly expressed and responsible for basal glucose uptake in many cell types – including pancreatic β-cells (*21, 161, 162*) and endothelial cells at the blood-brain barrier (*163*) -

yet post-translational mechanisms regulating GLUT1 activity, trafficking, and degradation remain poorly characterized.

In erythrocytes and endothelial cells GLUT1 has a Km for glucose transport of around 2 mM (*2*). Since this is below normal blood glucose concentration (~4-5 mM) the abundance of GLUT1 at the cell surface is likely a limiting factor for glucose uptake in many cells and tissues. Previous studies have identified three regulatory events that likely contribute to the PM stability of GLUT1. ***First***, phosphorylation of Ser226 in the major cytosolic loop by PKC was reported to promote GLUT1 PM stability and activity in Xenopus oocytes (*105*). Although the mechanism of positive regulation remains unclear (*164*) this is the only reported cytosolic post-translational modification of GLUT1. ***Second***, GLUT1 interaction with *t*hioredo*x*i*n* *i*nteracting *p*rotein (TXNIP), a member of the *arr*estin *d*omain-*c*ontaining (ARRDC) family of proteins, is reported to regulate its PM stability. Specifically, knocking down *TXNIP* increased steady state levels of GLUT1 in HepG2 cells, and TXNIP co-purified with GLUT1 in a manner that was negatively regulated by AMPK activity (*102*). TXNIP also co-purified with clathrin and subunits of the AP2 clathrin adaptor complex, and GFP-TXNIP co-localized with clathrin assemblies in the PM of HepG2 cells (*102*). ***Third***, the endosomal recycling retromer complex contributes to the PM stability of GLUT1. Specifically, GLUT1 interacts with the PDZ domain of the retromer subunit SNX27 (*97*), and loss of retromer function results in its aberrant trafficking to lysosomes (*97, 165, 166*). Upstream factors that antagonize retromer function – including the RabGAP protein TCB1D5 and the tumor suppressor and phosphatase PTEN – inhibit endosomal recycling of GLUT1 (*100, 167*). Taken together, these findings suggest that GLUT1 is regulated by a complex trafficking itinerary that involves clathrin-mediated endocytosis and endosomal recycling, both of which are potential points of regulation for controlling the abundance of GLUT1 at the

PM. However, several important questions remain: ***(i)*** Is TXNIP-mediated regulation of GLUT1 restricted to clathrin-mediated endocytosis, or does it regulate other sorting or trafficking events after internalization? ***(ii)*** What signals activate endocytosis and regulate endosomal sorting and recycling of GLUT1? ***(iii)*** Can GLUT1 bypass endosomal recycling for sorting and trafficking to alternative destinations such as lysosomes? A key limitation to addressing these questions is a lack of known regulators of GLUT1 trafficking in response to altered glucose availability.

We hypothesized that cells adapt to increased glucose availability by trafficking GLUT1 to lysosomes. To test this, we analyzed GLUT1 trafficking during a glucose shift time course, and we observed a subpopulation of GLUT1 that traffics to lysosomes as cells adapt to increased glucose availability. We further hypothesized that TXNIP and ubiquitin modification plays a role in the regulation of GLUT1 trafficking. However, specific ubiquitin modifications of GLUT1 have not been previously reported. Here, we present evidence that GLUT1 is ubiquitylated in response to glucose stimulation, and we determine that GLUT1 is ubiquitin-modified in its major cytosolic loop. Our results suggest that both TXNIP and ubiquitylation are critical for GLUT1 lysosomal trafficking, but TXNIP is dispensable for GLUT1 ubiquitylation. Based on our data, we propose a model where glucose triggers sequential regulation of GLUT1, first by TXNIP-mediated endocytosis and subsequently by ubiquitin modification of GLUT1 to promote trafficking to lysosomes. By elucidating the regulatory mechanisms that govern GLUT1 endocytic sorting and trafficking, these studies provide new insights into how cells adapt to changing glucose availability.

3.3 Results

3.3.1 Extracellular glucose stimulates GLUT1 endocytic trafficking to lysosomes

To investigate GLUT1 regulation in response to changing glucose availability, we performed surface biotinylation/capture assays to measure surface levels of endogenous GLUT1 in HeLa cells during a glucose shift time course (i.e., shifting from no glucose to 25 mM glucose at t=0). We chose these concentrations to represent physiological extremes, ranging from the glucose replete conditions of peripheral tissues to conditions endothelial cells might encounter during hyperglycemia. This assay revealed significant decline in the levels of surface-localized GLUT1 after 24 hours in high glucose media (**FIG 3.1A-B** and **FIG 3.2A-D**). In contrast, surface levels of the Na^+/K^+ ATPase were unchanged during the glucose shift time course (**FIG 3.1A** and **1C** and **FIG 3.2A-D**). Thus, switching from glucose depleted to glucose replete media triggers surface clearance of GLUT1 over a 24 hour period of adaptation.

To further examine this response to glucose, we performed immunofluorescence detection of GLUT1 in HeLa cells stably expressing mCherry-CaaX, a marker for the plasma membrane (PM). We observed that cells grown in media lacking glucose exhibit a large population of GLUT1 that co-localizes with mCherry-CaaX at the PM and this co-localization is decreased following glucose repletion (**FIG 3.1D-E**). Although mCherry-CaaX localizes primarily to the PM, it also exhibits some localization to internal puncta, which limits its fidelity as a specific marker of the PM. To address this limitation, we used pulse labeling of the lipophilic tracer dye FM4-64 to specifically label the PM. Although this improves specificity of PM labeling, FM4-64 is not fixable and thus must be imaged in live cells (i.e., it is incompatible with immunofluorescence). To accommodate this limitation, we generated HeLa cells stably expressing GLUT1-GFP

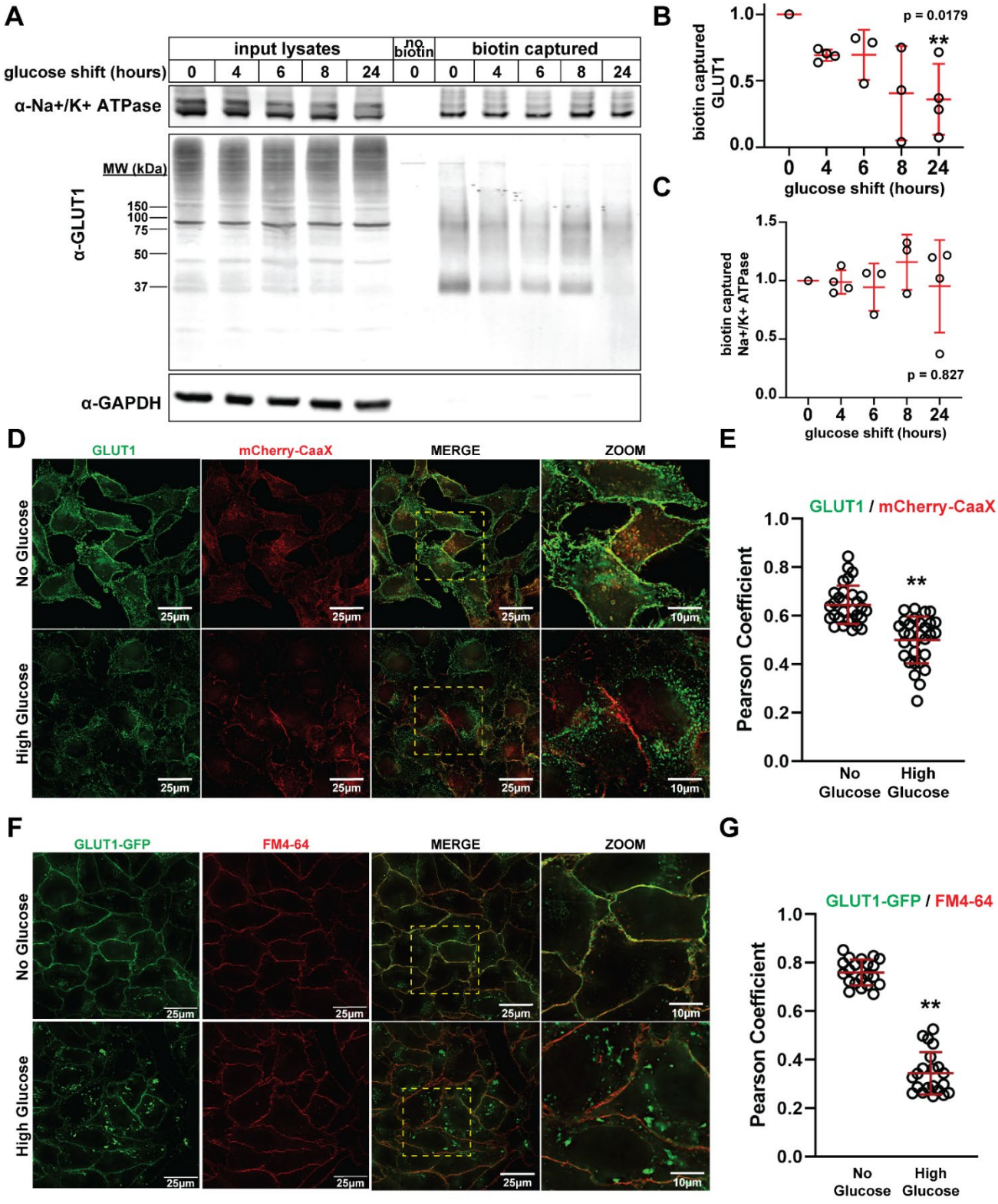

Figure 3.1 Excess glucose availability promotes GLUT1 clearance from the plasma membrane. **(A)** HeLa cells were cultured for 24 hours in media with no glucose, then switched to high glucose media (25mM) for the indicated amount of time. Biotin-labeling (**FIG 3.1** cont'd) was performed at the post-glucose shift time points. Following biotinylation, labeled cells were lysed and affinity purified with NeutrAavidin beads

(Thermo Scientific). Analysis was performed by SDS-PAGE and immunoblot with antibodies that recognize GLUT1, Na^+/K^+ ATPase, and GAPDH. **(B,C)** Quantification of captured GLUT1 **(B)** and Na^+/K^+ ATPase **(C)** for the experiment shown in (A) was performed over multiple biological replicates (n≥3). GLUT1 measurements were taken of the whole lane using FIJI. **(D)** HeLa cells stably expressing mCherry-CaaX were cultured in no glucose media for 24 hours then shifted to high glucose (25 mM) for the indicated time, at which point the samples were fixed for immunofluorescence detection with GLUT1 antibody (green). Zoomed images provided in the far right column correspond to the yellow dashed-line inset boxes to the left **(E)** Quantification of colocalization shown in (D) was measured by Pearson correlation on Softworx software (n=30 cells), $p=3.75x10^{-8}$) **(F)** HeLa cells stably expressing GLUT1-GFP were cultured using the conditions indicated in (D). Prior to imaging, cells were pulse-labelled with FM4-64 (red), a lipophilic tracer dye that inserts into the outer leaflet of the cell membrane. Live cells were incubated on ice in 8 μM cold FM4-64 for ~5 minutes before imaging. Zoomed images provided in the far right column correspond to the yellow dashed-line inset boxes to the left **(G)** Quantification of the results shown in (F). Pearson correlation coefficient was measured using Softworx software (n=30 cells), $p=1.69x10^{-24}$. For all experiments, p-values were computed using a two sample Student's t-Test in Microsoft Excel and data is present as mean +/- SEM.

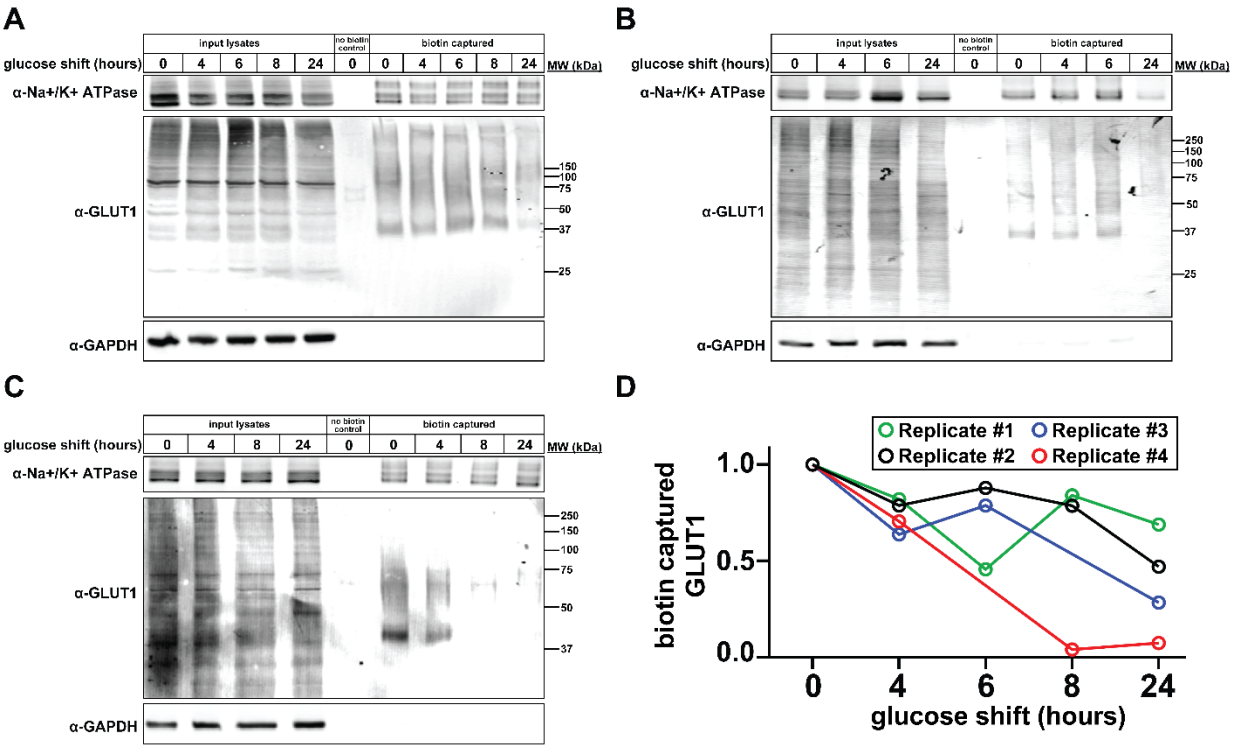

Figure 3.2. Additional evidence for glucose-stimulated clearance of GLUT1 from the plasma membrane using surface biotinylation assays, Related to Figure 3.1. **(A-C)** Biological replicates of the experiment shown in FIG 1A. Quantification of these replicate experiments are depicted in **FIG 3.1B** and **FIG 3.1C**. **(D)** Line graph representation of the results summarized in **FIG 3.1B**, showing the time course quantification of each biological replicate. Measurements were taken for the whole lane using FIJI.

and analyzed its surface localization during glucose adaptation by measuring co-localization with pulsed FM4-64 in live cells. This analysis revealed a significant decrease in co-localization of GLUT1-GFP with FM4-64 as cells adapt to increased glucose availability (**FIG 3.2F-G**). Combined, surface biotinylation assays and analysis of GLUT1 subcellular localization reveal significant internalization of GLUT1 in response to increased glucose availability.

We hypothesized that the glucose-stimulated clearance of GLUT1 from the PM corresponds to endocytosis and trafficking of GLUT1 to lysosomes. To test this, we performed immunofluorescence imaging of GLUT1 in HeLa cells during a glucose repletion time course. This analysis revealed significant internalization of GLUT1 and increasing co-localization with LAMP1, a lysosomal marker, as cells adapt to increased glucose availability (**FIG 3.3A**). We performed similar analysis of HeLa cells stably expressing GLUT1-GFP and similarly observed internalization and co-localization with LAMP1 over the glucose repletion time course (**FIG 3.3B**). Using automated image analysis tools (*168*) we also measured the fraction of total GLUT1-GFP co-localizing with LAMP1. This analysis revealed that in media lacking glucose 11.2% (±7.2) of GLUT1-GFP signal co-localizes with LAMP1, while a shift to high glucose media results in 36.4% (±10.0) of GLUT1-GFP co-localizing with LAMP1 (see Statistical Reporting document for **FIG 3.4B**). Glucose repletion also increased co-localization of GLUT1-GFP with LBPA and Lysotracker, two other markers of late endosomes and lysosomes (**FIG 3.4A-B**). Given the potential for artifacts associated with GFP tagging, particularly at the C-terminus of GLUT1 which harbors a PDZ-binding motif (*87*), we performed similar analysis with an N-terminal GFP-GLUT1 variant and also observed increased

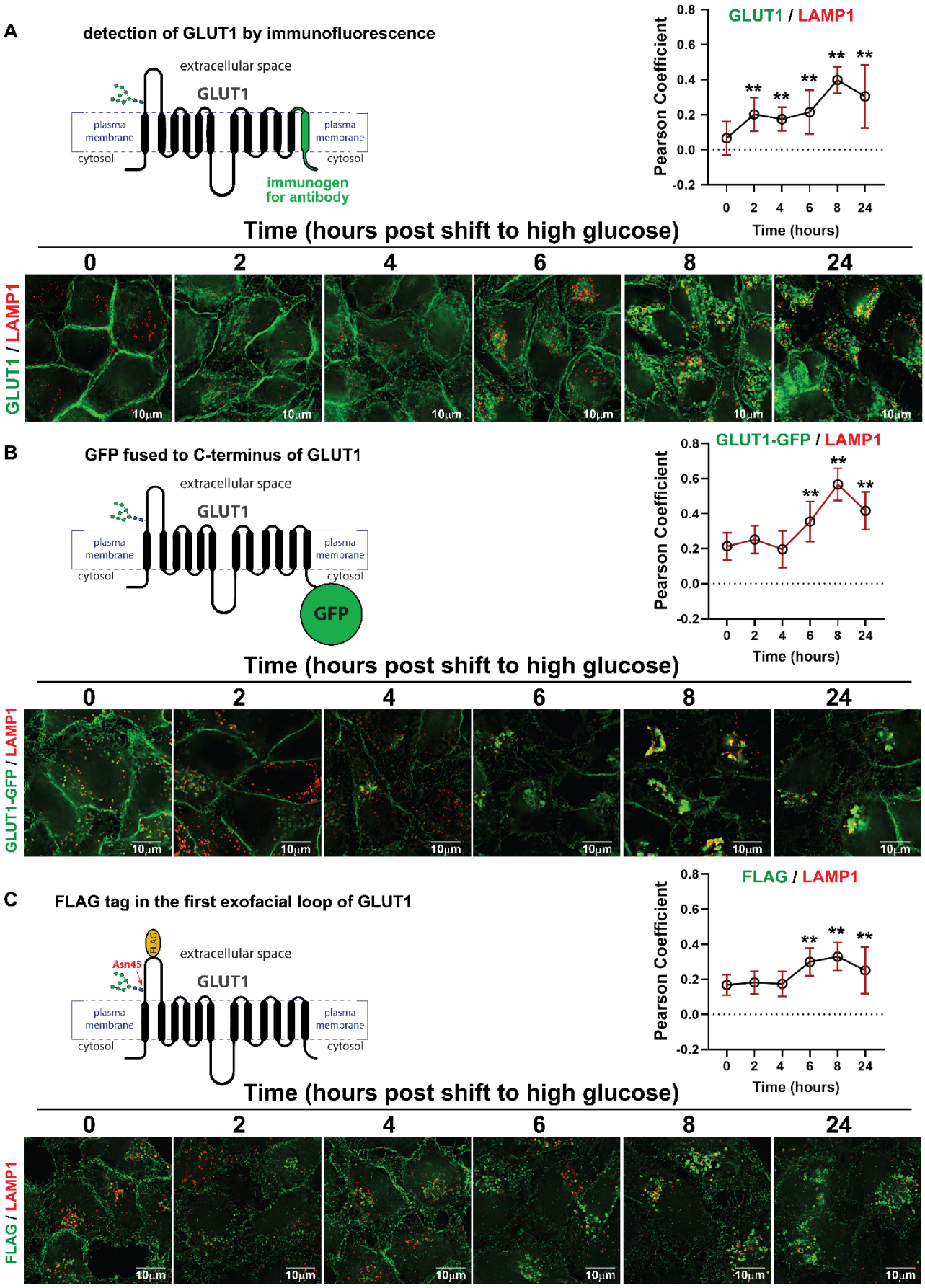
A
detection of GLUT1 by immunofluorescence
extracellular space
GLUT1
plasma membrane
cytosol
immunogen for antibody
GLUT1 / LAMP1
Pearson Coefficient
Time (hours)
Time (hours post shift to high glucose)
0
2
4
6
8
24
GLUT1 / LAMP1
10μm
B
GFP fused to C-terminus of GLUT1
GFP
GLUT1-GFP / LAMP1
C
FLAG tag in the first exofacial loop of GLUT1
Asn45
FLAG
FLAG / LAMP1

Figure 3.3. Glucose-stimulated clearance of GLUT1 results in trafficking to lysosomes. **(A)** Imaging of endogenous GLUT1 was performed in HeLa cells cultured in no glucose media for 24 hours then switched to high glucose media (25 mM) for the indicated time and fixed. Samples were imaged via immunofluorescence and probed with GLUT1 antibody (green) and LAMP1 antibody (red). A schematic of the detection strategy is shown in the top left of the panel. Quantification of colocalization (as measured by Pearson correlation on Softworx software (n=30 cells) is shown in the graph at the top right of the panel.$p < 1x10^{-5}$ **(B)** Imaging of stably expressed GLUT1-GFP was performed in HeLa cells cultured in no glucose media for 24 hours then switched to high glucose media (25 mM) for the indicated time and fixed. Samples were imaged via immunofluorescence and probed with LAMP1 antibody (red). A schematic of the detection strategy is shown in the top left of the panel. Quantification of colocalization as measured by Pearson correlation on Softworx software (n=30 cells) is shown in the graph at the top right of the panel. $p < 1x10^{-6}$ **(C)** Imaging of stably expressed GLUT1-FLAG, which harbors a FLAG tag on its first exofacial loop, was performed in HeLa cells cultured in no glucose media for 24 hours then switched to high glucose media (25 mM) for the indicated time and fixed. Samples were imaged via immunofluorescence and probed with FLAG antibody (green) and LAMP1 antibody (red). A schematic of the detection strategy is shown in the top left of the panel. Quantification of colocalization (as measured by Pearson correlation on Softworx software (n=30 cells) is shown in the graph at the top right of the panel. $p < 0.004$. For all experiments p-values were computed using a two sample Student's t-Test in Microsoft Excel and data is present as mean +/- SEM.

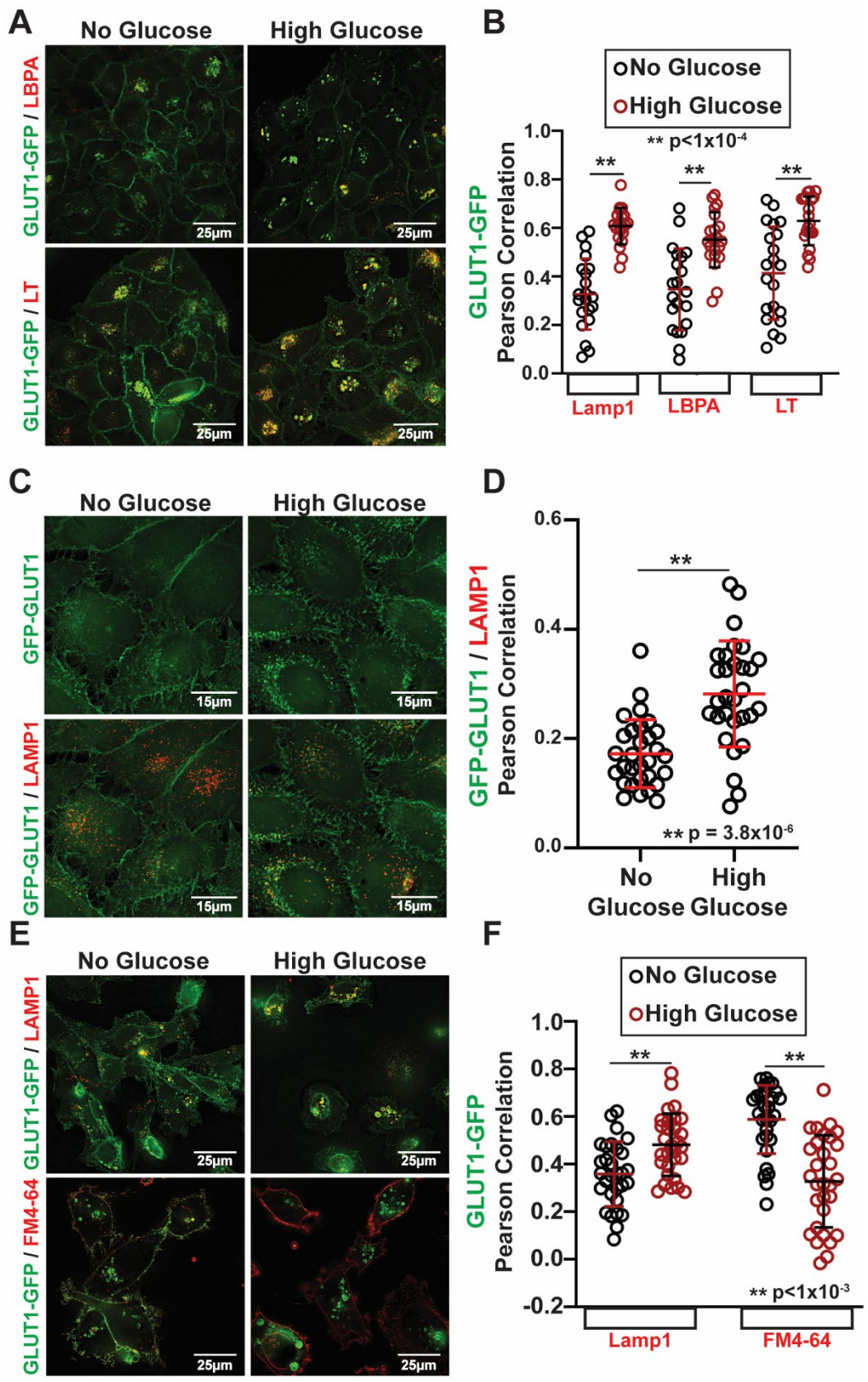

Figure 3.4. Additional evidence for glucose-stimulated clearance of GLUT1 from the plasma membrane using fluorescence microscopy assays, Related to **Figure 3.3. (A)** HeLa cells stably expressing GLUT1-GFP were cultured using the conditions indicated

in **FIG 3.3** prior to labeling with LysoTracker (LT; bottom row, red) or fixation and imaging for immunofluorescence detection of LBPA (top row, red). **(B)** Quantification of the results shown in panel (A) was done by measuring the Pearson coefficient of correlation for at least 21 cells (n≥21) with each condition indicated. **(C)** HeLa cells stably expressing N-terminally tagged GFP-GLUT1 were cultured using conditions indicated in **FIG 3.3** prior to fixation and imaging for immunofluorescence detection of Lamp1 (red). **(D)** Quantification of the results shown in panel (C) was done by measuring the Pearson coefficient of correlation for 30 cells (n=30) for each condition indicated. **(E)** MDA-MB-231 cells stably expressing GLUT1-GFP were cultured using the conditions indicated in **FIG 3.3** prior to pulse-labeling with FM4-64 (red, bottom row) and live cell imaging, or fixation followed by immunofluorescence detection of LAMP1 (red, top row). **(F)** Quantification of the results shown in panel (E) was performed by measuring Pearson coefficient of correlation of 30 cells (n=30) for each condition indicated. All p-values measured using a two sample Student's t-Test in Microsoft Excel. A P value < 0.05 was considered statistically significant and is indicated by **. Data are represented as mean +/- SEM. All measurements of Pearson coefficient of correlation were performed using Softworx software.

LAMP1 co-localization following glucose repletion (**FIG 3.4C-D**). To avoid any potential artifacts associated with GFP tagging on cytosol-facing termini of GLUT1, we also analyzed the subcellular localization of a GLUT1 variant harboring a FLAG epitope inserted into the first exofacial loop of the protein. Using immunofluorescence detection of the FLAG epitope, we found that glucose repletion triggered internalization and increasing co-localization of the FLAG-GLUT1 variant with LAMP1 (**FIG 3.3C**). Glucose-stimulated GLUT1 endocytosis and trafficking to lysosomes was also observed in MDA-MB-231 breast cancer cells (**FIG 3.4E-F**). Taken together, these results indicate that GLUT1 undergoes glucose-stimulated endocytosis and trafficking to lysosomes.

3.3.2 A subpopulation of GLUT1 traffics through ESCRT-associated endosomes

To better understand the glucose-stimulated GLUT1 trafficking itinerary, we analyzed GLUT1 subcellular localization using a panel of endosomal markers with the three GLUT1 detection strategies described in **FIG 3.3** (immunodetection of endogenous GLUT1, stable expression of GLUT1-GFP, and stable expression of a GLUT1 variant harboring a FLAG epitope in the first exofacial loop (FLAG-GLUT)). Previously, GLUT1 was found to co-localize with Vps35 (*97*), a retromer subunit and a marker of endosomal recycling. We observed glucose-stimulated co-localization of GLUT1 with Vsp35 (**FIG 3.5A-B**), as well the early endosomal markers EEA1 (**FIG 3.6**) and transferrin receptor (TfR) (**FIG 3.7**) and the late endosomal markers CD63 (**FIG 3.5C-D**) and VPS4A (**FIG 3.8**). In most cases, co-localization was observed when endogenous GLUT1 was detected by immunofluorescence, while co-localization with exogenous GLUT1-GFP or FLAG-GLUT1 was unchanged or slightly changed in response to glucose stimulation. One exception was the late endosomal marker CD63, which exhibited increased co-localization with both endogenous GLUT1 and GLUT1-

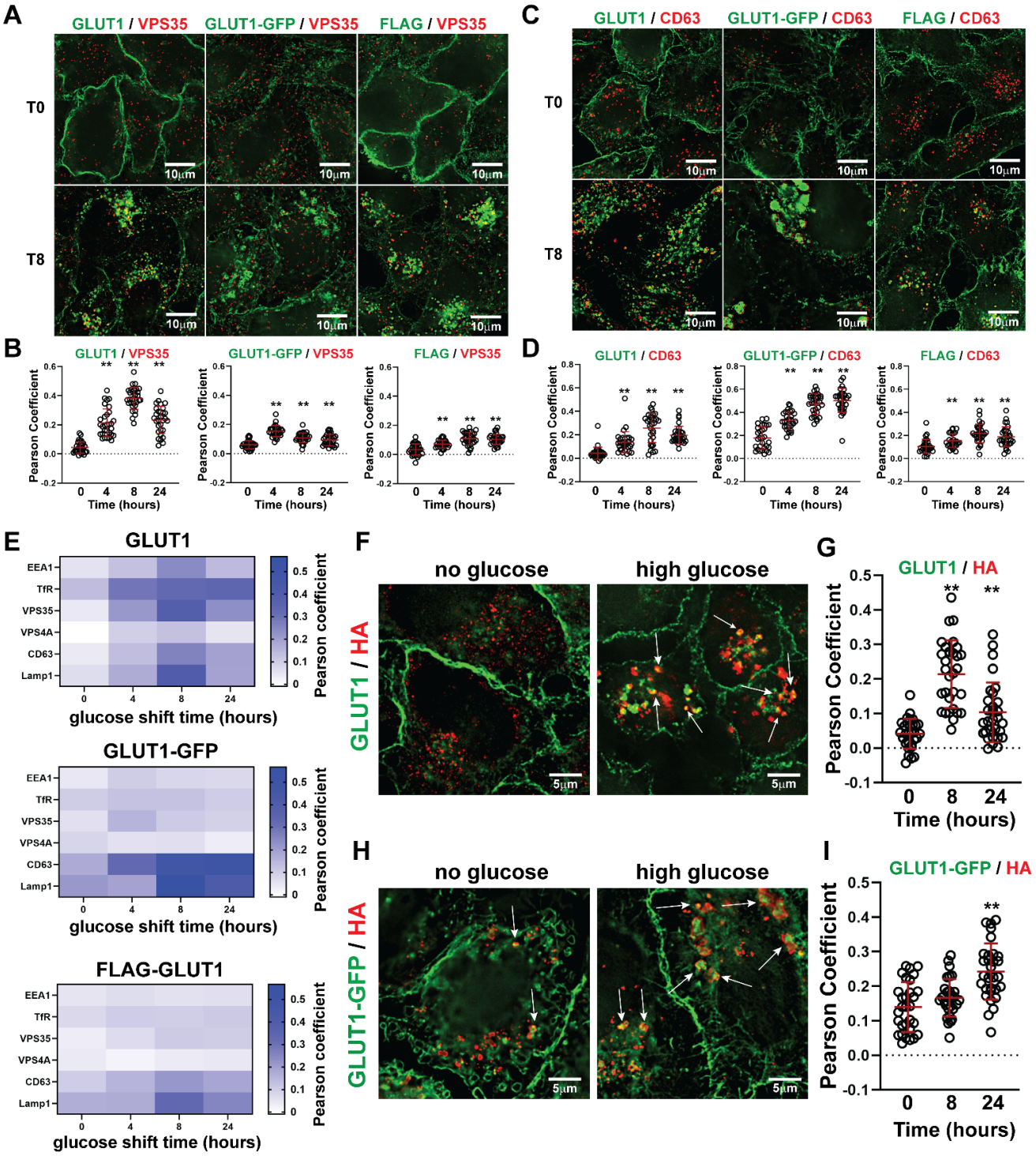

Figure 3.5. Characterization of the GLUT1 trafficking itinerary stimulated by excess glucose availability. HeLa cells expressing the three versions of GLUT1 described in **Figure 3.3** were cultured in media lacking glucose for 24 hours then either fixed or switched to high glucose media and fixed at the indicated time points. Cells were then probed by immunofluorescence for the endosomal proteins VPS35 **(A-B)** or CD63 **(C-D)** (**FIG3.5** cont'd) (red). In each case, co-localization was analyzed for endogenous GLUT1 (left), GLUT1-GFP (middle), or GLUT1-FLAG (right). Colocalization of GLUT1

signal with VPS35 **(B)** and CD63 **(D)** was quantified over the glucose stimulation time course. Measurements were done in Softworx using Pearson Correlation coefficient to measure colocalization (n=30 cells), $p < 0.001$. **(E)** Summarized profile of the GLUT1 trafficking itinerary stimulated by excess glucose availability. Heat maps showing colocalization of endogenous GLUT1 (top), GLUT1-GFP (middle), and exofacial GLUT1-FLAG (bottom) with different markers along the endocytic/endosomal trafficking route. For each time point and each marker, 30 measurements were taken of the Pearson coefficient of correlation using Softworx software. The color in each box is weighted based on the average Pearson coefficient ($n \geq 21$) at the indicated time point. **(F)** HeLa cells harboring a doxycycline-inducible dominant-negative VPS4 variant ($VPS4^{E228Q}$-HA) were cultured in no glucose media + 1 μg/ml doxycycline for 24 hours then fixed or switched to high glucose media + doxycycline and fixed at the indicated time point. Cells were then imaged for immunofluorescence detection of HA (red) and GLUT1 (green). $VPS4^{E228Q}$ is a dominant-negative mutant that accumulates on late-endosomal compartments responsible for sorting cargo into intraluminal vesicles. GLUT1 puncta that co-localize with, and are surrounded by, $VPS4^{E228Q}$-HA are marked with white arrows. **(G)** Quantification of the experiments represented in (F) by measuring the Pearson coefficient of correlation (n=30 cells) using Softworx software. $p < 0.001$ **(H)** HeLa cells stably expressing both GLUT1-GFP (green) and doxycycline-inducible $VPS4^{E228Q}$-HA were cultured as described in (F) and then imaged for immunofluorescence detection of HA (red). GLUT1-GFP puncta that co-localize with, and are surrounded by, $VPS4^{E228Q}$-HA are marked with white arrows. **(I)** Quantification of the experiments represented in (H) by measuring the Pearson coefficient of correlation (n=30 cells) using Softworx software, $p < 0.05$. For all experiments p-values were computed using a two sample Student's t-Test in Microsoft Excel and data is present as mean +/- SEM.

GFP, and to a lesser extent with FLAG-GLUT1. We organized co-localization data into heat maps that depict subcellular localization of endogenous GLUT1, GLUT1-GFP and FLAG-GLUT1 over the glucose stimulation time course (**FIG 3.5E**). Although we cannot exclude the possibility that trafficking of tagged GLUT1 variants (e.g., GLUT1-GFP or FLAG-GLUT1) is altered due to tag-associated artifacts, these variants recapitulate the lysosomal trafficking of endogenous GLUT1 in response to glucose (**FIG 3.5E**). Overall, the data support an itinerary where a subpopulation of GLUT1 is routed to late endosomal and lysosomal compartments as cells adapt to increased glucose availability.

Based on these observations, we hypothesized that glucose stimulation increases GLUT1 trafficking to the lysosome via the ESCRT sorting pathway. However, our analysis of GLUT1 trafficking did not reveal significant co-localization with VPS4A, a marker of late endosomes involved in ESCRT-mediated trafficking to lysosomes. VPS4A dynamically associates with the membrane of late endosomal compartments to regulate ESCRT-III disassembly, which is consistent with the diffuse, cytosolic staining pattern we observed by immunofluorescence imaging (**FIG 3.8A**). To test if GLUT1 traffics to lysosomes via the ESCRT pathway, we generated a HeLa cell line with a stably-integrated vector for inducible expression of a dominant negative Vps4A variant (Vps4A^{E228Q}-HA) which localizes to ESCRT sorting compartments (*169*). Doxycycline induction of this cell line resulted in expression of the Vps4A-HA fusion protein (**FIG 3.9A**) which was detected as subcellular puncta by immunofluorescence (**FIG 3.9B**). Using this cell line, we found that glucose stimulation increased co-localization of both endogenous GLUT1 (**FIG 3.5F-G**) and GLUT1-GFP (**FIG 3.5H-I**) with Vps4A^{E228Q}-HA over a glucose stimulation time course. In addition to co-localized GLUT1 and

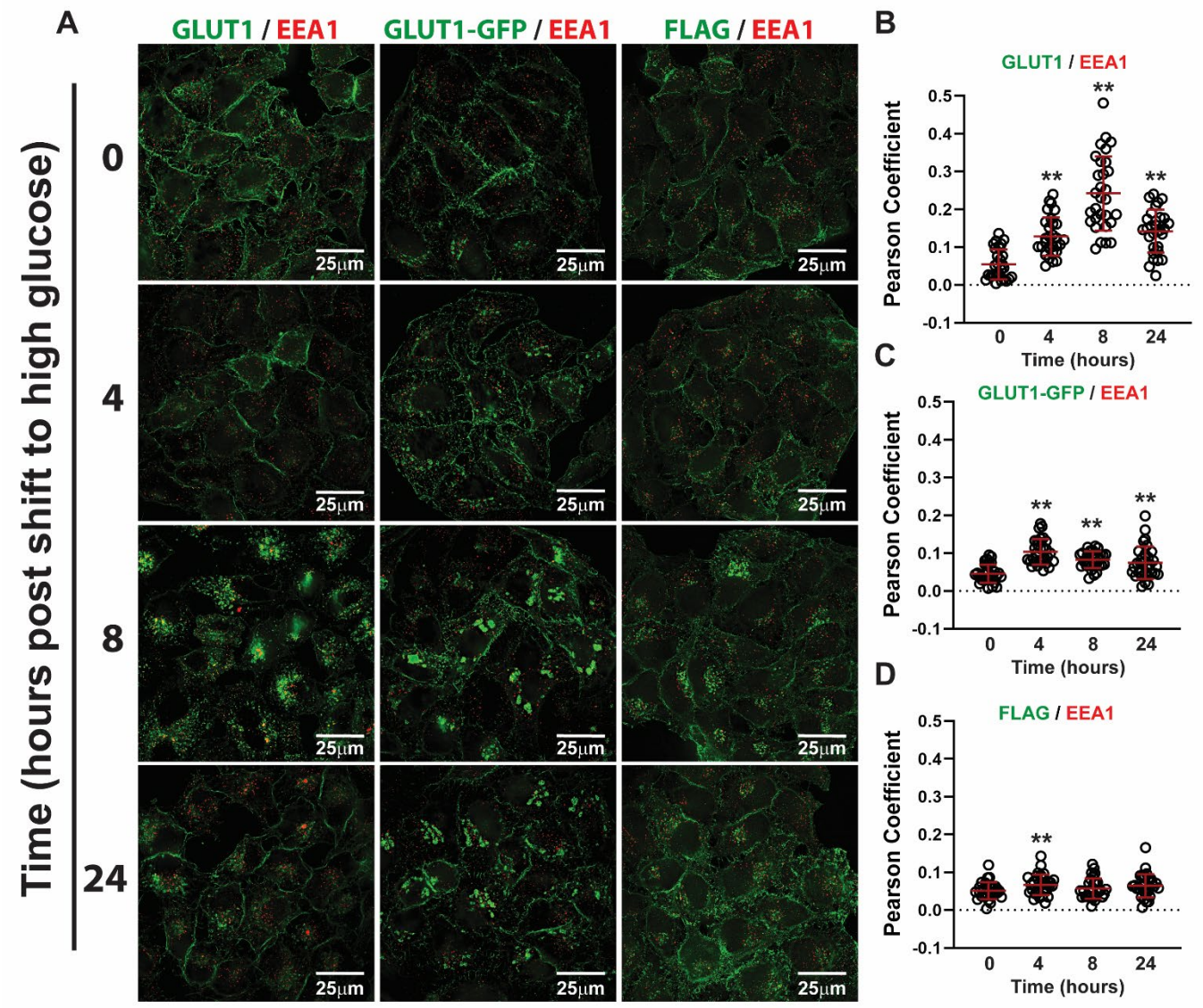

Figure 3.6: Analysis of GLUT1 localization to EEA1-positive early endosomal compartments following glucose-stimulated endocytosis, Related to **Figure 3.5**. **(A)** GLUT1 co-localization with the early endosomal marker EEA1 (red) during a glucose stimulation time course was analyzed by fluorescence microscopy. In the left column, endogenous GLUT1 in HeLa cells was detected by immunofluorescence (green). In the middle column, HeLa cells stably expressing GLUT1-GFP were analyzed. In the right column, HeLa cells stably expressing GLUT1 harboring an exofacial FLAG tag (green) were analyzed. These different approaches for detecting and imaging GLUT1 are summarized in **FIG 3.3**. **(B,C,D)** Quantification of the Pearson coefficients of correlation for the experiments represented in (A). Pearson measurements were made using Softworx software for 30 cells (n=30) per condition shown. For all experiments p-values were computed using a two sample Student's t-Test in Microsoft Excel. A P value < 0.05 was considered statistically significant and is indicated by **. Data are represented as mean +/- SEM.

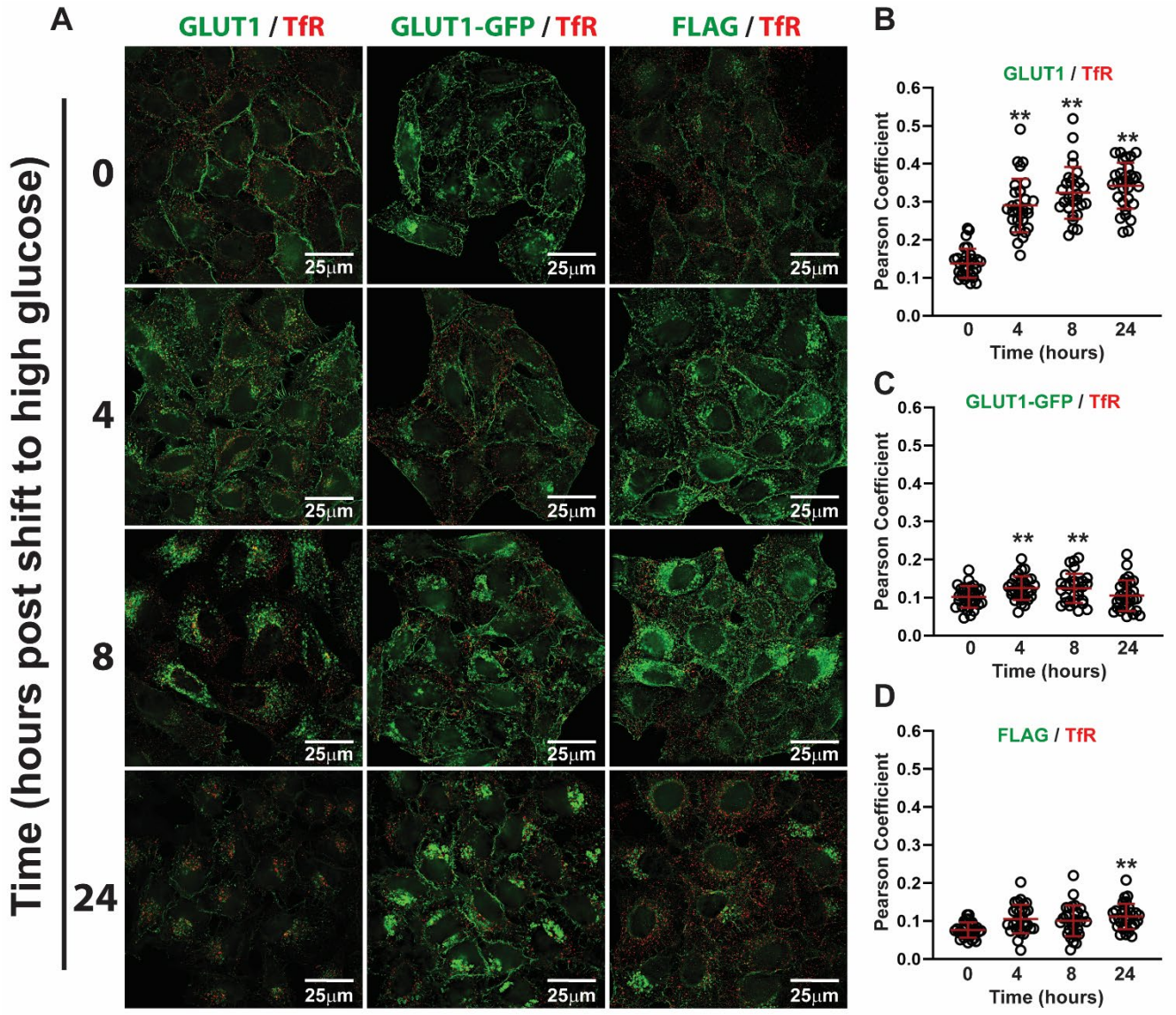

Figure 3.7: Analysis of GLUT1 localization to transferrin receptor (TfR)-positive endosomal compartments following glucose-stimulated endocytosis, Related to **Figure 3.5**. **(A)** GLUT1 co-localization with the endosomal marker TfR (red) during a glucose stimulation time course was analyzed by fluorescence microscopy. In the left column, endogenous GLUT1 in HeLa cells was detected by immunofluorescence (green). In the middle column, HeLa cells stably expressing GLUT1-GFP were analyzed. In the right column, HeLa cells stably expressing GLUT1 harboring an exofacial FLAG tag (green) were analyzed. These different approaches for detecting and imaging GLUT1 are summarized in **FIG 3.3**. **(B,C,D)** Quantification of the Pearson coefficients of correlation for the experiments represented in (A). Pearson measurements were made using Softworx software for 30 cells (n=30) per condition shown. For all experiments p-values were computed using a two sample Student's t-Test in Microsoft Excel. A P value < 0.05 was considered statistically significant and is indicated by **. Data are represented as mean +/- SEM.

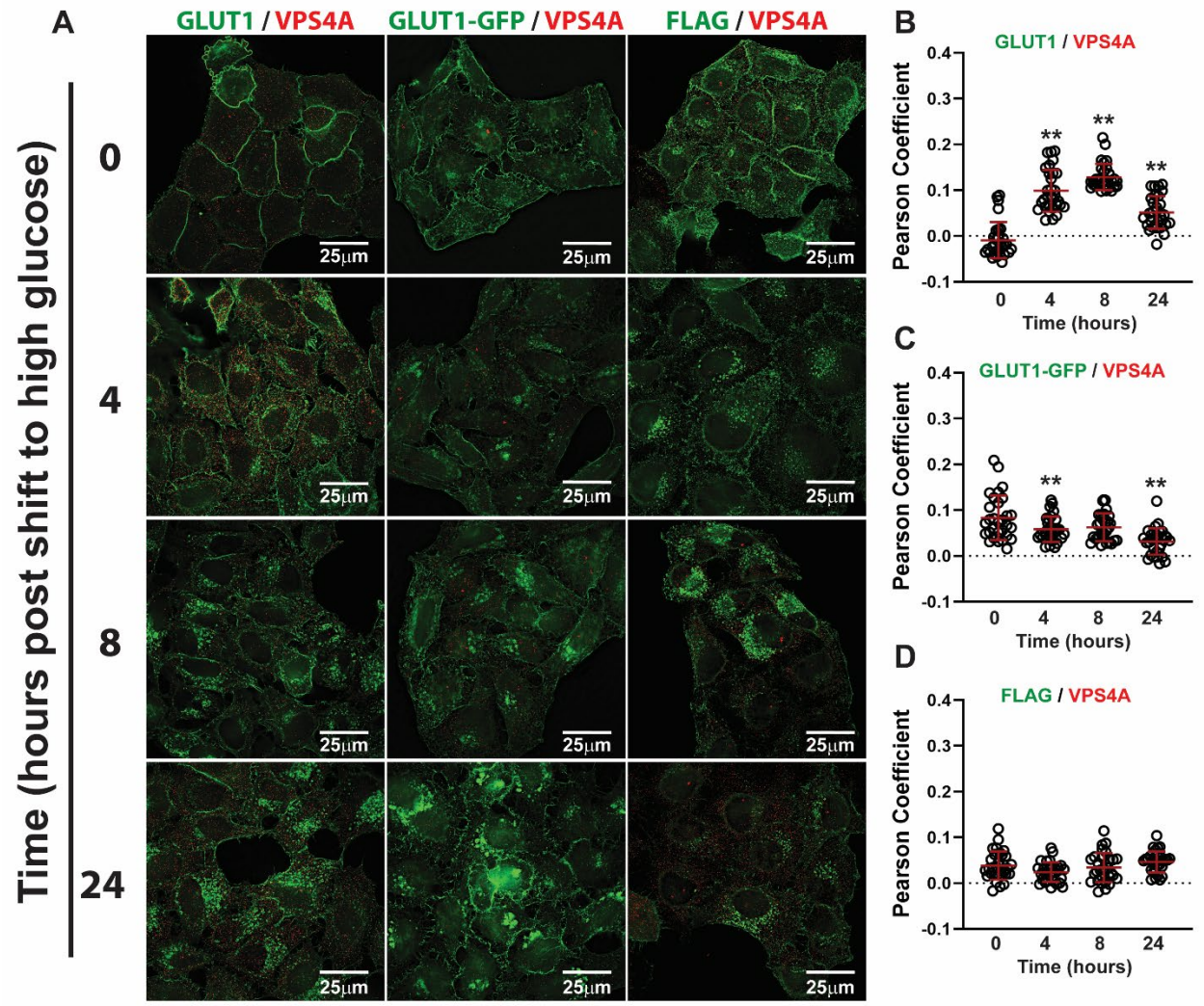

Figure 3.8: Analysis of GLUT1 localization to VPS4A-positive late endosomal compartments following glucose-stimulated endocytosis, Related to **Figure 3.5**. **(A)** GLUT1 co-localization with the late endosomal marker VPS4A (red) during a glucose stimulation time course was analyzed by fluorescence microscopy. In the left column, endogenous GLUT1 in HeLa cells was detected by immunofluorescence (green). In the middle column, HeLa cells stably expressing GLUT1-GFP were analyzed. In the right column, HeLa cells stably expressing GLUT1 harboring an exofacial FLAG tag (green) were analyzed. These different approaches for detecting and imaging GLUT1 are summarized in **FIG 3.3**. **(B,C,D)** Quantification of the Pearson coefficients of correlation for the experiments represented in (A). Pearson measurements were made using Softworx software for 30 cells (n=30) per condition shown. For all experiments p-values were computed using a two sample Student's t-Test in Microsoft Excel. A P value < 0.05 was considered statistically significant and is indicated by **. Data are represented as mean +/- SEM.

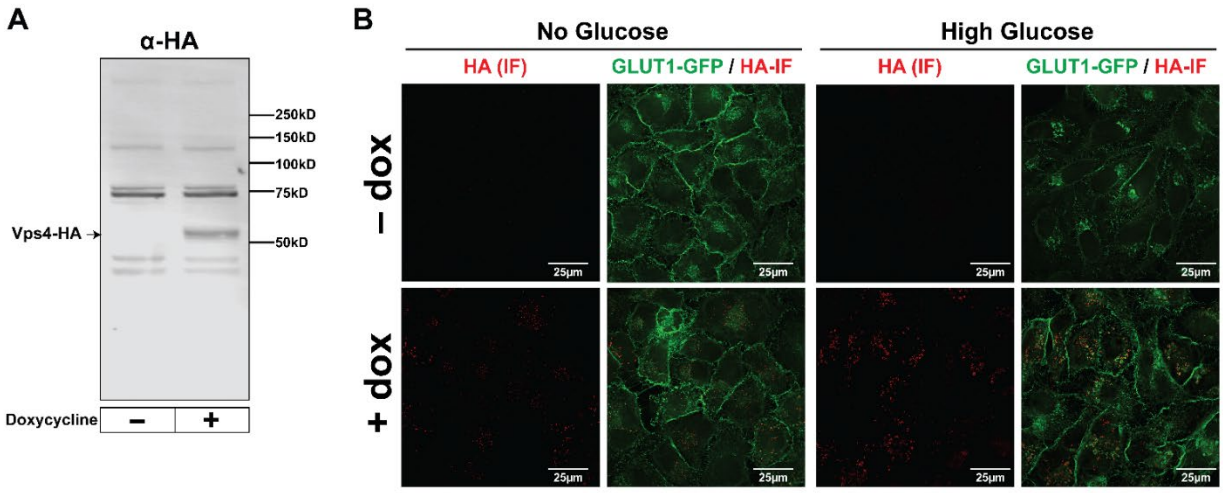

Figure 3.9: Validation of cell lines harboring a doxycycline-inducible dominant negative variant of Vps4, Related to **Figure 3.5**. **(A)** Immunoblot analysis of lysates prepared from HeLa cells stably transfected with an inducible expression vector for Vps4^{E228Q}-HA**.** **(B)** Fluorescence microscopy images of cells expressing GLUT1-GFP and harboring doxycycline-inducible VPS4^{E228Q}-HA. Cells with and without prior doxycycline induction were fixed and immunostained for HA.

Vps4A^{E228Q}-HA puncta we observed GLUT1/GLUT1-GFP puncta that appear to be encapsulated by a shell of Vps4A^{E228Q}-HA (**FIG 3.5F** and **3.5H**, white arrows), which may represent ESCRT sorting compartments frustrated by the accumulation of the dominant negative Vps4A variant. Taken together, our data reveal that glucose stimulation triggers internalization of GLUT1 from the PM and increases localization to ESCRT sorting compartments and lysosomes.

3.3.3 Endocytic trafficking of GLUT1 is stimulated by substrate transport

Since cells encounter a wide range of glucose concentrations, and since complete absence of glucose and 25 mM glucose are conditions seldom experienced in physiological contexts, we wanted to examine GLUT1 trafficking in response to a range of glucose levels. After starving HeLa cells of glucose for 24 hours, shifting to media containing 5 mM, 15 mM or 25 mM glucose resulted in similar kinetics of GLUT1 trafficking to lysosomes (**FIG 3.10A-B**). These concentrations represent a normal physiological range for glucose in human blood, but glucose concentrations encountered in peripheral tissues may be much lower. To simulate a range cells might experience in peripheral tissues, we analyzed GLUT1 trafficking in HeLa cells shifted from 1.5 mM to 15 mM glucose. In 1.5 mM glucose, GLUT1 localized primarily to the PM, while shifting to 15 mM triggered endocytic trafficking to lysosomes (**FIG 3.10C-F**). Notably, 1.5 mM is below the reported Km for GLUT1 (around 2 mM (*2*)) suggesting that endocytic trafficking of GLUT1 is triggered at concentrations of glucose above the Km.

Based on these findings, we hypothesized that substrate transport by GLUT1 is a trigger for its endocytic trafficking. Alternatively, GLUT1 trafficking could result from a negative feedback response to increased glucose metabolism. To distinguish between these possibilities, we compared GLUT1 trafficking stimulated by either glucose or 3-O-

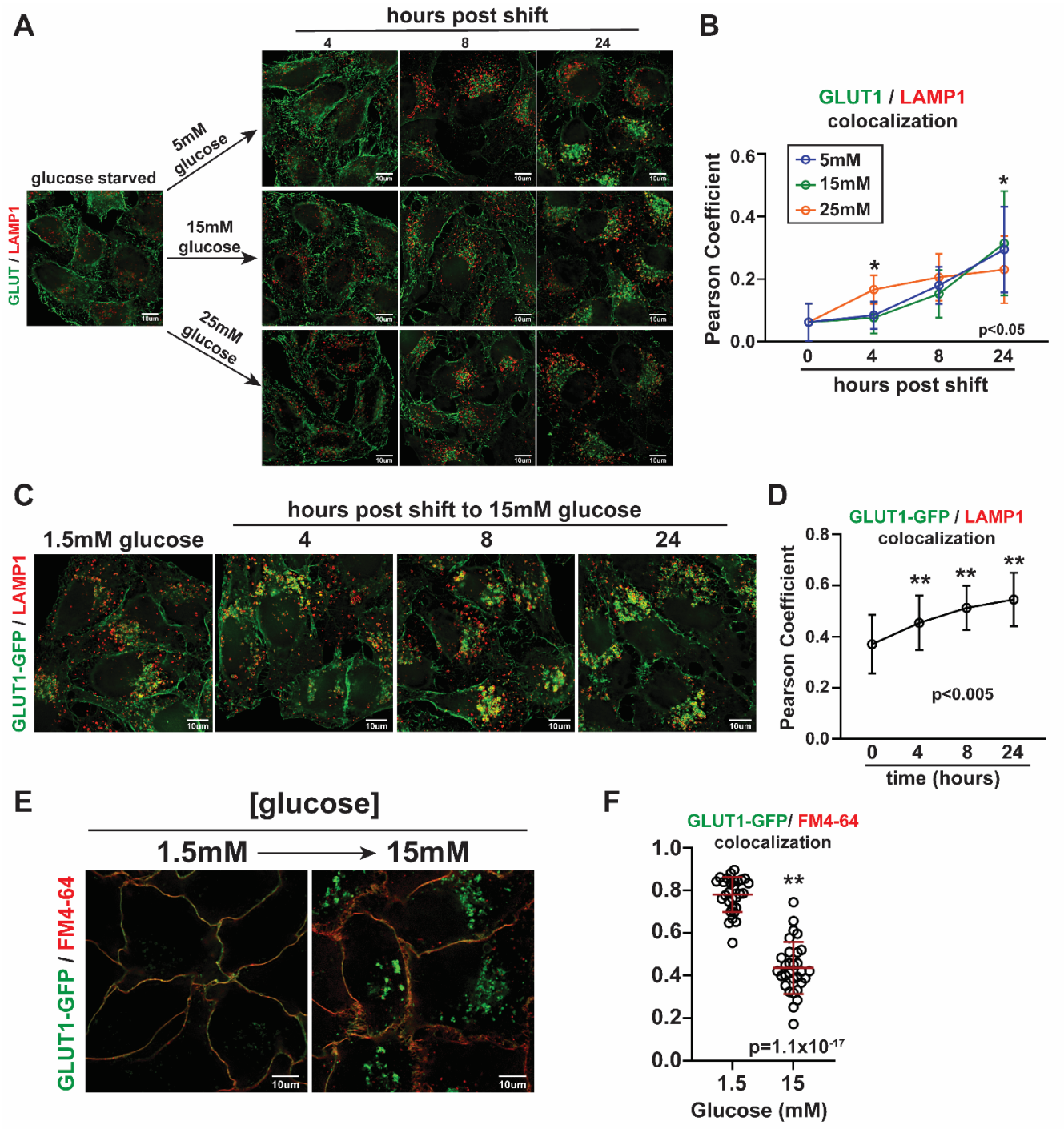

Figure 3.10: GLUT1 trafficking in physiological glucose concentrations, Related to **Figure 3.5**. **A)** HeLa cells were cultured for 24 hours in media with no glucose, then switched to either 5 mM, 15 mM, or 25 mM glucose media. Cells were fixed at the indicated time points for immunofluorescence detection with GLUT1 (green) and Lamp1 (red). **B)** Quantification of the experiments in (A). Measurements were done using the JACoP (BIOP version) FIJI plugin. Pearson correlation coefficient was measured for 30 cells under each condition (n=30). * indicates a statistically significant difference in the Pearson's coefficient between 5 mM and 25 mM glucose conditions. **C)** HeLa cells stably (**FIG 3.10** cont'd**)** expressing GLUT1-GFP were cultured in 1.5 mM glucose

media, then switched to 15 mM glucose media. The cells were fixed at the indicated times for immunofluorescence detection with Lamp1 (red). **D)** Quantification of the experiments in (C). Measurements were done using the JACoP (BIOP version) FIJI plugin. Pearson correlation coefficient was measured for 30 cells under each condition (n=30). ** indicates a statistically significant difference in Pearson's coefficient between the indicated time point and T=0. **E)** HeLa cells stably expressing GLUT1-GFP were cultured in 1.5 mM glucose media then switched to 15 mM glucose media for 24 hours. Prior to imaging, cells were placed on ice and switched to cold HBSS buffer containing 8 μM FM4-64 in order to label the plasma membrane. Cells were imaged before FM4-64 internalized. **F)** Quantification of the experiments in (E). Measurements were done using the JACoP (BIOP version) FIJI plugin. Pearson correlation coefficient was measured for 30 cells under each condition (n=30). For all experiments, p-values were computed using a two sample Student's t-Test in Microsoft Excel. A P value < 0.05 was considered statistically significant and is indicated by **. Data are represented as mean +/- SEM.

methyl-d-glucose (3-OMG), a glucose analog transported by GLUT1 but not metabolized by the cell. We observed that 3-OMG triggered GLUT1 endocytic clearance and lysosomal trafficking that mimicked the response to glucose (**FIG 3.11A-D**). These results indicate that substrate transport is sufficient to trigger GLUT1 endocytic trafficking and delivery to lysosomes.

3.3.4 GLUT1 trafficking requires both clathrin- and E3-binding domains of TXNIP

A previous study reported that TXNIP promotes GLUT1 PM clearance via clathrin-mediated endocytosis (*102*). To further explore the role of TXNIP in GLUT1 downregulation, we generated a stable HeLa cell line expressing both GLUT1-GFP (from a constitutive CMV promoter) and TXNIP (from a doxycycline-inducible (Tet-On) promoter). Induced TXNIP expression in this cell line (**FIG 3.12A**) led to glucose-independent trafficking of GLUT1-GFP to lysosomes (**FIG 3.12B-C**). Similarly, induced TXNIP expression in HeLa cells led to glucose-independent trafficking of endogenous GLUT1 to lysosomes (**FIG 3.13A-B**). Thus, induced TXNIP expression mimics the physiological response to glucose.

To test if TXNIP is required for glucose-stimulated GLUT1 endocytic trafficking, we generated HeLa cells lacking TXNIP using CRISPR/Cas9 with TXNIP-targeting gRNAs (**FIG 3.12D**). We isolated and characterized two distinct *txnip* knockout HeLa cell lines (**FIG 3.12E-F**) (which also expressed GLUT1-GFP), both of which exhibited defects in glucose-stimulated lysosomal trafficking of GLUT1 (**FIG 3.13C-D** and **FIG 3.12G-H**). We used *txnip* knockout clone 1 for additional experiments described in the remainder of this study.

To test if TXNIP expression restores glucose-stimulated GLUT1 trafficking in *txnip* knockout cells, we stably transfected an inducible TXNIP expression vector into

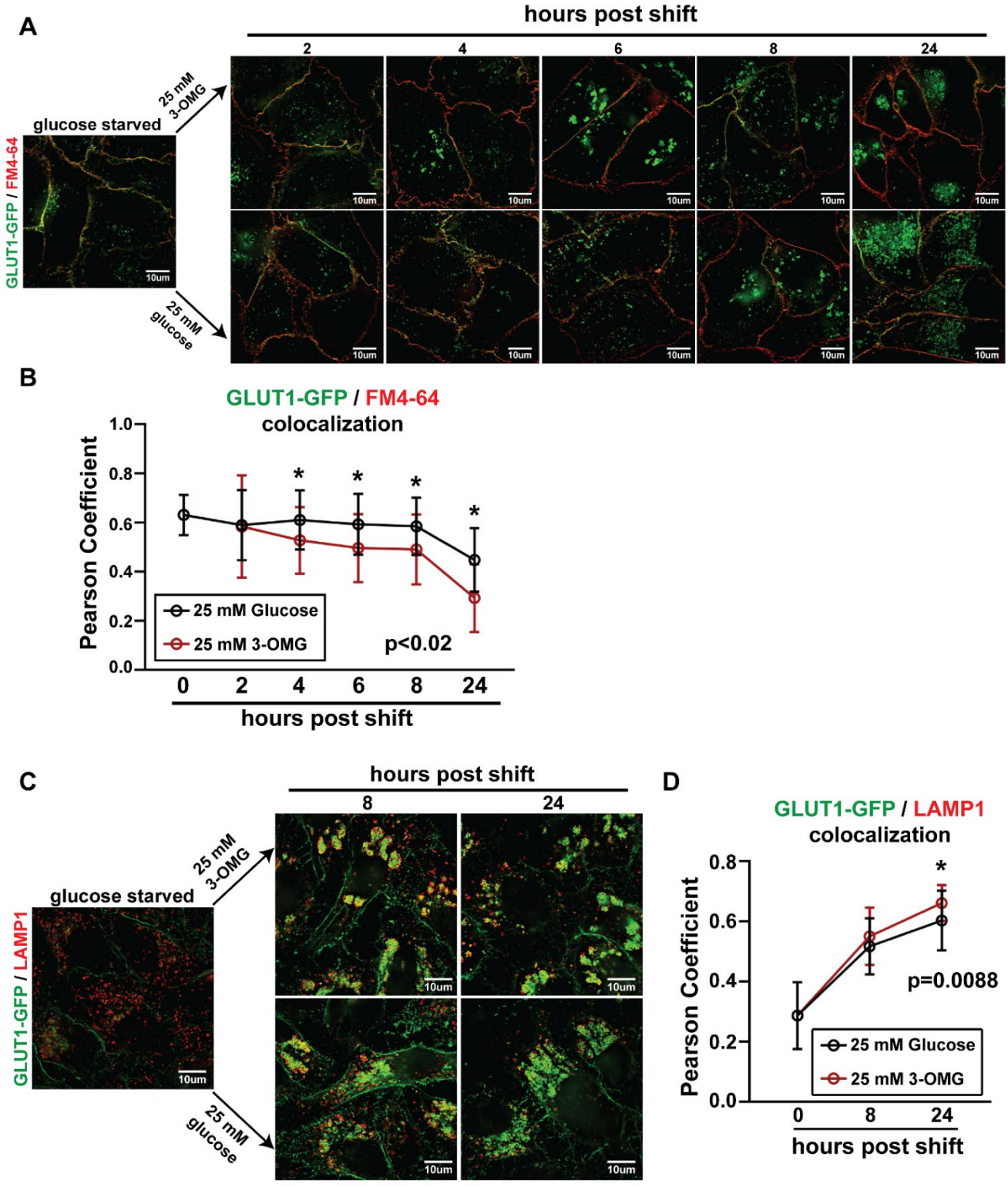

Figure 3.11: GLUT1 is trafficked from the plasma membrane in response to substrate transport, Related to **Figure 3.5**. **A)** HeLa cells stably expressing GLUT1-GFP were cultured for 24 hours in media with no glucose, then switched to either 25 mM glucose or 25 mM 3-OMG. Prior to imaging, cells were placed on ice and switched to cold HBSS (**FIG 3.11** cont'd) buffer containing 8 μM FM4-64 in order to label the plasma membrane. **B)** Quantification of the experiments in (A). Measurements were done using

the JACoP (BIOP version) FIJI plugin. Pearson coefficient of correlation was measured for 30 cells under each condition (n=30). * indicates a statistically significant difference in Pearson's coefficient between the glucose and 3-OMG condition at the indicated time point. **C)** HeLa cells stably expressing GLUT1-GFP were cultured in media without glucose for 24 hours then switched to either 25 mM glucose or 25 mM 3-OMG media. Cells were fixed at the indicated time points for immunofluorescence detection with Lamp1 (red). **D)** Quantification of the experiments in (C). Measurements were done using the JACoP (BIOP version) plugin. * indicates a statistically significant difference in Pearson's coefficient between the glucose and 3-OMG conditions at the 24 hour time point. Pearson correlation coefficient was measured for 30 cells under each condition (n=30). For all experiments, p-values were computed using a two sample Student's t-Test in Microsoft Excel. A P value < 0.05 was considered statistically significant and is indicated by **. Data are represented as mean +/- SEM.

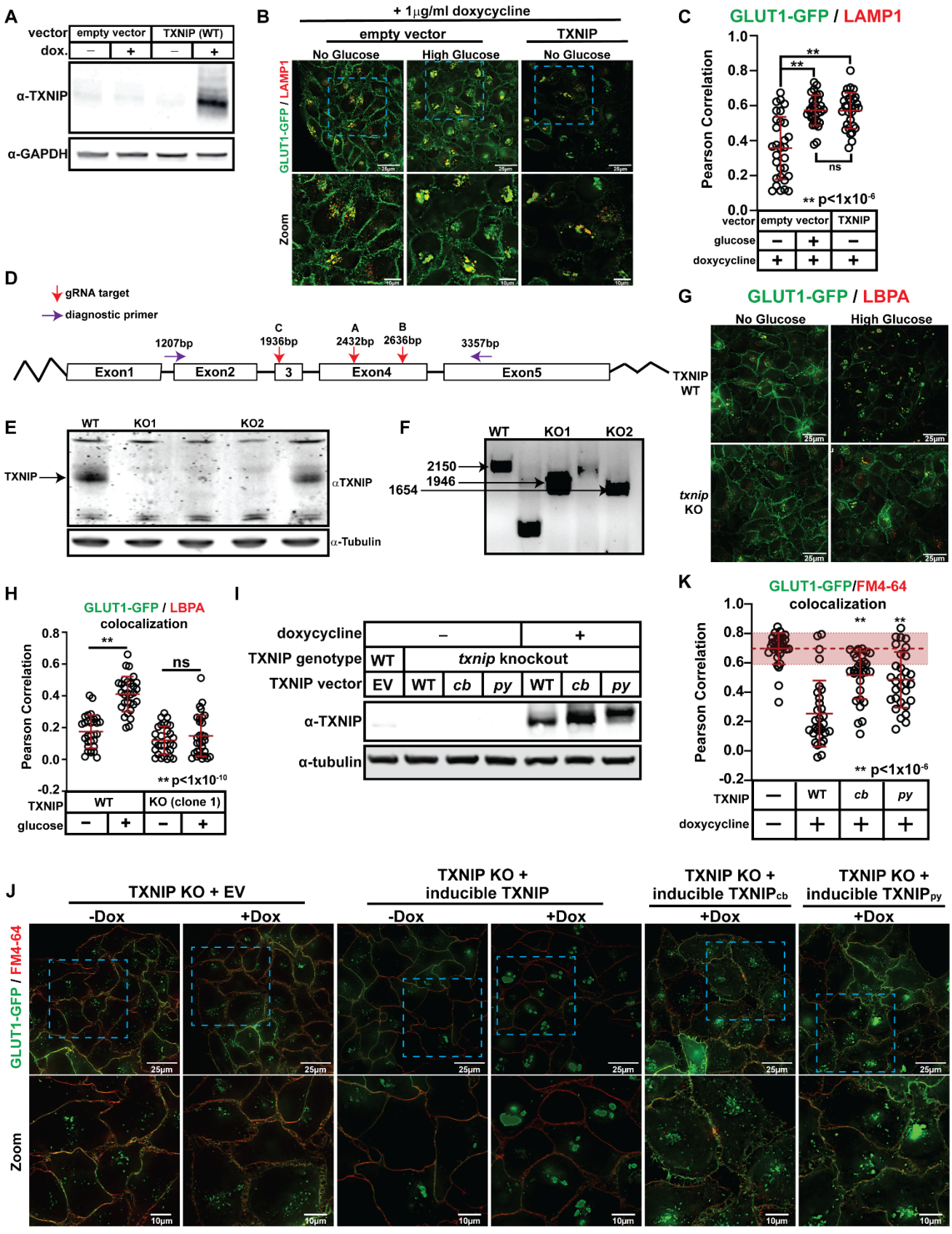

Figure 3.12: Characterization of the role of *TXNIP* in glucose-stimulated GLUT1 trafficking to lysosomes, Related to **Figure 3.13**. **(A)** HeLa cells were stably transfected

(**FIG 3.12** cont'd) with either empty vector (pINDUCER20) or vector expressing TXNIP under the control of Tet-on gene expression system. Doxycycline was added to induce expression of TXNIP for 24 hours prior to collection of cell lysate. Cell lysates were resolved by SDS-PAGE and analyzed by immunoblot. Immunoblotting of GAPDH was performed as a loading control. **(B)** HeLa cells stably expressing GLUT1-GFP and a doxycycline-induced expression vector were cultured using the conditions described in **FIG 3.1D** and, for the induced samples, additionally treated with 1 μg/ml doxycycline for the last 24 hours before fixation. Cells were fixed and imaged for detection of LAMP1 (red), a marker of lysosomal compartments. Zoomed images provided in the bottom row correspond to the blue dashed-line inset boxes of the top row. **(C)** Quantification of the experiments represented in panel (B) was performed by measuring the Pearson coefficient of correlation for 30 cells (n=30) with each condition shown. **(D)** A strategy to generate *txnip* knockout cell lines using CRISPR/Cas9 and gRNAs targeting exon 3 and 4 was developed. Cells were nucleofected twice with the TXNIP CRISPR/Cas9 KO plasmids (Santa Cruz Biotechnology), which target the *txnip* gene in 3 separate locations (red arrows) for a double strand break by the Cas9 nuclease. After recovering from electroporation, cells were sorted into 96 well plates for screening by immunoblot and PCR. **(E)** Clonal cell lines were isolated and screened for TXNIP expression by immunoblot. Two isolated clonal lines that lack detectable TXNIP expression are shown (KO1 and KO2). α-Tubulin was used as a loading control in immunoblots. **(F)** Clonal cell lines lacking TXNIP protein expression by immunoblot were further characterized for deletions at the chromosomal TXNIP locus. gDNA was collected from the two clones and the region of interest was amplified (purple arrows) and run on an agarose gel to compare with a wildtype sample. The size of the amplified DNA indicates at which gRNA target the *txnip* gene had been cut. KO1 is missing the region between gRNAs A and B while KO2 is missing the region between gRNAs A and C. **(G)** HeLa cells and *txnip* knockout equivalents (clone 1) stably expressing GLUT1-GFP were cultured as indicated in **Fig 3.1D** then fixed for immunofluorescence detection of LBPA (red), a marker of late endosomes. **(H)** Quantification of the experiments represented in panel (G) was performed by measuring the Pearson coefficient of correlation for 30 cells (n=30) with each condition shown. All p-values were measured using a two sample Student's t-Test in Microsoft Excel. All measurements of Pearson coefficient of correlation were performed using Softworx software. **(I)** HeLa cells stably expressing GLUT1-GFP were stably transfected with either empty vector (pINDUCER20) or vector expressing wildtype, clathrin binding mutant, or PY motif mutant TXNIP under the control of Tet-on gene expression system. Doxycycline was added to induce expression of TXNIP for 24 hours prior to collection of cell lysate. Cell lysates were resolved by SDS-PAGE and analyzed by immunoblot. Immunoblotting of α-tubulin was performed as a loading control. **(J)** Complementation analysis of HeLa cells stably expressing GLUT1-GFP with the *txnip* gene knocked out via CRISPR/Cas9. The knockout cells were complemented with either an empty vector, wildtype TXNIP, a clathrin binding mutant, or a PY motif mutant expressed in a doxycycline-induced vector. Cells were cultured in media containing doxycycline to induce expression of the indicated protein. Prior to imaging, cells were placed on ice and switched to cold (4°C) buffer containing the lipophilic tracer dye FM4-64 (8 μM) (red) in order to label the plasma membrane.

Live (**FIG 3.12** cont'd) cells were imaged in cold buffer immediately to ensure retention of FM4-64 at the plasma membrane. **(K)** Quantification of the results shown in panel (J) was performed by measuring the Pearson coefficient of correlation of 30 cells (n=30) for each condition indicated. All p-values were measured using a two sample Student's t-Test in Microsoft Excel. A P value < 0.05 was considered statistically significant and is indicated by **. Data are represented as mean +/- SEM. In panel K, the significant difference applies for comparison with conditions of no TXNIP expression and WT TXNIP expression. All measurements of Pearson coefficient of correlation were performed using Softworx software. Dotted red line on graphs indicated the average Pearson coefficient of correlation for the no TXNIP, no doxycycline condition and the shaded red area indicates the standard deviation.

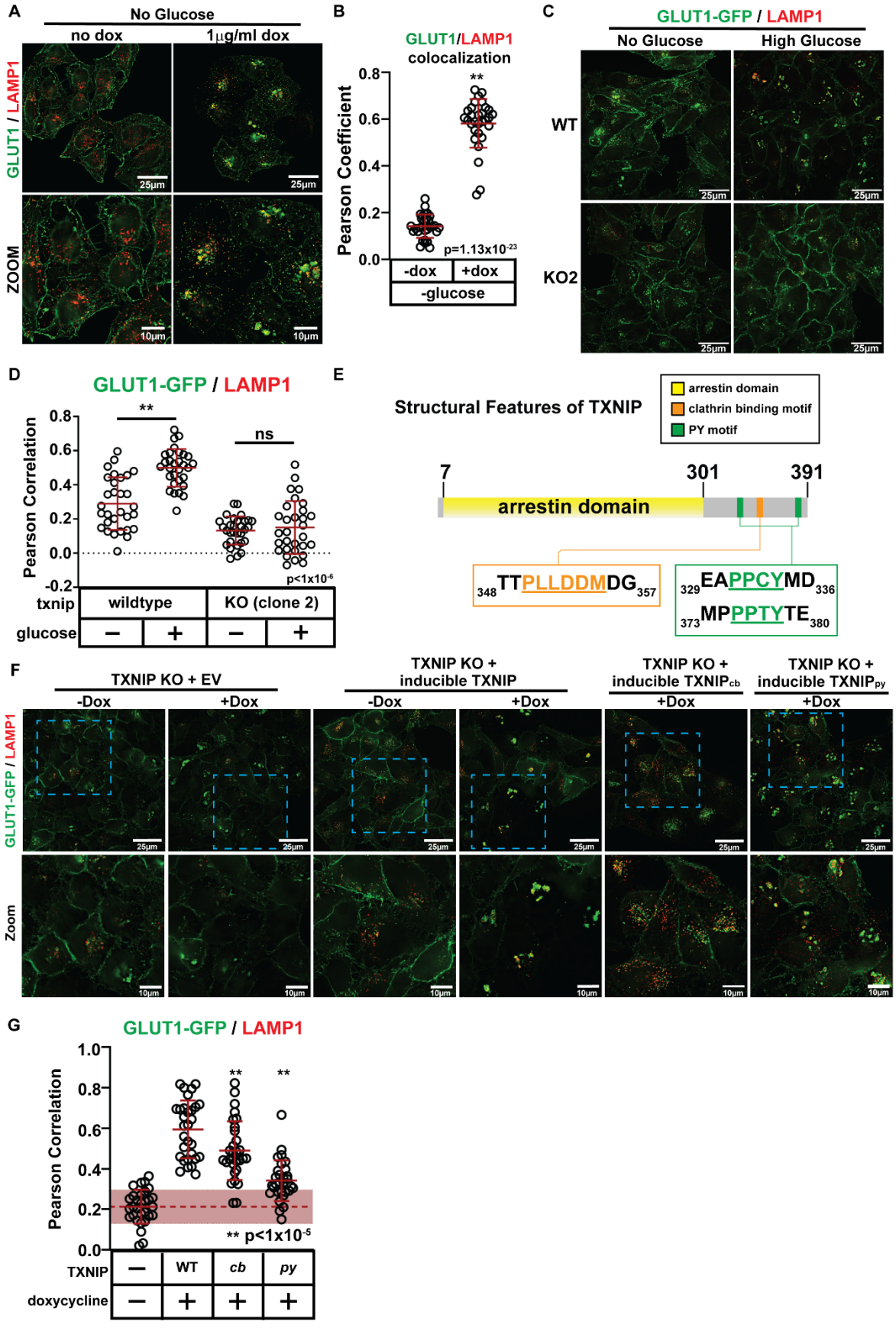

Figure 3.13. The clathrin binding motif and PY motifs of TXNIP are required for glucose-mediated GLUT1 trafficking to lysosomes. **(A)** HeLa cells stably expressing a

(**FIG 3.13** cont'd) doxycycline-inducible expression vector were cultured using the conditions described in **FIG 3.1D** and, for the induced samples, additionally treated with 1 μg/ml doxycycline for the last 24 hours before fixation. Cells were fixed and imaged for detection of LAMP1 (red), a marker of lysosomal compartments. Zoomed images provided in the bottom row correspond to the blue dashed-line inset boxes of the top row. **(B)** Quantification of the experiments represented in panel (A) was performed by measuring the Pearson coefficient of correlation for 30 cells (n=30) with each condition shown. **(C)** HeLa cells and *txnip* knockout equivalents (clone 2) stably expressing GLUT1-GFP were cultured as indicated in (A) then fixed for immunofluorescence detection of LAMP1 (red), a marker of lysosomal compartments. **(D)** Quantification of the experiments represented in panel (C) was performed by measuring the Pearson coefficient of correlation for 30 cells (n=30) with each condition shown. **(E)** Schematic representation of TXNIP illustrating the predicted arrestin fold domain (yellow), the clathrin binding motif (orange), and the two PY motifs (green). **(F)** Complementation analysis of HeLa cells stably expressing GLUT1-GFP with the *txnip* gene knocked out via CRISPR/Cas9. The knockout cells were complemented with either an empty vector, wildtype TXNIP, a clathrin binding mutant (*cb*), or a PY motif mutant (*py*) expressed in a doxycycline-induced vector. Cells were cultured as indicated in **Fig 3.1D** with doxycycline added the last 24 hours to induce expression of the indicated protein. Cells were fixed and imaged by immunofluorescence for detection of LAMP1 (red), a marker of lysosomal compartments. **(G)** Quantification of the results shown in panel (F) was performed by measuring the Pearson coefficient of correlation for 30 cells (n=30) for each condition indicated. The dashed line and area shaded in red indicate the average Pearson's coefficient and standard deviation for the GLUT1-GFP, *txnip* KO cells with a Dox-inducible WT TXNIP vector that is kept in no glucose media without Dox. All p-values were measured using a two sample Student's t-Test in Microsoft Excel and data is present as mean +/- SEM. All measurements of Pearson coefficient of correlation were performed using Softworx software.

txnip knockout cells. Induction of TXNIP expression in these cells resulted in TXNIP protein levels greater than that detected for endogenous TXNIP in parental HeLa cells (**FIG 3.12I**) and complemented the GLUT1 trafficking defect in *txnip* knockout cells, as evidenced by increased GLUT1-GFP co-localization with LAMP1 (**FIG 3.13E-G**) and decreased co-localization with PM-localized FM4-64 (**FIG 3.12J-K**) upon induction of TXNIP expression. We decided to use this complementation system to characterize the structural features of TXNIP involved in regulating GLUT1 endocytic trafficking.

TXNIP contains an N-terminal arrestin fold domain and C-terminal motifs that bind to clathrin and NEDD4 family E3 ubiquitin ligases (**FIG 3.13E**). Specifically, TXNIP binds to clathrin via a di-leucine motif near its C-terminus (P**LL**DDM$_{355}$) and mutation of this motif (L351A, L352A) decreased TXNIP localization to sites of clathrin-mediated endocytosis and decreased the rate of GLUT1 endocytosis (*102*). PY motifs at the C-terminus of TXNIP (P**P**C**Y**$_{334}$ and P**P**T**Y**$_{378}$) interact with WW domains of NEDD4 family E3 ubiquitin ligases, including ITCH (*138, 153*) and WWP1 (*170, 171*) although their contribution to GLUT1 trafficking remains unknown. To determine how these C-terminal features of TXNIP contribute to GLUT1 trafficking, we induced expression of TXNIP variants harboring mutations that disrupt clathrin binding (TXNIP$_{cb}$: L351A, L352A) or E3 binding (TXNIP$_{py}$: PPCY$_{334}$ → PACA$_{334}$ and PPTY$_{378}$ → PATA$_{378}$) in *txnip* knockout cells. Compared to the wildtype variant, both TXNIP$_{cb}$ and TXNIP$_{py}$ exhibited increased stability following induced expression (**FIG 3.12I**). Interestingly, TXNIP$_{py}$ stabilization was observed for a lower mobility form of the protein, which was previously reported and attributed to phosphorylated TXNIP (*102*). In contrast, TXNIP$_{cb}$ stabilization was observed without apparent alterations to mobility by SDS-PAGE as detected by immunoblot (**FIG 3.12I**). We next tested if induced expression of these TXNIP variants

restored GLUT1-GFP trafficking in *txnip* knockout cells. Both TXNIP mutations conferred partial loss of function, with GLUT1-GFP exhibiting significantly lower co-localization with the lysosomal marker LAMP1 (**FIG 3.13F-G**) and increased co-localization with PM-localized FM4-64 (**FIG 3.12J-K**) compared to wildtype TXNIP. Taken together, these results indicate that both di-leucine and PY motifs contribute to TXNIP-mediated trafficking of GLUT1.

3.3.5 TXNIP interacts with WWP1 via its C-terminal PY motifs

Since GLUT1 co-purifies with TXNIP (*102*) (*172*) and TXNIP interacts with ITCH (*153*) and WWP1 (*171*), both E3 ubiquitin ligases of the NEDD4 family, we hypothesized that TXNIP functions as an E3 ubiquitin ligase adaptor. Previous studies reported that the second PY motif of TXNIP (PY2, $PPTY_{378}$) binds to the WW domains of ITCH (*153*), but the basis for TXNIP interaction with WWP1 has not been determined. To test if the PY motifs of TXNIP are critical for interaction with WWP1 we incubated recombinant FLAG-WWP1 with lysates from *txnip* knockout HeLa cells harboring inducible TXNIP expression constructs (WT, *cb*, and *py* variants). Affinity purification of FLAG-WWP1 from these lysates revealed co-purification with WT TXNIP and the *cb* variant which doesn't bind clathrin (**FIG 3.14A**). In contrast, mutations disrupting the C-terminal PY motifs of TXNIP resulted in loss of co-purification with FLAG-WWP1 (**FIG 3.14A**). Similar experiments using FLAG-tagged TXNIP as bait also revealed co-purification with WWP1 that was lost in a $TXNIP^{py}$ mutant (**FIG 3.14B**). This analysis reveals that TXNIP interacts with WWP1 via its C-terminal PY motifs. It also reveals that GLUT1 interacts with both TXNIP and WWP1 independently and in a manner that does not require the TXNIP-WWP1 interaction (**FIG 3.14A-B**).

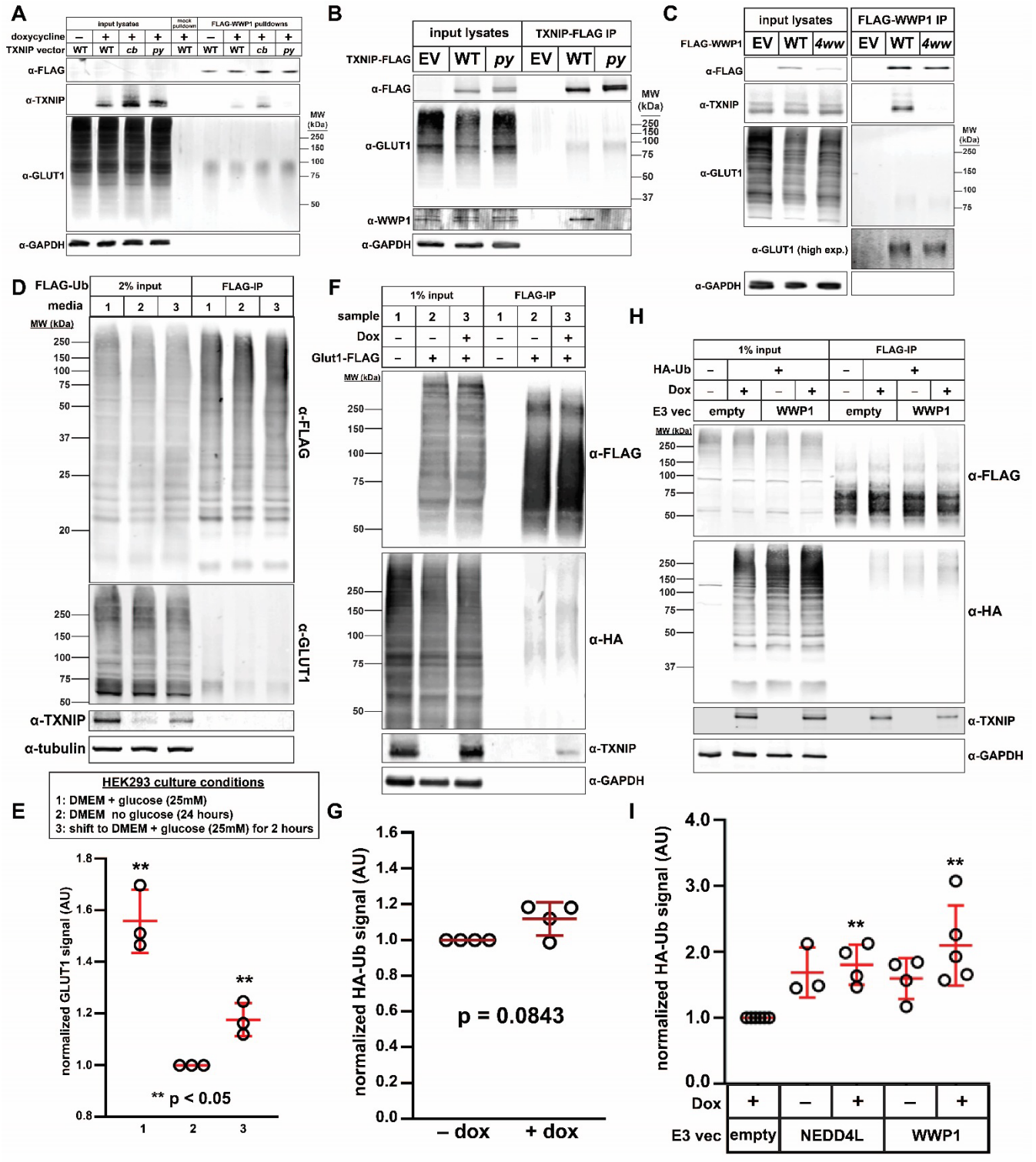

Figure 3.14. TXNIP is dispensable for GLUT1 ubiquitin modification. **(A)** HeLa cells stably expressing GLUT1-GFP were stably transfected with either empty vector (pINDUCER20) or vector expressing wildtype, clathrin binding mutant (*cb*), or PY motif mutant *(py)* TXNIP under the control of Tet-on gene expression system. 1 μg/ml doxycycline was added to induce expression of TXNIP for 24 hours prior to collection of cell lysate. Cell lysates were incubated with recombinant WWP1-FLAG at 4°C overnight (**FIG 3.14** cont'd) then WWP1-FLAG was pulled down using αFLAG magnetic beads.

Elution was performed using FLAG peptide. Lysates and eluates were resolved by SDS-PAGE and analyzed by immunoblot. Immunoblotting of GAPDH was performed as a loading control. **(B)** HeLa cells stably expressing GLUT1-GFP were transiently transfected with either a wildtype or PY mutant TXNIP expression plasmid. When cells reached 100% confluence, they were collected in lysis buffer and incubated with αFLAG magnetic beads for 1 hour at 4°C with rotation. TXNIP-FLAG was eluted with FLAG peptide and samples were resolved by SDS-PAGE then analyzed by immunoblot. GAPDH was used as a loading control. **(C)** HeLa cells stably expressing GLUT1-GFP and a dox-inducible clathrin binding mutant TXNIP were transiently transfected with either wildtype WWP1-FLAG or a mutant WWP1-FLAG with all 4 ww domains mutated. $TXNIP_{CB}$ was induced with 1 μg/ml doxycycline 24 hours before collecting lysates. Cells were then collected in lysis buffer and incubated with αFLAG magnetic beads for 1 hour at 4°C with rotation. WWP1 was eluted using FLAG peptide and samples were resolved by SDS-PAGE and analyzed by immunoblot. GAPDH was used as a loading control. **(D)** HEK293T cells stably expressing FLAG-Ub were split into either 1) regular 25 mM glucose DMEM media, 2) DMEM media with no glucose, or 3) no glucose DMEM media to be switched to 25 mM glucose media 2 hours before collection. All cells were transiently transfected with a GLUT1-GFP expression plasmid. When cells reached 100% confluency, sample 3 cells were switched to high glucose (25 mM) DMEM media and lysates were collected 2 hours later then incubated with magnetic FLAG affinity beads for 1 hour at 4° with rotation. FLAG-Ub was eluted using FLAG peptide, samples were resolved by SDS-PAGE, and analyzed by immunoblot. α-Tubulin was used as a loading control. **(E)** Quantification of the eluate GLUT1 signal for three biological replicates (n=3) of the experiment shown in (D). ****** indicates a significant difference ($p < 0.05$) compared to the no glucose condition (lane 2). **(F)** *txnip* knockout HeLa cells stably expressing constitutive GLUT1-FLAG and a dox-inducible TXNIP expression plasmid were transiently transfected with HA-Ub. 24 hours before collecting lysates, cells were either mock-treated (sample 2) or treated with 1 μg/ml doxycycline (sample 3) to induce TXNIP expression. As a control, HeLa cells expressing endogenous TXNIP with a stably integrated empty vector (i.e., no GLUT1-FLAG expression) were also analyzed (sample 1). Lysates were incubated with magnetic αFLAG affinity beads for 1 h at 4°C with rotation and eluted using FLAG peptide. Samples were resolved by SDS-PAGE and analyzed by immunoblot. GAPDH was used as a loading control. **(G)** Quantification of the eluate HA-Ub signal in four biological replicates (n=4) of the experiment shown in (F). **(H)** HeLa cells stably expressing constitutive GLUT1-FLAG and dox-inducible TXNIP vectors were transiently transfected with either empty vector, HA-Ub, and/or WWP1 as indicated in the figures. 24 hours after inducing TXNIP with 1 μg/ml doxycyxline, cells were collected in lysis buffer and incubated with magnetic αFLAG affinity beads for 1 hour at 4°C with rotation. GLUT1-FLAG was eluted with FLAG peptide and samples were resolved by SDS-PAGE then analyzed by immunoblot. GAPDH was used as a loading control. **(I)** Quantification of HA-Ub signal for at least three biological replicates (n≥3) of the experiments shown in (H). Double asterisk (**) indicates a significant difference ($p < 0.05$) compared to the empty vector control (lane 1). All p-values were measured using a two sample Student's t-Test in Microsoft Excel and data is present as mean +/- SEM.

To determine if TXNIP interacts with the WW domains of WWP1, we transiently transfected vectors expressing full length FLAG-WWP1 (wildtype or a *4ww* mutant (W377F, P380A, W409F, P412A, W484F, P487A, F524A, P527A) which disrupts PY motif binding at all four WW domains) (*171*) and analyzed co-purification with TXNIP. We observed co-purification of TXNIP with wildtype FLAG-WWP1, but not the *4ww* mutant (**FIG 3.14C**), indicating that TXNIP binds to the WW domains of WWP1. By comparison, GLUT1 co-purified with both wildtype WWP1 and the 4ww variant, indicating the GLUT1-WWP1 interaction does not require intact WW domains. Together, these data indicate that GLUT1 interactions with TXNIP and WWP1 are mutually exclusive, which is inconsistent with the hypothesis that TXNIP functions as an adaptor that recruits WWP1 to modify GLUT1.

3.3.6 GLUT1 ubiquitin modification is regulated by glucose availability

Based on our results, we hypothesized that ubiquitin modification of GLUT1 promotes its trafficking to the lysosome for degradation. However, GLUT1 ubiquitylation has not previously been reported. Our analysis of GLUT1 in cell lysates by SDS-PAGE and immunoblot detected GLUT1 across a wide range of mobilities (**FIG 3.14**), suggesting many modified forms despite the fact that few post-translational modifications of GLUT1 have been reported. One documented modification of GLUT1 is N-linked glycosylation at Asn45 in the first extracellular loop (*79, 173*). Indeed, we found that treatment of affinity-purified GLUT1 with PNGase F (a deglycosylating enzyme specific for cleavage of N-glycans) altered its mobility by SDS-PAGE (**FIG 3.15A**), leading to accumulation of a lower MW form (around 40 kDa) which could represent unmodified GLUT1 (although the predicted MW of unmodified GLUT1 is 54 kDa).

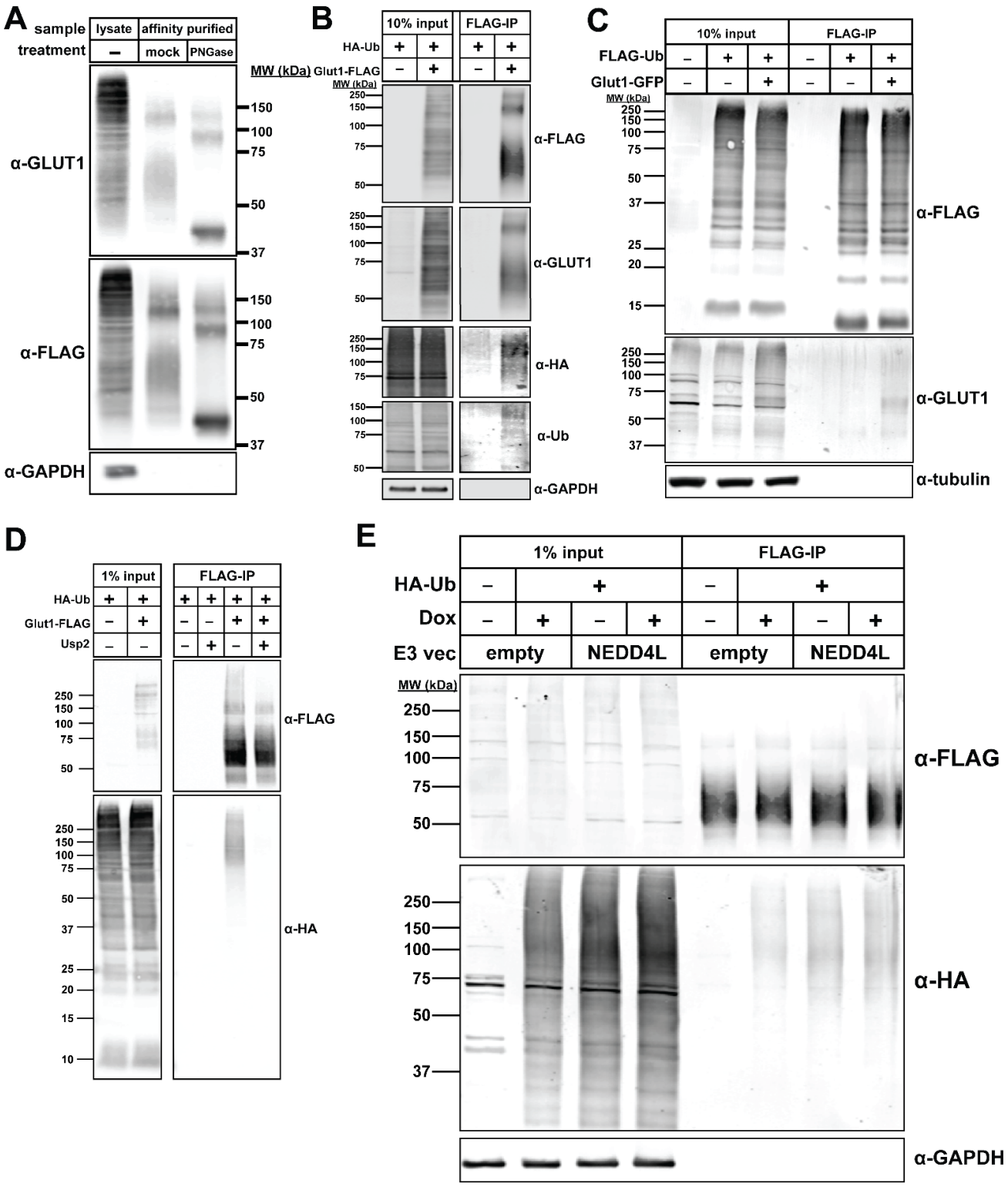

Figure 3.15: Characterization of GLUT1 ubiquitin modification, Related to **Figure 3.14**. **(A)** GLUT1-FLAG stably expressed in HeLa cells was affinity purified from cell lysates and either mock-treated or treated with PNGase F at 37ºC for an hour. **(B)** HeLa cells stably expressing an empty vector or GLUT1-FLAG were transiently transfected with an (**FIG 3.15** cont'd) HA-Ub expression vector and cultured to 100% confluency before cell lysates were collected. Lysates were incubated with αFLAG magnetic beads followed

by elution using FLAG peptide. Samples were resolved by SDS-PAGE and analyzed by immunoblot. GAPDH was used as a loading control. **(C)** HEK293T cells stably expressing FLAG-Ub were transiently transfected with a GLUT1-GFP expression plasmid. When cells reached 100% confluency, lysates were collected and incubated with αFLAG magnetic beads. FLAG-Ub was eluted using FLAG peptide. Samples were resolved by SDS-PAGE and analyzed by immunoblot. α-tubulin was used as a loading control. **(D)** HeLa cells stably expressing an empty vector or GLUT1-FLAG were transiently transfected with an HA-Ub expression vector and cultured to 100% confluency before cell lysates were collected. Lysates were incubated with α-FLAG magnetic beads followed by elution using FLAG peptide. Half of each eluate was incubated with Usp2 at 37ºC for an hour. Samples were resolved by SDS-PAGE and analyzed by immunoblot. **(E)** HeLa cells stably expressing constitutive GLUT1-FLAG and Dox-inducible TXNIP vectors were transiently transfected with either empty vector, HA-Ub, and/or Nedd4L, as indicated in the figures. 24 hours after inducing TXNIP with 1 μg/ml doxycyxline, cells were collected in lysis buffer and incubated with α-FLAG magnetic beads for 1 hour at 4ºC with rotation. GLUT1-FLAG was eluted with FLAG peptide and samples were resolved by SDS-PAGE then analyzed by immunoblot. GAPDH was used as a loading control. Quantification of results is provided in **FIG 3.14I**.

Interestingly, several high MW species persisted after PNGase F treatment (**FIG 3.15A**), suggesting the existence of high MW forms of GLUT1 that cannot be attributed to N-linked glycosylation.

To test the possibility that GLUT1 may be regulated by ubiquitin modification, we transiently transfected a vector expressing HA-tagged ubiquitin into HeLa cells expressing GLUT1-FLAG and then affinity purified GLUT1-FLAG from cell lysates. SDS-PAGE and immunoblot analysis revealed ubiquitin co-purifying with GLUT1-FLAG (**FIG 3.15B**). Similarly, using HEK293 cells stably expressing FLAG-Ubiquitin, we observed GLUT1 co-purifying with FLAG-Ub – and this co-purification was elevated when GLUT1-GFP was expressed exogenously in these cells (**FIG 3.15C**). Additionally, our analysis of affinity-purified GLUT1-FLAG revealed high molecular weight species that were decreased following treatment with the deubiquitylating enzyme USP2 (**FIG 3.15D**). In order to determine if GLUT1 ubiquitylation is regulated by glucose availability, we generated HEK293 cells stably expressing FLAG-Ubiquitin and measured GLUT1 co-purification with FLAG-Ubiquitin in the context of changing glucose availability. We observed a significant decrease (~50%) in the amount of GLUT1 co-purifying with FLAG-Ubiquitin following a switch from high (25 mM) glucose media to media without glucose (**FIG 3.14D-E**). Additionally, glucose repletion of starved cells triggered a significant increase in ubiquitin modification of GLUT1 (**FIG 3.14D-E**), indicating that ubiquitin modification of GLUT1 is increased in conditions that promote its endocytic trafficking.

Since GLUT1 ubiquitylation correlated with TXNIP expression (**FIG 3.14D**) we hypothesized that TXNIP may promote GLUT1 ubiquitylation in the presence of glucose. Indeed, high glucose levels are reported to increase TXNIP expression (*102,*

174). To test this hypothesis, we transiently expressed HA-tagged ubiquitin in *txnip* knockout HeLa cells which stably harbor *(i)* a doxycycline-inducible TXNIP expression vector, and *(ii)* a vector for constitutive expression of FLAG-tagged GLUT1. In these cell lysates, HA-ubiquitin co-purified with FLAG-GLUT1, but the amount of ubiquitin co-purification did not significantly change when TXNIP expression was induced (**FIG 3.14F-G**). To test if NEDD4 family E3 ubiquitin ligases regulates the ubiquitin modification of GLUT1, we performed the same experiment except we included a plasmid expressing either NEDD4L (a NEDD4 family member not known to interact with GLUT1 or TXNIP) or WWP1. We found that expression of either WWP1 or NEDD4L increased GLUT1 ubiquitin modification, but this increase was only statistically significant when TXNIP expression was induced (**FIG 3.14H-I** and **FIG 3.15E**). Taken together, these results indicate that GLUT1 ubiquitylation can be induced by co-expression of WWP1 or NEDD4L with TXNIP, but given the relatively modest effect these experiments do not strongly support an E3 adaptor function for TXNIP.

3.3.7 GLUT1 is ubiquitin modified on its major cytosolic loop

While our findings are consistent with ubiquitin modification of GLUT1 they do not exclude the possibility that GLUT1 may co-purify with interacting proteins that are ubiquitin modified. However, in an unbiased analysis of the ubiquitin-modified proteome of MDA-MB-231 cells we resolved a ubiquitin remnant (diGly) peptide from GLUT1 corresponding to ubiquitylation at Lys245 (**FIG 3.16A**). This position occurs within the large cytosolic loop of GLUT1, which contains multiple other lysine residues (**FIG 3.16B**). Due to the distribution of Lys and Arg residues, much of the GLUT1 major cytosolic loop is a tryptic “blind spot” for proteomic detection (**FIG 3.16B**). Thus, while our results indicate that GLUT1 can be modified at Lys245 we cannot exclude the

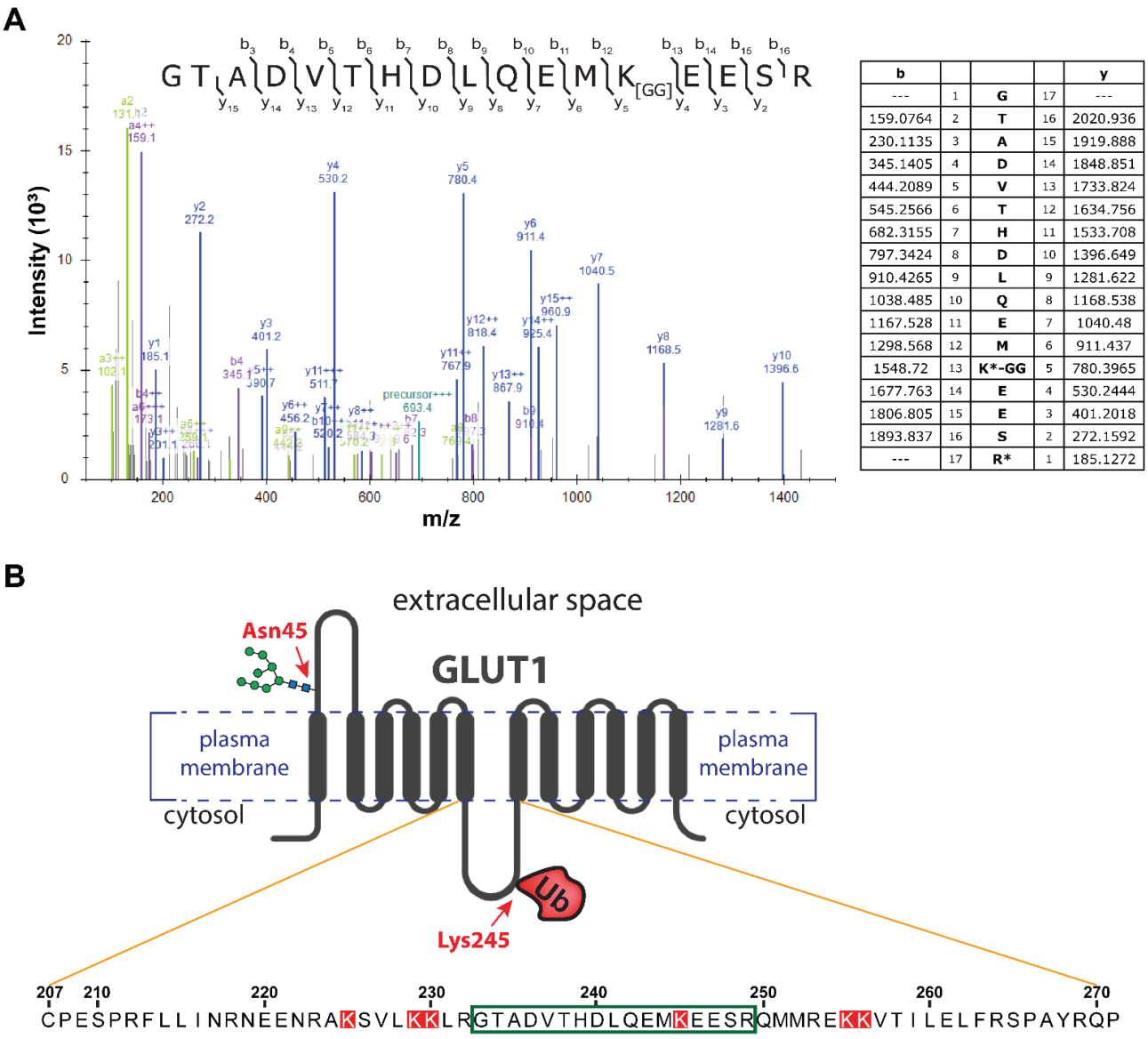

b				y
---	1	G	17	---
159.0764	2	T	16	2020.936
230.1135	3	A	15	1919.888
345.1405	4	D	14	1848.851
444.2089	5	V	13	1733.824
545.2566	6	T	12	1634.756
682.3155	7	H	11	1533.708
797.3424	8	D	10	1396.649
910.4265	9	L	9	1281.622
1038.485	10	Q	8	1168.538
1167.528	11	E	7	1040.48
1298.568	12	M	6	911.437
1548.72	13	K*-GG	5	780.3965
1677.763	14	E	4	530.2444
1806.805	15	E	3	401.2018
1893.837	16	S	2	272.1592
---	17	R*	1	185.1272

Figure 3.16: Evidence of GLUT1 ubiquitin modification on its major cytosolic loop, Related to **Figure 3.14**. **(A)** Enrichment of peptides containing ubiquitin remnant modifications (di-Gly) from tryptic digestion of MDA-MB-231 cell lysates revealed ubiquitin modification of GLUT1 at Lys245. The MS2 spectra of the peptide is shown at the top and the predicted fragmentation ions for the peptide is shown in the table below (generated using MS-Product (UCSF)). **(B)** Schematic of GLUT1 in the plasma membrane, illustrating the portions facing the cytosol. The detected ubiquitin modification on the major cytosolic loop of GLUT1 is shown. Below, the sequence corresponding to the major cytosolic loop of human GLUT1 is shown. All lysine residues in the major cytosolic loop, which represent potential sites of ubiquitin modification, are highlighted in red. The green box illustrates the ubiquitin-modified peptide that was resolved in (A).

possibility that other lysine residues in the major cytosolic loop are also ubiquitin-modified, or that additional ubiquitin modification occurs at other cytosol-facing Lys residues on the N- and C-terminal cytosolic tails.

3.3.8 Cytosol-facing lysines in GLUT1 regulate lysosomal trafficking in response to glucose

Given the role that ubiquitylation plays in regulating the trafficking of signaling receptors like GPCRs and EGFR (*175, 176*) we hypothesized that ubiquitylation of GLUT1 contributes to the regulation of its endocytosis and lysosomal trafficking in response to glucose stimulation. To test this, we generated HeLa cell lines stably expressing either wildtype GLUT1-GFP or a variant with Lys245 mutated to arginine (K245R) and we analyzed lysosomal trafficking in response to glucose stimulation. The K245R GLUT1 variant robustly trafficked to lysosomes following glucose stimulation, albeit with slightly lower LAMP1 co-localization compared to wildtype GLUT1 (**FIG 3.17A-B**). This result suggests that K245 is not required for glucose-stimulated lysosomal trafficking of GLUT1, although there may be multiple redundant ubiquitylation sites on GLUT1. To examine this possibility, we characterized the glucose-stimulated trafficking of a GLUT1 variant with all cytosolic lysine residues substituted for arginine ($11K_{cyto}\rightarrow R$; see **Table 3.1** for specific description of mutations). This variant exhibited a defect in glucose-stimulated lysosomal trafficking (**FIG 3.18A-B**) and was instead partially retained at the PM with some $11K_{cyto}\rightarrow R$ GLUT1-GFP internalized (**FIG 3.17C-D**). We hypothesized this internalized pool may localize to early endosomal compartments, given the low level of co-localization with LAMP1 (**FIG 3.18A-B**). Indeed, this GLUT1 variant exhibited increased colocalization with EEA1 following glucose

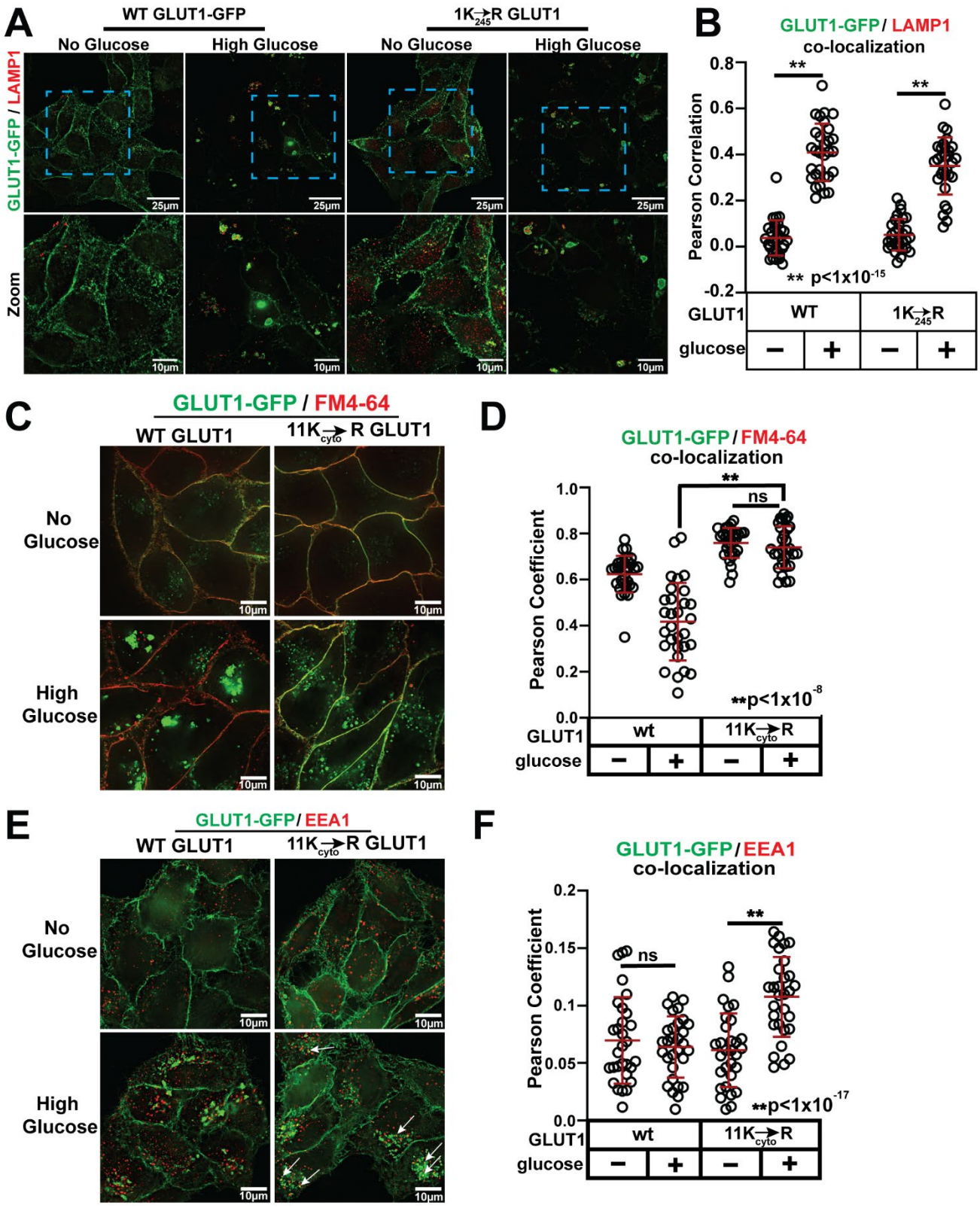

Figure 3.17: Characterization of the role of cytosol-facing lysine residues in glucose-stimulated GLUT1 trafficking to lysosomes, Related to **Figure 3.18. (A)** HeLa cells stably expressing either wildtype GLUT1-GFP or GLUT1-GFP with lysine 245 mutated

(**FIG 3.17** cont'd) to arginine ($1K_{245}$→R) were cultured as indicated prior to fixation and imaging for immunofluorescence detection of LAMP1 (red), a marker of lysosomal compartments. **(B)** Quantification of the results shown in panel A was performed by measuring the Pearson coefficient of correlation for 30 cells (n=30) with each condition indicated. **(C)** HeLa cells stably expressing either wildtype GLUT1-GFP or GLUT1-GFPwith all cytosolic lysines mutated to arginine ($11K_{cyto}$→R GLUT1) were cultured as indicated. Prior to imaging, cells were placed on ice and switched to cold (4°C) buffer containing the lipophilic tracer dye FM4-64 (8 μM) (red) in order to label the plasma membrane. Live cells were imaged in cold buffer immediately to ensure retention of FM4-64 at the plasma membrane. **(D)** Quantification of the results shown in panel C was performed by measuring the Pearson coefficient of correlation for 30 cells (n=30) with each condition indicated. **(E)** HeLa cells stably expressing either wildtype GLUT1-GFP or GLUT1-GFP with all cytosolic lysines mutated to arginine ($11K_{cyto}$→R) were cultured as indicated prior to fixation and imaging for immunofluorescence detection of EEA1 (red), a marker of early endosomal compartments. **(F)** Quantification of the results shown in panel E was performed by measuring the Pearson coefficient of correlation for 30 cells (n=30) with each condition indicated. All p-values were measured using a two sample Student's t-Test in Microsoft Excel. A P value < 0.05 was considered statistically significant and is indicated by **. Data are represented as mean +/- SEM. All measurements of Pearson coefficient of correlation were performed using Softworx software.

Designation	Protein	Variant	Description
WT	GLUT1	Wildtype, isoform 1 (canonical)	wildtype
$1K_{245}\rightarrow R$	GLUT1	K245R	K245R mutation
$11K_{cyto}\rightarrow R$	GLUT1	K6R, K7R, K225R, K229R, K230R, K245R, K255R, K256R, K451R, K456R, K477R	All cytosolic-facing Lys residues mutated to Arg
$6K_{loop}\rightarrow R$	GLUT1	K225R, K229R, K230R, K245R, K255R, K256R	All cytosolic loop Lys residues mutated to Arg
$5K_{tails}\rightarrow R$	GLUT1	K6R, K7R, K451R, K456R, K477R	All N- and C-terminal tail Lys residues mutated to Arg
1K245	GLUT1	K6R, K7R, K225R, K229R, K230R, K255R, K256R, K451R, K456R, K477R	Single Lys variant: K245
WT	TXNIP	Wildtype, isoform 1 (canonical)	wildtype
cb	TXNIP	L351A, L352A	Clathrin binding domain mutated
py	TXNIP	$PPCY_{334} \rightarrow PACA_{334}$ and $PPTY_{378} \rightarrow PATA_{378}$	Two C-terminal PY motifs mutated
WT	WWP1	Wildtype, isoform 1 (canonical)	wildtype
4ww	WWP1	W377F, P380A, W409F, P412A, W484F, P487A, F524A, P527A	All four WW domains mutated

Table 3.1: . Designations for mutant variants of GLUT1, TXNIP, and WWP1 used in this study.

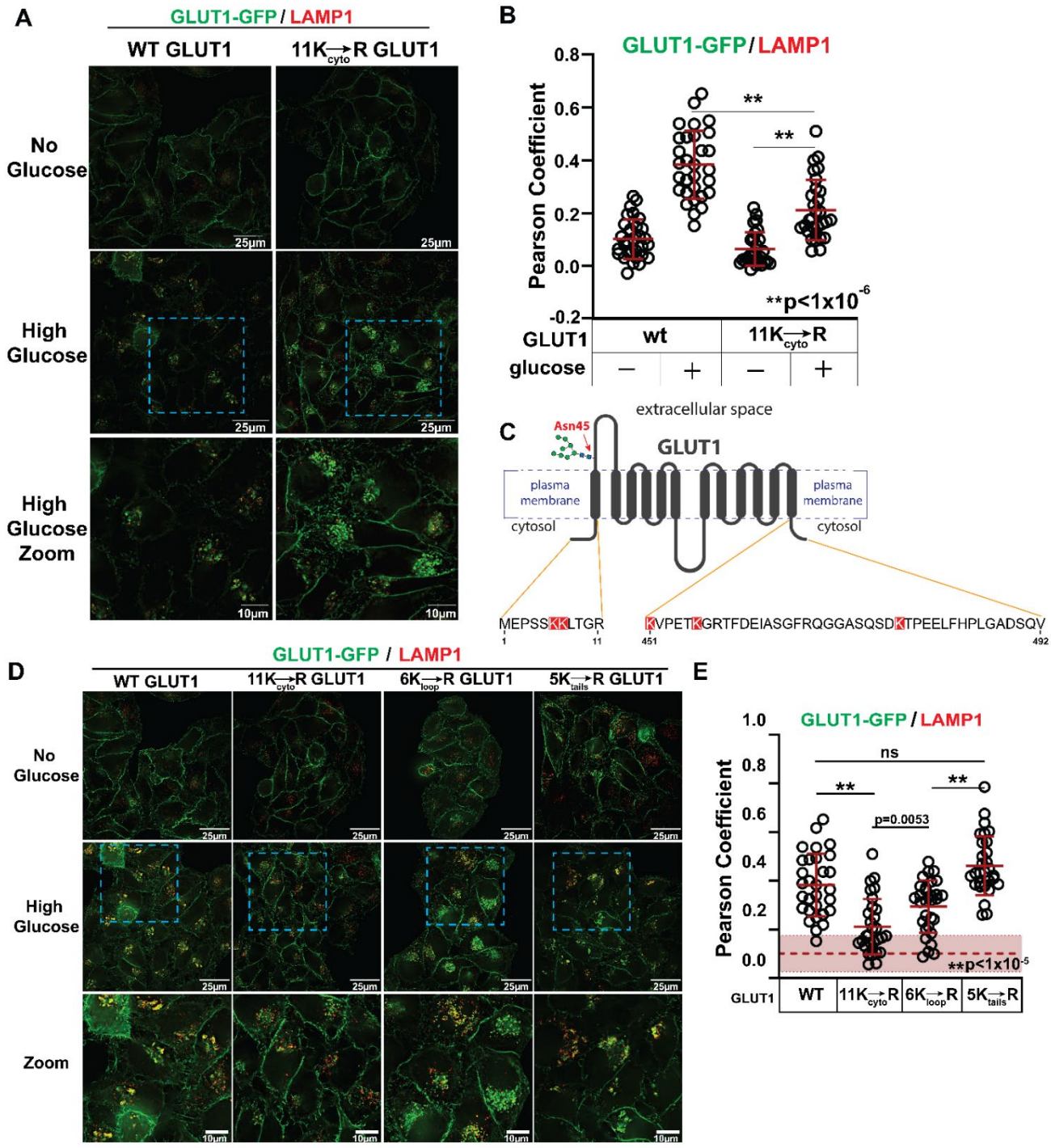

Figure 3.18. Mapping of cytosolic lysines required for lysosomal trafficking of GLUT1. **(A)** HeLa cells stably expressing either wildtype GLUT1-GFP or GLUT1-GFP with all cytosolic lysines mutated to arginine ($11K_{cyto}$→R) were cultured in media lacking glucose for 24 hours then cultured for another 24 hours in fresh media lacking glucose ("no glucose") or shifted to fresh media with high glucose (25 mM) for 24 hours ("high glucose") prior to fixation and imaging for immunofluorescence detection of LAMP1 (red). **(B)** Quantification of the results shown in (A) was performed by measuring the (**FIG3.18** cont'd) Pearson coefficient of correlation for 30 cells (n=30) with each condition indicated. **(C)** Schematic of GLUT1 illustrating the primary amino acid

sequence of N-terminal and C-terminal cytosolic tails. Lysine residues in the N-terminal and C-terminal cytosolic tails are highlighted in red. A similar schematic illustrating the lysine residues in the major cytosolic loop is shown in **FIG 3.16B**. **(D)** HeLa cells stably expressing either wildtype GLUT1-GFP, GLUT1-GFP with all cytosolic lysines mutated to arginine ($11K_{cyto}\rightarrow R$), GLUT1-GFP with the 6 lysines on the major cytosolic loop mutated to arginine ($6K_{loop}\rightarrow R$), or GLUT1-GFP with the 5 cytosolic lysines outside of the major loop mutated to arginine ($5K_{tails}\rightarrow R$) were cultured as in (A) prior to fixation and imaging for immunofluorescence detection of LAMP1 (red). **(E)** Quantification of the results shown in panel D was performed by measuring the Pearson coefficient of correlation for 30 cells (n=30) with each condition indicated. The dashed line and area shaded in red indicate the average Pearson's coefficient and standard deviation for the WT GLUT1-GFP colocalization with LAMP1 under glucose-starved conditions. All measurements of Pearson coefficient of correlation were performed using Softworx software. All p-values were measured using a two sample Student's t-Test in Microsoft Excel.

stimulation (**FIG 3.17E-F**), consistent with the interpretation that a portion of the $11K_{cyto}\rightarrow R$ GLUT1-GFP is retained at early endosomal compartments.

To test if K245 in the major cytosolic loop is sufficient to restore lysosomal trafficking of the $11K_{cyto}\rightarrow R$ GLUT1 variant, we analyzed glucose-stimulated trafficking of a GLUT1 variant harboring K245 as the only cytosol-facing Lys residue. This GLUT1 variant (designated 1K245) exhibited a defect in glucose-stimulated lysosomal trafficking compared to wildtype GLUT1 (**FIG 3.19A-B**), although this trafficking response was slightly greater compared to the $11_{cyto}K\rightarrow R$ variant (**FIG 3.18A-B**). Similarly, the 1K245 variant exhibited some retention at the plasma membrane compared to wildtype GLUT1 (**FIG 3.19C-D**), although the defect was not as severe as that observed for the $11_{cyto}K\rightarrow R$ variant (**FIG 3.17C-D**). These findings reveal that a single Lys residue in the 245 position of the cytosolic loop can facilitate some endocytic trafficking, although it is not sufficient to restore normal lysosomal trafficking in response to glucose stimulation.

In addition to the six Lys residues present in its major cytosolic loop (**FIG 3.16B**) GLUT1 also harbors two Lys residues at its N-terminal cytosolic tail and three Lys residues at its C-terminal cytosolic tail (**FIG 6C**). No other cytosol-facing Lys residues are present in the canonical GLUT1 isoform sequence used in this study, although we cannot exclude the possibility that other cytosol-facing Lys residues may exist in other isoforms or natural variants in human populations. To better understand how Lys residue position contributes to glucose-stimulated trafficking of GLUT1 we generated GLUT1 variants where all Lys residues in the major cytosolic loop or all N- and C-terminal tail Lys residues were substituted with Arg ($6K_{loop}\rightarrow R$ or $5K_{tails}\rightarrow R$, respectively) (**Table 3.1**). For the GLUT1 variant lacking Lys residues in the major

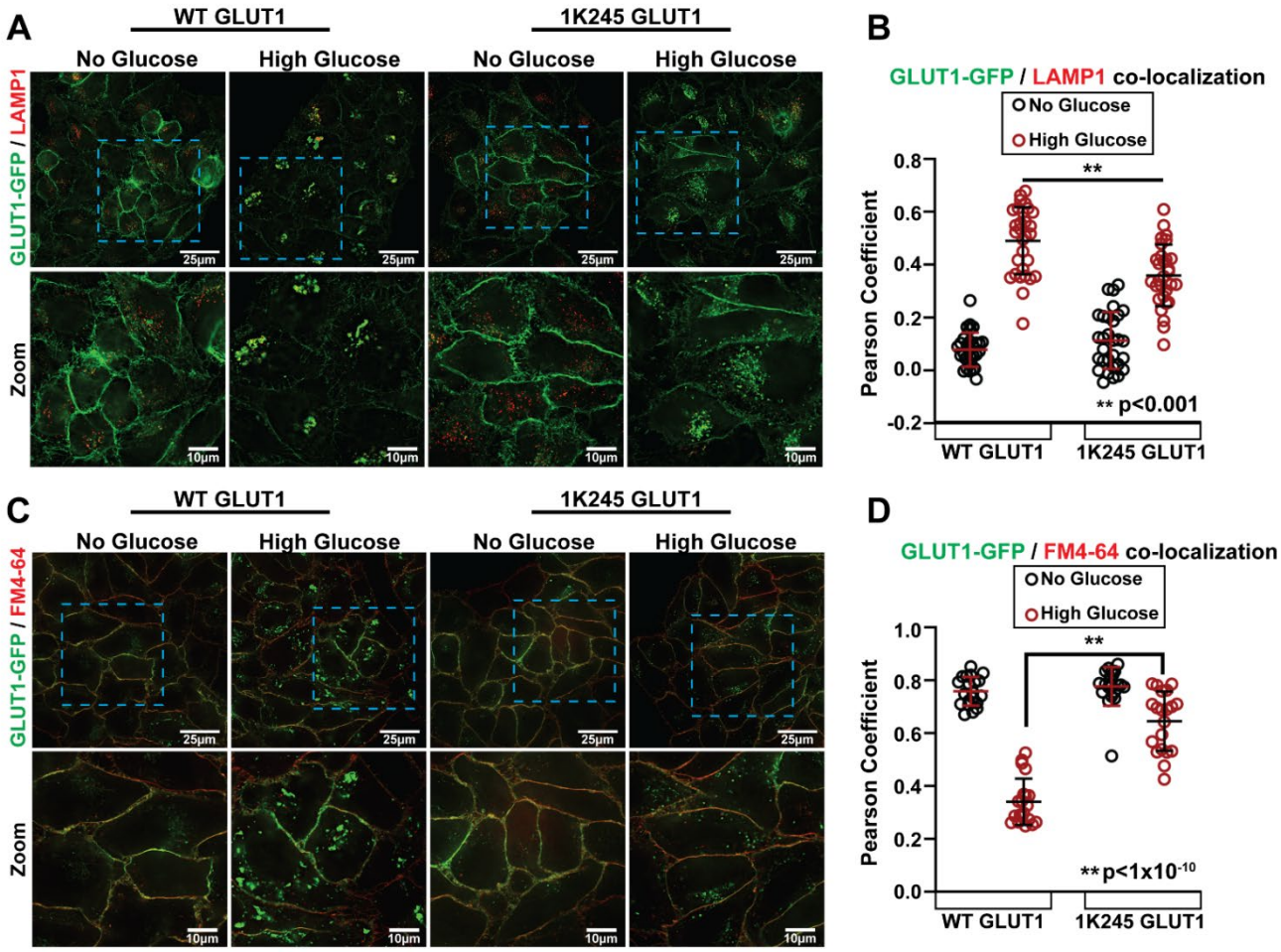

Figure 3.19: A GLUT1 variant harboring a single cytosolic lysine (K245) only partially restores glucose-stimulated endocytic trafficking, Related to **Figure 3.18**. **(A)** HeLa cells stably expressing either wildtype GLUT1-GFP or GLUT1-GFP with all cytosolic lysines mutated to arginine except K245 (1K245) were cultured as indicated prior to fixation and imaging for immunofluorescence detection of LAMP1 (red), a marker of lysosomal compartments. **(B)** Quantification of the results shown in panel A was performed by measuring the Pearson coefficient of correlation for 30 cells (n=30) with each condition indicated. **(C)** HeLa cells stably expressing either wildtype GLUT1-GFP or GLUT1-GFP (green) with all cytosolic lysines mutated to arginine except K245 (1K245) were cultured as indicated. Prior to imaging, cells were placed on ice and switched to cold (4°C) buffer containing the lipophilic tracer dye FM4-64 (8 μM) (red) in order to label the plasma membrane. Live cells were imaged in cold buffer immediately to ensure retention of FM4-64 at the plasma membrane. **(D)** Quantification of the results shown in panel C was performed by measuring the Pearson coefficient of correlation for 20 cells (n=20) with each condition indicated. All p-values were measured using a two sample Student's t-Test in Microsoft Excel. A P value < 0.05 was considered statistically significant and is indicated by **. Data are represented as mean +/- SEM. All measurements of Pearson coefficient of correlation were performed using Softworx software.

cytosolic loop ($6K_{loop}\rightarrow R$) we observed defects in glucose-stimulated lysosomal trafficking (**FIG 3.18D-E**) despite observing a significant decrease in PM localization (**FIG 3.20A-B**). These findings suggest retention of the GLUT1 $6K_{loop}\rightarrow R$ variant in endosomal compartments, which is consistent with an increase in observed co-localization with EEA1 (**FIG 3.20C-D**). In contrast, the GLUT1 variant lacking Lys residues at N- and C-terminal tails ($5K_{tails}\rightarrow R$) exhibited slight PM retention but no defect in lysosomal trafficking (**FIG 3.18D-E** and **FIG 3.20A-B**). The $5K_{tails}\rightarrow R$ variant did not exhibit early endosomal retention, based on co-localization with EEA1 (**FIG 3.20C-D**). Taken together, our results indicate that Lys residues in the major cytosolic loop appear to regulate endosomal sorting of GLUT1, while Lys residues at the N- and C-terminal tails may contribute to the regulation of GLUT1 endocytosis. However, loss of all cytoplasmic facing Lys residues results in a much more dramatic trafficking defect, indicating that Lys residues at each of these locations contributes to GLUT1 trafficking following glucose stimulation.

3.3.9 Cytosol-facing lysines in GLUT1 are required for its TXNIP-mediated endocytic trafficking

Our results indicate that glucose-stimulated trafficking of GLUT1 requires both TXNIP and ubiquitin modification, but the relationship between these two factors remains unclear – particularly given the lack of evidence supporting an E3 adaptor function for TXNIP. To better understand the relationship between TXNIP and ubiquitination in the regulation of GLUT1 trafficking, we tested if lysosomal trafficking of GLUT1 induced by TXNIP overexpression (as shown in **FIG 3.13A-B** and **FIG 3.12B-C**) requires ubiquitin modification, taking advantage of the $11K_{cyto}\rightarrow R$ GLUT1 variant which lacks cytosol-facing Lys residues. We found that the $11K_{cyto}\rightarrow R$ GLUT1 variant was

unresponsive to induced TXNIP overexpression, failing to traffic to lysosomes (**FIG 3.21A-B**) and instead exhibiting increased PM retention (**FIG 3.21C-D**). Thus, TXNIP-mediated GLUT1 endocytosis and lysosomal trafficking requires cytosol-facing Lys residues of GLUT1. These results are consistent with a role for ubiquitin modification in the regulation of GLUT1 downstream of TXNIP, however we cannot exclude the possibility that other lysine modifications (e.g., acetylation) may also play a role in the regulation of GLUT1 trafficking.

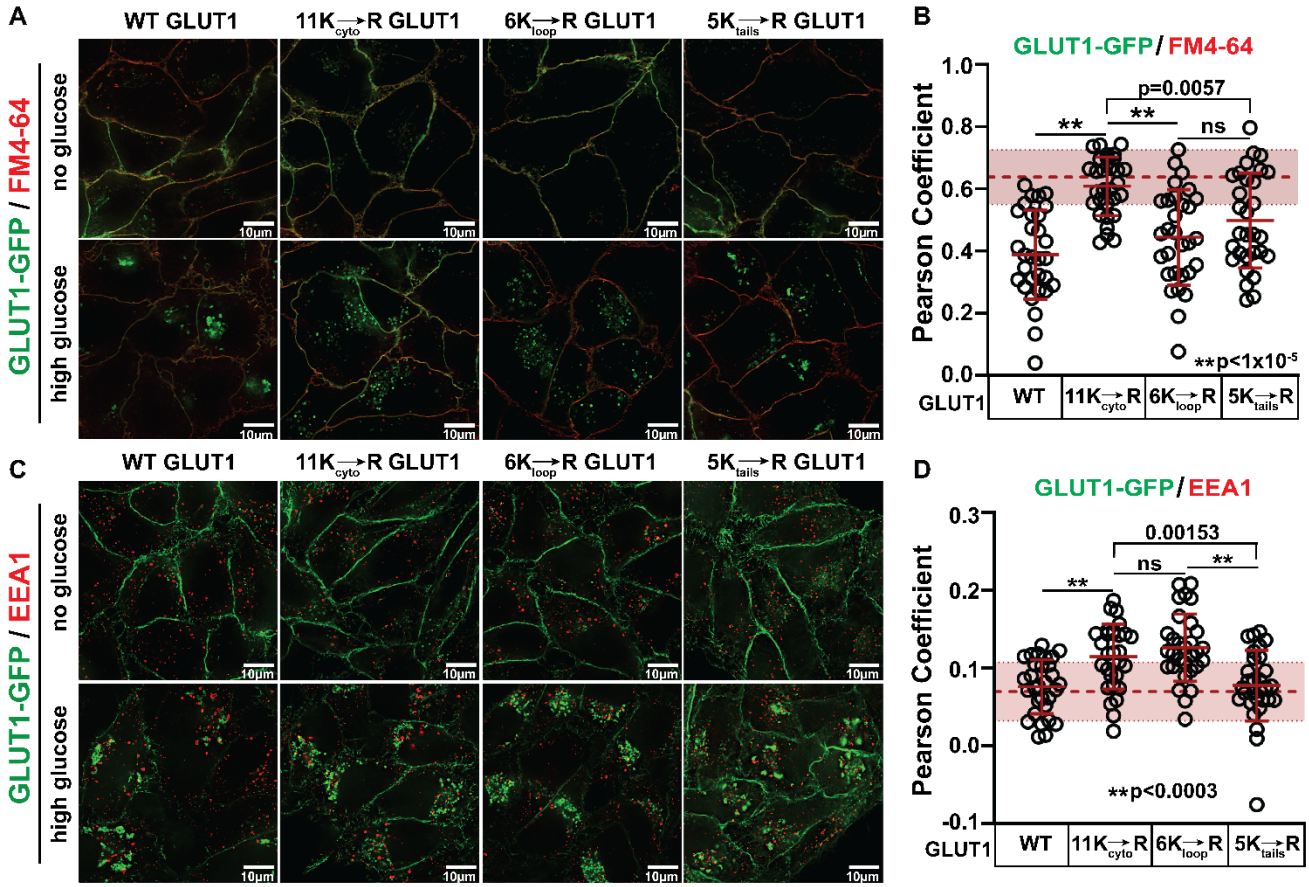

Figure 3.20: Characterization of the role of cytosol-facing lysine residues in glucose-stimulated GLUT1 trafficking, Related to **Figure 3.18. (A)** HeLa cells stably expressing either wildtype GLUT1-GFP, GLUT1-GFP with all cytosolic lysines mutated to arginine ($11K_{cyto}$→R), GLUT1-GFP with the 6 lysines on the major cytosolic loop mutated to arginine ($6K_{loop}$→R), or GLUT1-GFP with the 5 cytosolic lysines outside of the major loop mutated to arginine ($5K_{tails}$→R) were cultured as in **Fig3.1D.** Prior to imaging, cells were placed on ice and switched to cold (4°C) buffer containing the lipophilic tracer dye FM4-64 (8 μM) (red) in order to label the plasma membrane. Live cells were imaged in cold buffer immediately to ensure retention of FM4-64 at the plasma membrane. **(B)** Quantification of the results shown in panel (C) was performed by measuring the Pearson coefficient of correlation for 30 cells (n=30) with each condition indicated. The red dashed line indicates the average Pearson's coefficient for WT GLUT1-GFP with FM4-64 in "no glucose" media. The shaded area represents the standard deviation. **(C)** HeLa cells stably expressing either wildtype GLUT1-GFP, GLUT1-GFP with all cytosolic lysines mutated to arginine ($11K_{cyto}$→R), GLUT1-GFP with the 6 lysines on the major cytosolic loop mutated to arginine ($6K_{loop}$→R), or GLUT1-GFP with the 5 cytosolic lysines outside of the major loop mutated to arginine ($5K_{tails}$→R) were cultured as in **Fig 3.1D** prior to fixation and imaging for immunofluorescence detection of EEA1 (red). **(D)** Quantification of the results shown in panel (C) was performed by measuring the Pearson coefficient of correlation for 30 cells (n=30) with each condition indicated. The red dashed line indicates the average Pearson's coefficient for WT GLUT1-GFP with EEA1 in "no glucose" media. All p-values were measured using a two sample Student's

(**FIG3.20** cont'd) t-Test in Microsoft Excel. A P value < 0.05 was considered statistically significant and is indicated by **. Data are represented as mean +/- SEM. All measurements of Pearson coefficient of correlation were performed using Softworx software.

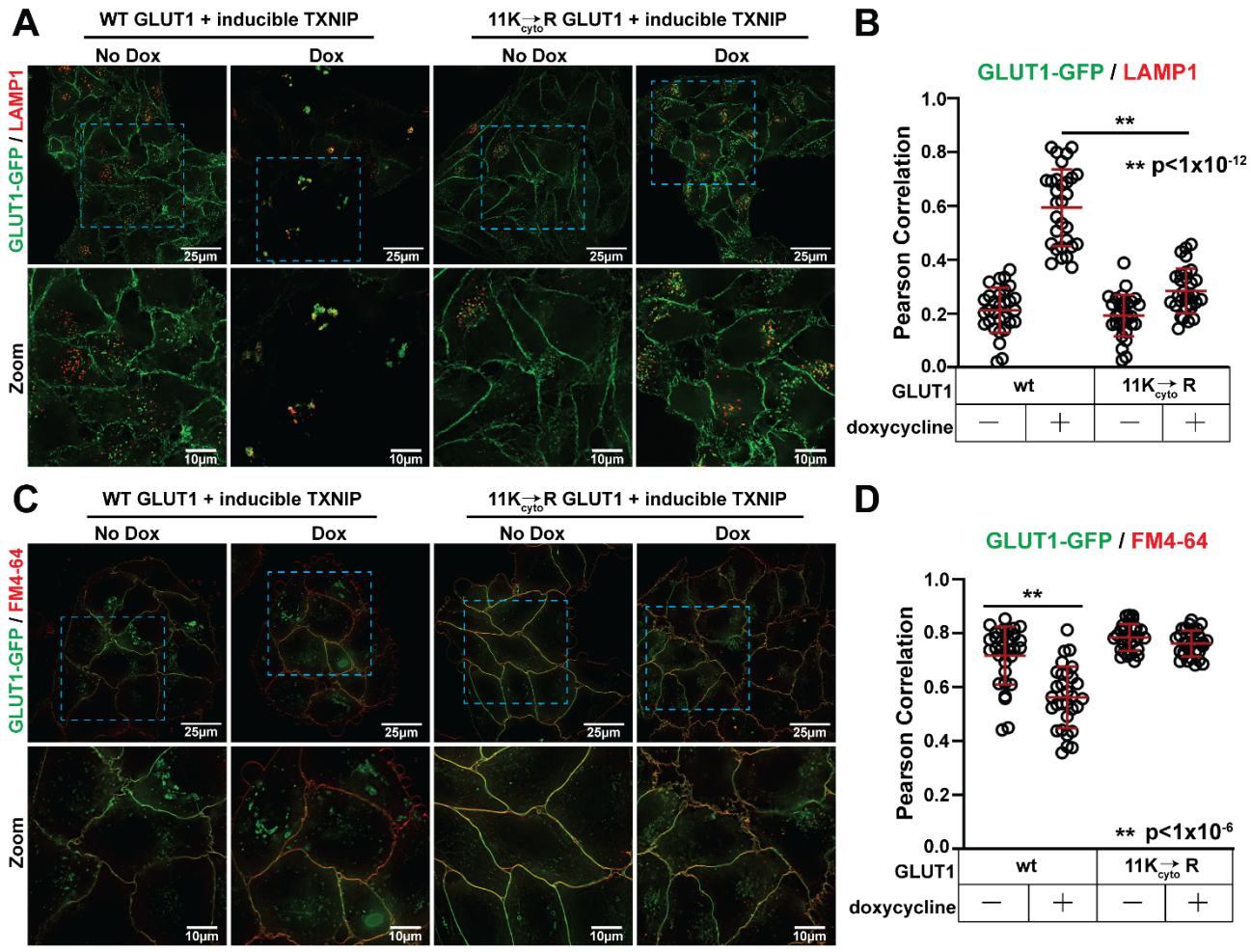

Figure 3.21. TXNIP-mediated trafficking of GLUT1 requires its cytosolic lysine residues. **(A)** HeLa cells stably expressing either wildtype GLUT1-GFP or GLUT1-GFP with all cytosolic lysines mutated to arginine ($11K_{cyto}\rightarrow R$) were also stably transfected with a doxycycline-inducible vector harboring wildtype TXNIP. Cells were cultured as indicated in **Figure 3.1D** prior to fixation and imaging for immunofluorescence detection of LAMP1 (red), a marker of lysosomal compartments. **(B)** Quantification of the results shown in panel A was performed by measuring the Pearson coefficient of correlation for 30 cells (n=30) with each condition indicated. **(C)** HeLa cells stably expressing either wildtype GLUT1-GFP or GLUT1-GFP with all cytosolic lysines mutated to arginine ($11K_{cyto}\rightarrow R$ GLUT1) were also stably transfected with a doxycyclin-inducible vector harboring wildtype TXNIP. Cells were cultured as indicated in **Figure 3.1D**. Prior to imaging, cells were placed on ice and switched to cold (4°C) buffer containing the lipophilic tracer dye FM4-64 (8 μM) (red) in order to label the plasma membrane. Live cells were imaged in cold buffer immediately to ensure retention of FM4-64 at the plasma membrane. **(D)** Quantification of the results shown in panel C was performed by measuring the Pearson coefficient of correlation for 30 cells (n=30) with each condition indicated. All p-values were measured using a two sample Student's t-Test in Microsoft Excel. All measurements of Pearson coefficient of correlation were performed using Softworx software.

3.4 Discussion

By characterizing the trafficking itinerary of GLUT1 during cellular adaptation to increased glucose availability, we have identified novel factors that regulate GLUT1 trafficking to lysosomes. We found that glucose concentrations above the Km trigger GLUT1 endocytosis and trafficking to lysosomes, and that substrate transport is sufficient to trigger this response. Furthermore, we report that ***(i)*** TXNIP variants defective for binding to NEDD4 E3 ubiquitin ligases are impaired for glucose-stimulated lysosomal trafficking of GLUT1, ***(ii)*** ubiquitin modifications associated with GLUT1 are regulated by glucose availability and are promoted by NEDD4L and WWP1, ***(iii)*** GLUT1 is ubiquitin modified on its major cytosolic loop, and multiple cytosol-facing Lys residues are involved in the regulation of GLUT1 trafficking, and ***(iv)*** these cytosol-facing Lys residues are required for TXNIP-mediated endocytic trafficking of GLUT1. Our results are consistent with a model of serial regulation of GLUT1 by TXNIP and ubiquitin modification, with a critical role for ubiquitin that occurs downstream of TXNIP-mediated regulation (**Figure 3.22)**.

3.4.1 Regulation of GLUT1 trafficking by TXNIP

TXNIP is reported to regulate GLUT1 endocytosis via its interaction with clathrin (*102*), and our analysis of a TXNIP variant defective for clathrin binding ($TXNIP^{cb}$) is consistent with this previous analysis (**FIG 3.13**). However, we also found that a TXNIP variant defective for binding to NEDD4 family E3 ubiquitin ligases ($TXNIP^{py}$) exhibited less glucose-stimulated GLUT1 lysosomal trafficking than both $TXNIP^{WT}$ and $TXNIP^{cb}$ variants (**FIG 3.13**) – despite the fact that both mutant variants are stabilized compared to wildtype TXNIP (**FIG 3.12I**). Expression of either TXNIP variant resulted in increased PM retention of GLUT1 compared to wildtype (**FIG 3.12J-K**), although GLUT1 PM

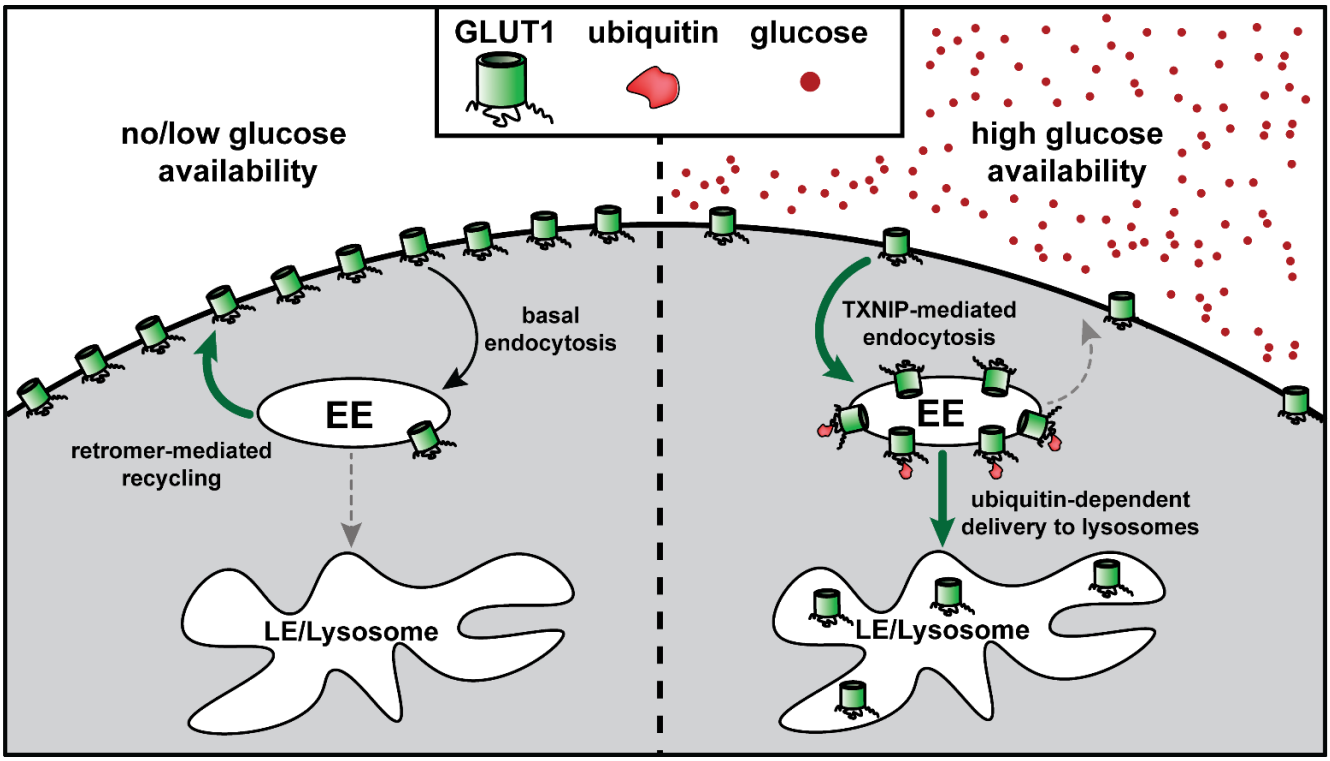

Figure 3.22: Model illustrating the glucose-induced trafficking of GLUT1 to the lysosome. In no/low glucose conditions, GLUT1 is recycled back to the membrane to maintain high levels of GLUT1 at the PM. In high glucose conditions, TXNIP induces endocytosis and the ubiquitin-dependent trafficking of GLUT1 to the late endosome/lysosome.

retention was slightly greater of in the case of TXNIP^{cb} expression. Indeed, when the TXNIP^{py} variant is expressed, GLUT1 appears to exhibit increased accumulation inside the cell (**FIG 3.13F** and **3.12J**) suggesting it may be retained on early endosomal compartments. These findings indicate that TXNIP plays multiple roles at distinct steps in the GLUT1 trafficking itinerary, with clathrin binding important for endocytic clearance from the PM and PY motifs important for regulating endosomal sorting and the decision to recycle or commit to lysosomal trafficking. Since TXNIP has also been implicated in the insulin-stimulated trafficking of GLUT4 (*154*) it will be interesting for future studies to determine if clathrin-binding and E3-binding motifs of TXNIP also contribute to the regulation of GLUT4.

Based on studies of arrestin-related proteins in yeast (*175, 177*) we hypothesized that TXNIP may function as an adaptor for human NEDD4 family members. As expected, mutation of the C-terminal PY motifs in TXNIP abolished binding to WWP1 (**FIG 3.14A-B**) and ITCH (*138, 153*), and this mutant variant of TXNIP was impaired for glucose-stimulated GLUT1 trafficking (**FIG 3.13**). Unexpectedly, we found that ubiquitin modification of GLUT1 and its association with WWP1 occurs independently of TXNIP. These findings do not support an adaptor function for TXNIP, despite revealing a critical role for TXNIP PY motifs in glucose-stimulated clearance of GLUT1. One possible explanation is that TXNIP, although dispensable for recruitment of NEDD4 family E3s to GLUT1, might promote activation of E3 activity (*178, 179*), perhaps by relieving an inhibitory state in response to glucose. Similarly, TXNIP may not contribute to recruitment of NEDD4 family E3 ligases to GLUT1 but may instead confer glucose-sensitive regulation of E3 activity towards GLUT1. However, since the PY motifs of

TXNIP may not interact exclusively with NEDD4 family E3 ubiquitin ligases, we cannot exclude the possibility that they regulate GLUT1 trafficking via other regulatory interactions which have not yet been characterized. It will be important to determine how the PY motifs of TXNIP contribute to the regulation of GLUT1, since this mechanism appears to be distinct and independent of clathrin binding.

3.4.2 Regulation of GLUT1 trafficking by ubiquitylation

Despite its broad expression and importance for basal glucose uptake in many cells and tissues, not much is known about post-translational mechanisms of GLUT1 regulation, in part because few GLUT1 post-translational modifications (PTMs) have been reported and characterized. To our knowledge, the only PTMs previously reported for GLUT1 are N45 glycosylation (*79*) and S226 phosphorylation (*105*). In this study, we present evidence that GLUT1 is subject to additional regulation by ubiquitylation, with specific ubiquitin modification detected on Lys245 within the major cytosolic loop. Since cytosol-facing Lys residues are required for glucose-stimulated trafficking of GLUT1, we propose that ubiquitin conjugation to GLUT1 at multiple Lys residues is critical for this response. In particular, Lys residues of the major cytosolic loop are critical for glucose-stimulated GLUT1 trafficking (**FIG 3.18**) – although Lys245 by itself is dispensable for GLUT1 trafficking to the lysosome in HeLa cells (**FIG 3.17A-B**). Our analysis of GLUT1 mutant variants targeting different combinations of cytosol-facing Lys residues reveals the potential for complex regulation of GLUT1 by ubiquitin conjugation at multiple sites.

GLUT1 mutations are associated with GLUT1 Deficiency Syndrome (GLUT1-DS) (*113, 180, 181*), and we examined patient mutations to determine if any mapped to Lys residues in the major cytosolic loop. Interestingly, one GDS patient was reported to harbor the K256V mutation (*180*) in the major cytosolic loop of GLUT1. Some have

speculated this mutation could affect GLUT1 interactions with negatively charged lipid head groups (*113*). However, the K256V mutation could also prevent ubiquitin modification – although further experimental analysis will be required to distinguish between these possibilities.

Our data also reveal a role for NEDD4 family E3 ubiquitin ligases in the regulation of GLUT1 and its associated ubiquitin modifications (**FIG 3.14H-I**). Specifically, both NEDD4L and WWP1 promoted ubiquitylation associated with GLUT1, and this activity was slightly enhanced in the presence of TXNIP. We cannot exclude the possibility that other ARRDC family proteins may function redundantly in the targeting of GLUT1 for ubiquitylation. Additional experiments will be needed to address the role of WWP1, NEDD4L, and other NEDD4 family E3 ubiquitin ligases in the regulatory trafficking of GLUT1.

3.4.3 An emerging model for GLUT1 trafficking in response to glucose stimulation

Despite established roles for GLUT1 regulation by TXNIP (*102*) and retromer (*97, 100, 167*) many gaps remain in our understanding of GLUT1 trafficking. In this study, we address some of those gaps by identifying a role for ubiquitin modification as a regulator of GLUT1 lysosomal trafficking. Our data suggests that TXNIP has multiple functions that regulate GLUT1 trafficking – including clathrin binding and binding to E3 ubiquitin ligases. Likewise, mutational analysis of GLUT1 suggests that ubiquitin modifications are involved in the regulation of endosomal sorting and lysosomal trafficking. Based on our results, we propose the following model for glucose-regulated GLUT1 trafficking. In conditions of glucose starvation, TXNIP is degraded and ubiquitin association with GLUT1 is low, leading to low levels of endocytic clearance from the PM and a higher efficiency of retromer-mediated recycling on endosomes. In this state,

GLUT1 remains relatively stable at the PM. In conditions of high extracellular glucose, TXNIP is stabilized and ubiquitylation of GLUT1 is increased, leading to an increased rate of endocytosis and decreased efficiency of retromer-mediated recycling on endosomes. It is possible that ubiquitylation of GLUT1 on its cytosolic loop interferes with recognition by retromer while also facilitating capture by ubiquitin binding elements of the ESCRT pathway, sorting it into the MVB pathway for delivery to lysosomes. Together, TXNIP association and ubiquitin modification both contribute to the steady state localization of GLUT1, toggling between a state of PM stability and one of targeting for delivery to lysosomes. Lysosomal delivery is typically associated with degradation, however we cannot exclude the possibility that GLUT1 may transport glucose across lysosomal membranes. But many important questions remain surrounding the mechanisms that regulate GLUT1 ubiquitin modification in response to changing glucose levels. Ultimately, deeper understanding of how glucose availability and sensing pathways toggle between these states will facilitate new insights into mechanisms of disease and possibly identify new targets for therapeutic intervention

ACKNOWLEDGEMENTS

We are grateful to T. Graham and N. Hepowit for critical reading of the manuscript. We are also grateful to K. Rose, O. McDonald, Q. Zhang, R. Coffey, J. Goldenring, L. Lapierre, and Y. Mao for technical advice and insightful discussions. This study was funded by NIH grants RG35M144112 (to JAM) and a Vanderbilt-Ingram Cancer Center GI-SPORE pilot award (P50CA236733).

Chapter 4

Biochemical characterization of the TXNIP-GLUT1 axis

4.1 Summary

In this chapter, I present a series of experiments to better characterize the biochemical features of TXNIP and GLUT1. First, I share the results from a TXNIP interaction profile performed using SILAC-mass spectrometry (MS). Next, I present experiments investigating the post-translation modifications (PTMs) found on GLUT1. Finally, I further characterize the components involved in regulation of GLUT1.

4.2 TXNIP Interaction profile

In order to characterize the TXNIP protein interaction profile, I adopted the stable isotope labelling with amino acids in cell culture mass spectrometry (SILAC-MS) approach. First, I generated cells expressing FLAG-TXNIP and labeled them with regular ("light") lysine and arginine, while control cells expressing an empty FLAG-tag vector were labeled with heavy lysine and arginine (containing ^{13}C and ^{15}N isotopes). After FLAG affinity purification from both lysates, samples were combined and digested with trypsin before peptide clean up and analysis by LC-MS/MS. MaxQuant software was used to analyze the data and calculate a light-to-heavy ratio for each peptide detected. We considered a protein a hit if it exhibited a light: heavy ratio greater than 5 based on quantification of at least three peptides (**Table 4.1**). This analysis identified several proteins already known to interact with TXNIP such as thioredoxin, ubiquitin, clathrin heavy chain, and GLUT1. My analysis also revealed a number of interactions that have not previously been reported. These fall into three functional categories: ubiquitin ligases, trafficking proteins, and proteins involved in metabolism. Two E3 ubiquitin ligases, NEDD4L and UBR4, were shown to be TXNIP interactors. NEDD4L is a member of the NEDD4 family of ubiquitin ligase and contains WW domains that could potentially interact with the PY motifs on TXNIP. Also I demonstrated in **Chapter 3** that NEDD4L increases ubiquitylation of GLUT1 **(Figures 3.14I** and **3.15E)**. It would be

SILAC-based interaction profile of TXNIP in MDA-MB-231 cells		
Hit	**% Coverage**	**Description**
TXNIP	75.2	ARRDC family protein; bait
Thioredoxin	49.5	redox homeostasis
Ubiquitin	46.2	protein degradation
NEDD4L	13.4	E3 ubiquitin ligase
Clathrin heavy chain	12.5	vesicle coat protein
GLUT1	8.5	glucose transporter
DLDH*	8.4	lipoamide dehydrogenase
GCN1*	6.8	kinase activator; integrated stress response
Dynamin-2*	5.2	GTPase; vesicle scission
UBR4	2.9	E3 ubiquitin ligase
Myoferlin*	2.8	Membrane fusion; endocytic recycling

Table4.1: Cells expressing empty vector (heavy) and cells expressing TXNIP-FLAG (light) were compared by SILAC-MS. Table selected shows hits using the following criteria: (1) number of peptides quantified ≥ 3; (2) L:H ratio > 5. (*indicates a previously unidentified interactor)

interesting to investigate the role of NEDD4L in GLUT1 regulation more in depth. UBR4 was found to be interact with TXNIP in conjunction with two other E3 ubiquitin ligases, UBR5 and HUWE1. When these three ligases are knocked down, ITCH-dependent degradation of TXNIP is significantly impaired (*182*). UBR4 is a member of the ubiquitin ligases of the N-end rule pathway (UBR) family of E3 ligases that bind to destabilizing N-terminal residues, or N-degrons. The UBR family is highly conserved across eukaryotes. While they remain poorly characterized, UBRs have been reported to be involved in protein quality control, G-protein-coupled receptors, apoptosis, and mitochondrial control (*183, 184*). The TXNIP interactome also revealed two previously unidentified interactors involved in trafficking: Dynamin-2, a GTPase involved in vesicle scission from the PM during endocytosis (*185*) and Myoferlin, a membrane-anchored protein involved in membrane fusion, repair, and trafficking (*186*). Lastly, the TXNIP interaction profile revealed two proteins involved with metabolism and stress response. Dihydrolipoamide dehydrogenase (DLDH) is part of a series of enzymes that convert pyruvate into acetyl-coA, oxidizing dihydrolipoamide and producing ROS in the process (*186*). As discussed in **Chapter 1,** TXNIP is involved in redox balance, inhibiting thioredoxin and consequently increasing ROS. GCN1 is a protein kinase that is activated as part of the integrated stress response in cells (*187*). TXNIP is also involved in signaling pathways that respond to stress. For example, it is phosphorylated by AMPK, which is activated when the cell is under metabolic stress. Identification of a TXNIP-GCN1 interaction raises the possibility that TXNIP could be a substrate of GCN1. Although these data may fuel new hypotheses about the regulation and function of TXNIP, future studies will need to validate these interactions using biochemical methods such as co-immunoprecipitation.

4.3 Post-translational modifications of GLUT1

Despite its broad significance for glucose metabolism, very little is known about the post-translation modifications that regulate GLUT1. There is evidence that N-glycosylation of GLUT1 is required for proper glucose transport, subcellular localization, and stability (*103, 188*). There is one study that shows phosphorylation of GLUT1

enhances cell surface localization and glucose uptake (*105*). Ubiquitylation of GLUT1 has not been reported previously. In my analysis of GLUT1, I sought to better characterize the post-translational modifications of GLUT1, which may lead to a better understanding of how GLUT1 is regulated.

4.3.1 Identifying other PTMs on GLUT1

GLUT1 resolved by SDS-PAGE and immunoblotting exhibits a smeared pattern, suggestive of extensive post-translational modification. When GLUT-FLAG was treated with PNGase F (which removes N-glycosylation), the smears are converted to two clear bands (one around 40kD and one around 100kDa) and a high molecular weight smear **(Figure 4.1)**. This pattern indicates that N-glycosylation of GLUT1 contributes to the smear by SDS-PAGE, but additional modification results in multiple forms of GLUT1 from cell lysates. To probe the nature of these forms, I treated purified GLUT1 with Usp2, a promiscuous deubiquitylase that removes most polyubiquitin modifications, and shrimp alkaline phosphatase (SAP), which reverses protein phosphorylation. In **Figure 4.1A**, purified GLUT1 was treated with each enzyme individually. The PNGase F had the most dramatic effect,; however, there is a clear change in banding pattern with both Usp2 and SAP treatment **(Figure 4.1A-B)**. This indicates that GLUT1 is subjected to ubiquitylation and phosphorylation. In **Figure 4.1C**, Usp2 and SAP were added to GLUT1 along with PNGase F, and then all three enzymes were incubated with the protein at once. Layering Usp2, SAP, or both on top of PNGase F had a virtually indistinguishable effect on the banding pattern of the GLUT1 on the immunoblot. Taken together, this data indicates that GLUT1 is subjected to extensive glycosylation and, while there is phosphorylation and ubiquitylation present, it is hard to resolve by SDS-PAGE and immunoblot.

Because the low molecular weight band shown in PNGase F-treated GLUT1 immunoblots is smaller than the predicted weight of GLUT1 (~55kDa) (**Figure 4.1**), I designed an experiment to confirm this was not the result of proteolytic processing. An HA-tag was added to the first exofacial loop of GLUT1 (after residue 53) in addition to the FLAG-tag on the C-terminus of the protein. This HA-GLUT1-FLAG construct was subsequently expressed in cells then purified and treated with PNGase F. Analysis by SDS-PAGE and immunoblot shows that the same low molecular weight band remains in GLUT1, HA, and FLAG immunoblots **(Figure 4.2)**, which suggest that the band is the

result of full length GLUT1 protein. However, because the HA tag is in the first exofacial loop rather than the N-terminus of GLUT1, a proteolytic event in the first 53 residues cannot be ruled out.

To further investigate phosphorylation and ubiquitylation, other approaches are needed, such as the lysine-to-arginine mutations performed in **Chapter 3 (Figure 3.18).** This effectively renders GLUT1 unable to be ubiquitylated on its cytosolic face so that any effect on GLUT1 trafficking can be observed. Similarly, phosphorylation can be interrogated by observing any GLUT1 trafficking phenotype that arises from mutation of potential phosphorylation sites (cytoplasmic serine, threonine, and tyrosine residues) to alanine residues. Mass spectrometry experiments are another approach for identifying PTMs. I have previously attempted SILAC-MS analysis of GLUT1; however, I was not able to resolve any peptides. I suspect that the SILAC-MS protocol I utilized would need to be optimized for membrane proteins. Alternatively, quantitative ubiquitin remnant profiling is an unbiased approach for identifying ubiquitylated proteins in the cell. This method was used to identify the ubiquitylation of Lys245 reported in **Chapter 3** (**Figure 3.16**). This experiment could yield more ubiquitin remnants on GLUT1 if an alternative enzyme was used to digest the purified protein, such as ArgC, which cleaves at the C-terminus of arginine residues. The major cytosolic loop of GLUT1 is a tryptic “blind spot” due to the amino acid sequence having a large number of lysines and arginines, which is where trypsin cuts.

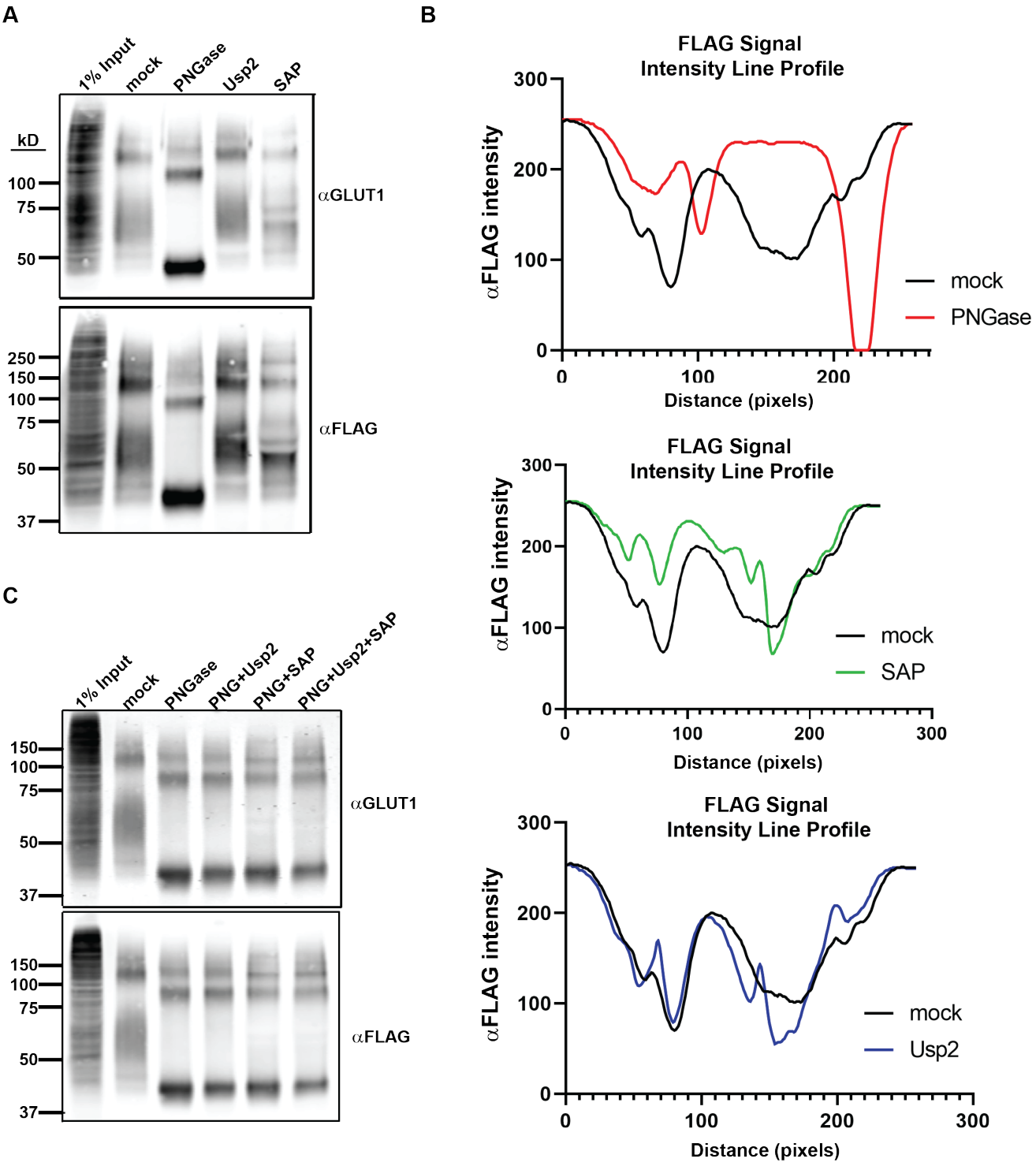

Figure 4.1: Treatment of GLUT1-FLAG IP with various enzymes. A) GLUT1-FLAG is pulled down using αFLAG beads and treated with either mock, PNGase F, Usp2, or SAP. B) Line profile of the FLAG signal intensity for the immunoblot in (A). C) GLUT1-FLAG pull down as shown in (A), with enzymes used in combination with PNGase F.

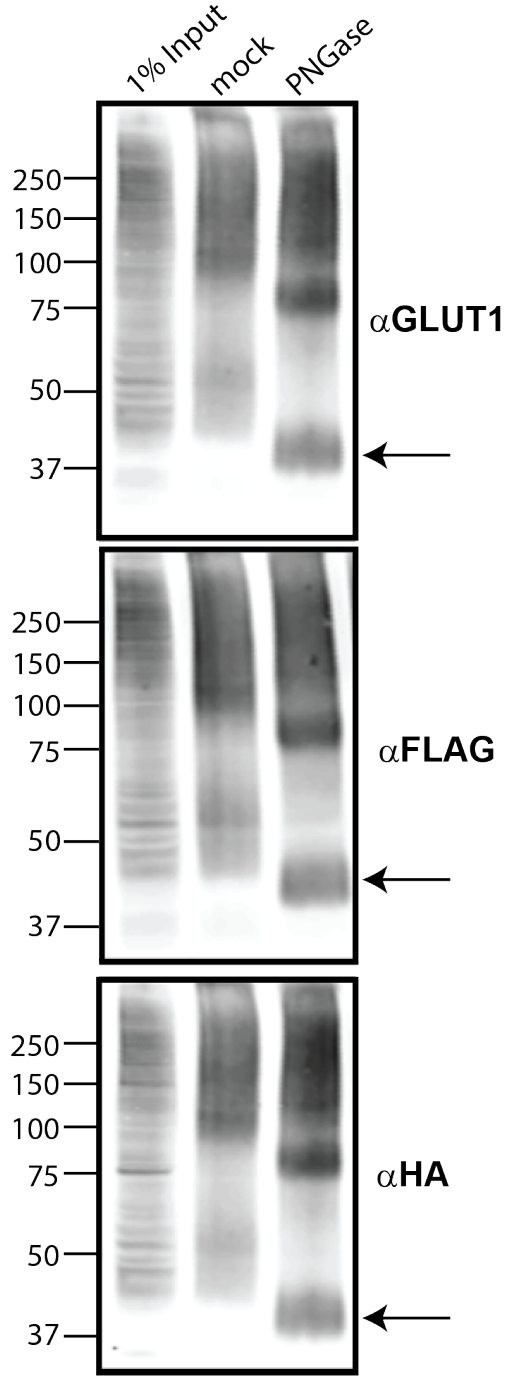

Figure 4.2: PNGase treatment of HA-GLUT1-FLAG IP. Immunoblot was probed with GLUT1, FLAG, and HA antibodies to confirm the low molecular weight is full length GLUT1. Arrows indicate the low molecular weight band in question.

4.4 Validation of GLUT1 lysosomal delivery by GFP clipping

GFP is resistant to the acidity and proteases of the lysosomal compartment (*189*), which results in a free, 25 kD GFP band on immunoblots "clipped" from the degraded protein when visualizing GFP-tagged proteins by immunoblot. The quantity of free GFP correlates with the quantity of degraded protein. I used GFP clipping analysis to measure the effect of various conditions on GLUT1 degradation.

4.4.1 Investigating the role of TXNIP PY motifs on GLUT1-GFP degradation

In order to interrogate the requirement of TXNIP PY motifs in lysosomal trafficking of GLUT1, I compared the accumulation of clipped GFP when GLUT1-GFP HeLa cells were transfected with either WT or PY mutant TXNIP. When quantified on an immunoblot, the accumulation of free GFP was significantly increased with WT TXNIP overexpression. Overexpression of $TXNIP_{PY}$, on the other hand, showed no significant difference in free GFP in comparison to the empty vector control **(Figure 4.3)**. This suggests a role for the PY motifs of TXNIP in GLUT1 trafficking and degradation. This is consistent with the defect in GLUT1-GFP trafficking seen with $TXNIP_{PY}$ expression in **Figure 3.13F-G.**

The experiments in this chapter have provided additional characterization of TXNIP's interactors, PTMs on GLUT1, and the negative regulation of GLUT1. The results presented here raise several questions: what is the functional purpose of TXNIP's interaction with these newly discovered interactors? Are there more ubiquitylation and phosphorylation sites on GLUT1 in addition to the few that have been reported. And why are the PY motifs of TXNIP needed for GLUT1 degradation?

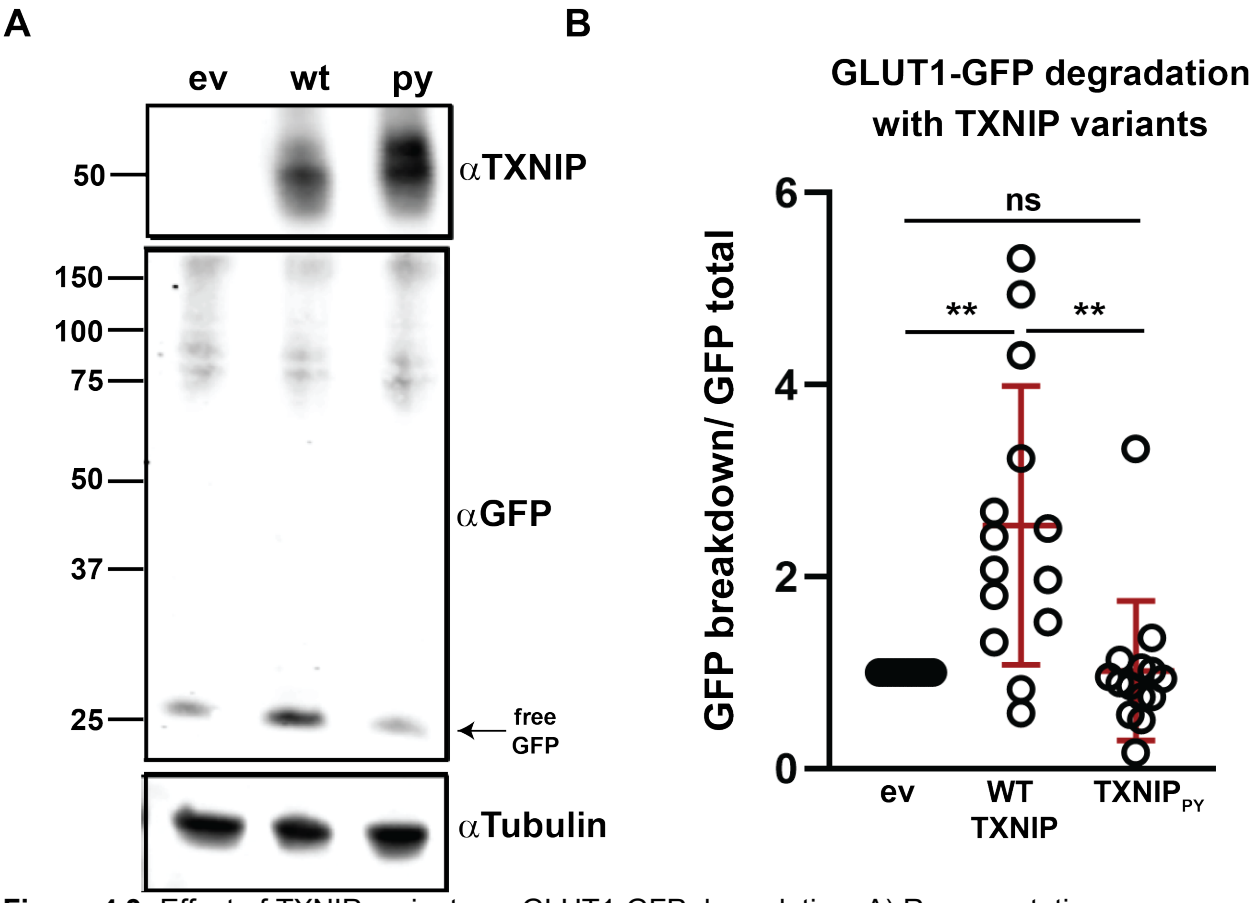

Figure 4.3: Effect of TXNIP variants on GLUT1-GFP degradation. A) Representative immunoblot showing the change in free GFP (at 25kD). Empty vector (ev), wild type TXNIP (wt), and $TXNIP_{py}$ (py) overexpression vectors were transfected into GLUT1-GFP HeLa cells. Whole cell lysates were collected and analyzed by immunoblot. B) Quantification of free GFP**:** total GFP under each condition. n=14 biological replicates. Quantification of blots performed using FIJI. Student's t-test done in Microssoft Excel, **<0.005.

Chapter 5

Discussion

5.1 Summary

In **Chapter 3,** I presented evidence that **(i)** GLUT1 traffics through endocytic compartments to lysosomes in response to increased glucose, **(ii)** both the clathrin-binding site and E3-binding PY motifs of TXNIP are required for GLUT1 trafficking, **(iii)** GLUT1 ubiquitylation is regulated by glucose availability, **(iv)** GLUT1 is ubiquitylated on its major cytosolic loop, and **(v)** the cytosolic lysines of GLUT1 are required for regulation of endocytic trafficking downstream of TXNIP. In **Chapter 4,** I report the results of a TXNIP interaction profile using SILAC-MS and share additional experiments characterizing the role of ubiquitin and TXNIP in GLUT1 regulation. These findings contribute to our understanding of the mechanisms regulating GLUT1 and glucose uptake needed to maintain glucose homeostasis.

5.2 Models of GLUT1 trafficking regulation by TXNIP and ubiquitin

The data presented in **Chapters 3** and **4** demonstrate that GLUT1 is ubiquitylated in response to increased glucose levels and that the lysines of GLUT1 are important for proper GLUT1 lysosomal trafficking. The data also suggest that the clathrin-binding motif and PY motifs of TXNIP are necessary for proper GLUT1 trafficking to the lysosome. **Figure 3.22** presents a general model for this TXNIP- and ubiquitin-dependent trafficking of GLUT1 to lysosomes under high glucose conditions; however, the details of this trafficking regulation still needs to be elucidated. Here I will propose various models that could account for the roles of TXNIP and ubiquitin in GLUT1 trafficking.

5.2.1 Ubiquitin is sufficient, but not required, for GLUT1 endocytosis

The data in this thesis have demonstrated that while GLUT1 has an increased presence at the surface, it is still able to be endocytosed without any lysines available

for ubiquitin modification. However, GLUT1 is stalled in an unknown post-endocytic compartment without these cytosolic lysines intact (**Figure 3.17** and **3.18)**. One explanation for this phenotype is that ubiquitin is not needed for GLUT1 endocytosis but is required for post-endocytic sorting and trafficking to the lysosome. EGFR, for instance, was shown to internalize at a similar rate whether its cytosolic lysines were mutated or not. However, the EGFR turnover rate was drastically increased with the loss of cytosolic lysines, resulting in accumulation in early endosomes (*190*). Perhaps GLUT1 regulation functions in a similar fashion. Ubiquitin modification is not necessarily needed for GLUT1 endocytosis, but the protein must be ubiquitylated at some point between endocytosis and early endosome co-localization in order to be properly sorted for trafficking to the lysosome versus the recycling pathway.

5.2.2 GLUT1 ubiquitylation as a signal for the ESCRT machinery

Following endocytosis, membrane proteins can be recycled back to the PM or trafficked to the lysosome. When the membrane protein is ubiquitylated, the ESRCT machinery recognizes it and sorts it into the multivesicular bodies (MVB) pathway for lysosomal degradation (*191*). In the absence of ubiquitylation, the protein is recycled back to the surface rather than trafficked to the lysosome. It is possible that GLUT1 ubiquitylation is required for sorting to the ESCRT pathway rather than serving as an internalization signal. This model is consistent with the literature on GLUT1 regulation as well as the data presented in this thesis. As previously shown, TXNIP is involved in GLUT1 endocytosis (*102*) and the data presented in **Chapter 3** suggests that GLUT1 ubiquitylation is TXNIP-independent and downstream of TXNIP's action on GLUT1. TXNIP would help to facilitate ubiquitin-independent endocytosis of GLUT1 through interactions with clathrin and/or AP-2. Before reaching the early endosome, GLUT1 is ubiquitylated so that the ESCRT complexes in the early endosome can recognize the glucose transporter, stop its recycling, and sequester it into MVBs along with other ubiquitylated cargo. Then GLUT1 will be trafficked to the lysosome, passing through the ESCRT-III associated VPS4A^{+} compartments as shown in **Figure 3.5F-I.** This would be consistent with the high colocalization of lysine-mutant GLUT1 with the PM (**Figure 3.17C-D**) as the inability to ubiquitylate GLUT1 for ESCRT complex recognition would lead to recycling of the transporter rather than trafficking to the lysosome.

5.2.3 A role for TXNIP PY motifs in preventing GLUT1 recycling

TXNIP negatively regulates GLUT1, but how the protein carries out this regulation is not completely understood. Experiments presented in **Chapter 3** demonstrate that clathrin-adapter binding and PY motifs of TXNIP are necessary for proper trafficking of GLUT1. The clathrin-binding domain, a di-leucine motif at L351 and L352, is involved in endocytosis (*102*), while the role of the two PY motifs of TXNIP in GLUT1 trafficking has not been explained.

There are many examples of α-arrestins (called arrestin-related trafficking adaptors or "ARTs" in *S. cerevisiae*) using PY motifs to interact with Nedd4 family E3 ubiquitin ligases. The α-arrestins bind to WW domains of ligases via the PY motifs (*192*). **Figure 5.2** shows a schematic of the published interaction between TXNIP and Nedd4 family ligase Itch (*138, 153*). In *S. cerevisiae*, ART1 serves as an adaptor for the Nedd4-like E3 ligase, Rsp5, to ubiquitylate the arginine transporter, Can1. In response to ubiquitin modification, Can1 is endocytosed and trafficked to the vacuole (*193*). ART2 binds to the manganese transporter, Smf1, allowing Rsp5 to ubiquitylate the transporter for endocytosis and trafficking to the vacuole (*194*). The human α-arrestin, ARDDC3, interacts with E3 ligase NEDD4 to facilitate the ubiquitylation and subsequent endocytosis and degradation of the β2-adrenergic receptor (*195*). These reported cases of α-arrestins serving as adaptors for ligases to ubiquitylate membrane proteins led us to hypothesize that TXNIP regulates GLUT1 by a similar mechanism. However, the data presented in **Chapter 3** are not consistent with the hypothesis **(Figure3.14)**. We observed GLUT1 ubiquitylation independent of TXNIP, and it remains unclear why TXNIP PY motifs are needed for GLUT1 lysosomal trafficking. An alternative hypothesis is that TXNIP is an adaptor for ubiquitin modification of a different factor involved in GLUT1 trafficking. The TXNIP interactome presented in **Chapter 4 (Table 4.1)** reveals that other E3 ubiquitin ligases (NEDD4L, UBR4) interact with TXNIP. Perhaps NEDD4L ubiquitylates an unknown trafficking component along the GLUT1 trafficking pathway, such as myoferlin. As presented in **Table 4.1**, TXNIP interacts with myoferlin, a protein known to be involved in endocytic recycling (*196*) and reported to interact with Snx27 of the retromer recycling pathway in a SILAC-based interaction profile (*97*). Perhaps TXNIP facilitates an interaction between myoferlin and Nedd4L, targeting myoferlin for degradation and therefore inhibiting GLUT1 recycling. This would be a secondary role

for TXNIP in addition to its involvement in endocytosis. It is reported that myoferlin deletion in myoblasts causes delayed transferrin recycling, but does not completely block recycling (*196*). Based on this data, it is likely that loss of myoferlin ubiquitylation would result in a gain of function phenotype due to its stabilization, but would likely not fully obstruct GLUT1 recycling as myoferlin is not necessary for recycling. Hence, the partial rescue phenotype seen in the $TXNIP_{py}$ experiment.

It is also possible that abolishing the already-established interaction between TXNIP and Itch by mutating the PY motifs is responsible for the observed GLUT1 trafficking phenotype **(Figure 3.13F)**. The degradation of TXNIP via Itch ubiquitylation may be necessary to dissociate TXNIP from the machinery somewhere along the endocytic pathway and allow trafficking to continue. The PY motif mutant leads to a greater loss of GLUT1/LAMP1 colocalization than seen in the clathrin-binding mutant **(Figure 3.13G)**. This could indicate that GLUT1 stalls in pre-lysosomal compartments due to TXNIP's continued association with the endocytic machinery. Further experimentation will be needed to determine what is truly responsible for the observed GLUT1 trafficking defects. Zhang et. al. demonstrated that Itch ubiquitylates Lys212 (*153*). Observing GLUT1 trafficking in the presence of a TXNIP Lys212Arg mutant would reveal any involvement in GLUT1 regulation.

5.2.4 A role for ARRDCs in GLUT1 Ubiquitylation

In **Chapter 3**, experimental data revealed GLUT1 ubiquitylation independent of TXNIP **(Figure 3.14G)**. However, overexpression of NEDD4 family ligases WWP1 and NEDD4L both increased ubiquitylation of GLUT1 significantly and a statistically insignificant boost in ubiquitylation was observed when TXNIP was added on top of the ligases **(Figure3.14I)**. Similarly, there is a statistically insignificant increase in GLUT1 ubiquitylation when TXNIP is reintroduced to knockout cells **(Figure 3.14G).** Although its role in GLUT1 trafficking appears not to be redundant, these results leave open the possibility that TXNIP's role in GLUT1 ubiquitylation is redundant. There are 5 additional human ARRDCs (ARRDC1-5, although ARRDC5 does not have PY motifs) that are not as well characterized as TXNIP. ARRDC3 and ARRDC4 have previously been implicated in glucose regulation (*142, 152, 197*), and others have proposed a role for ARRDC4 in GLUT1 regulation (*198*). A SILAC-MS interaction profile performed in the MacGurn lab revealed that WWP1 interacts with both TXNIP and ARRDC1 (*171*).

Perhaps the rise in ubiquitylation upon TXNIP addition was not larger due to the presence of one or more redundant E3 ligase adaptors. ARTs in *S. cerevisiae* tend to have redundant adaptor functions (*177*); therefore, redundancy in human α-arrestins would not be unprecedented. It would be interesting to examine the remaining α-arrestins in the context of GLUT1 regulation. While there is not much known about expression levels of ARRDCs, ARRDC3 protein levels are very low in colon, thymus, spleen, bone marrow, small intestine, and bladder (*199*).

5.3 GLUT1 Trafficking in Disease

There have been many reports of mutations in GLUT1-DS patients **(Table5.1)**; however, there is a lack of understanding with regards to how these mutations result in glucose deficiency. Some have suggested that mutations in GLUT1 can lead to loss of protein stability, misfolding, or aggregation (*113*). Others have pointed at mutations among residues involved in transport activity or substrate binding that can prevent glucose from crossing the BBB (*18*). There has also been one report of a missense mutation introducing a dileucine motif that promotes clathrin-dependent trafficking (*111*). Here, I discuss my findings in the context of mutations linked to GLUT1-DS.

5.3.1 GLUT1-DS patients have lysine mutations

Mutational analysis of 15 GLUT1-DS patients revealed two patients with mutations involving lysine residues. One patient had heterozygous Lys256Val and Arg126Leu mutations, each on a different allele. The patient's mother had the Lys256Val mutation on a single allele and presented no symptoms related to misregulated glucose. They suggest the two missense mutations, when combined, have a synergistic effect that leads to the patient's symptoms (*180*). It would be informative to perform a trafficking assay with the Lys256Val GLUT1 variant expressed in a cell line. Perhaps the loss of Lys256 affects the GLUT1 trafficking itinerary, leading to mistrafficking and therefore decreased glucose uptake. Another patient was found to have a Glu146Lys mutation (*180, 200*). It has been suggested that changing the negatively charged glutamate to a positively charged lysine residue abolishes an electrostatic interaction with Arg92 (*113*). While this is a valid explanation, it is interesting to consider the possibility that the gain of a cytoplasmic Lys residue could result in unwanted trafficking to the lysosome or

another intermediate endocytic compartment **(Figure 5.1).** WT GLUT1 has cytoplasmic lysine residues exclusively on the major cytoplasmic loop and the N-terminal and C-terminal tails of the protein. As discussed in **Chapter 3**, mutations of different cytosol-facing lysine residues (N-terminal tail, major cytosolic loop, or C-terminal tail) result in trafficking defects **(Figure 3.18D)**. This suggests that ubiquitylation impacts the endocytic trafficking of GLUT1 to varying degrees dependent on the position of modification. Perhaps the introduction of a Lys residue, as seen in a GLUT1-DS patient, on a cytoplasmic loop that was previously unable to be ubiquitylated leads to improper trafficking of GLUT1 away from the cell surface and results in decreased glucose uptake. Future studies on GLUT1-DS associated mutations should seek to characterize how patient mutations affect the trafficking of GLUT1, using assays similar to what I presented in **Chapter 3.**

Mutation	Structural Position	Patient Phenotype	Mechanism of Action
Ser66Phe (*180*)	1st extracellular loop	Classical	Unknown
Arg126Leu (*180*)	4th TM domain	Classical	Unknown
Arg126His (*201*)	4th TM domain	Classical	Unknown
Arg126Cys (*202*)	4th TM domain	Seizures, apnea, shaky eye movement	Glucose transport
Glu146Lys (*180*)	Cytoplasmic loop between TM4 and TM5	Classical	Glucose transport
Lys256Val (*180*)	Major cytoplasmic loop between TM6 and TM7	Classical	Unknown
Arg333Trp (*180*)	Cytoplasmic loop between TM8 and TM9	Classical	Membrane topology
Arg333Gln (*203*)	Cytoplasmic loop between TM8 and TM9	Late-onset classical	Membrane topology
Gly91Asp (*204*)	3rd TM domain	Unknown	Membrane topology
Thr310Ile (*205*)	8th TM domain	Classical	Unknown
Asn34Ile (*206*)	1st extracellular loop	Non-classical	Glucose transport
Asn34Ser (*201*)	1st extracellular loop	Classical	Unknown
Asn34Tyr (*203*)	1st extracellular loop	Classical	Unknown
Gly130Ser (*201*)	4th TM domain	Mild, 50-75% of wt function	Glucose transport
Arg153Cys (*201*)	Cytoplasmic loop between TM4 and TM5	Classical	Unknown
Arg153His (*203*)	Cytoplasmic loop between TM4 and TM5	Non-classical	Unknown
Ala275Thr (*207*)	7th TM domain	Classical	Unknown
Thr295Met (*201*)	Extracellular loop between TM7 and TM8	Classic	Glucose transport
Gly314Ser (*207*)	8th TM domain	Classical	Unknown
Arg93Trp (*208*)	3rd TM domain	Intermittent ataxia, late onset seizures, developmental delay	Unknown
Ser95Ile (*209*)	3rd TM domain	Unknown	Unknown
Met96Val (*203*)	3rd TM domain	Classical	Unknown
Ala155Val (*203*)	Cytoplasmic loop between TM4 and TM5	Classical	Glucose transport
Val165Ile (*210*)	5th TM domain	Classical	Unknown
Arg212Cys (*203*)	Major cytoplasmic loop between TM6 and TM7	Classical	Unknown
Arg212His (*203*)	Major cytoplasmic loop between TM6 and TM7	Classical	Unknown
Arg223Trp (*203*)	Major cytoplasmic loop between TM6 and TM7	Late-onset Classical	Unknown
Asn317Thr (*209*)	8th TM domain	Unknown	Unknown

Ser324Leu (*211*)	8th TM domain	Developmental delay, epilepsy	Unknown
Glu329Gln (*203*)	Cytoplasmic loop between TM8 and TM9	Classical	Glucose transport
Gly382Asp (*203*)	10th TM domain	Classical	Glucose transport, decreased expression
Ala405Asp (*203*)	11th TM domain	Late-onset Classical	Glucose transport
Pro485Leu (*111, 203*)	C-terminal tail (cytoplasmic)	Classical	Aberrant trafficking
Ser294Pro (*212*)	Extracellular loop between TM7 and TM8	Classical	Unknown
Arg468Trp (*213*)	C-terminal tail (cytoplasmic)	Classical	Glucose transport

Table 5.1 Mutations found in GLUT1-DS patients. List of patient amino acid mutations leading to GLUT1 deficiency syndrome along with the location in the protein, the phenotype in patients, and the mechanism of action. In addition to the missense mutations listed here, there are many documented splice site and nonsense mutations that also lead to GLUT1-DS. Patient phenotypes: Classical= epilepsy, developmental delay, movement disorders; Non-classical= developmental delay, movement disorders, no epilepsy.

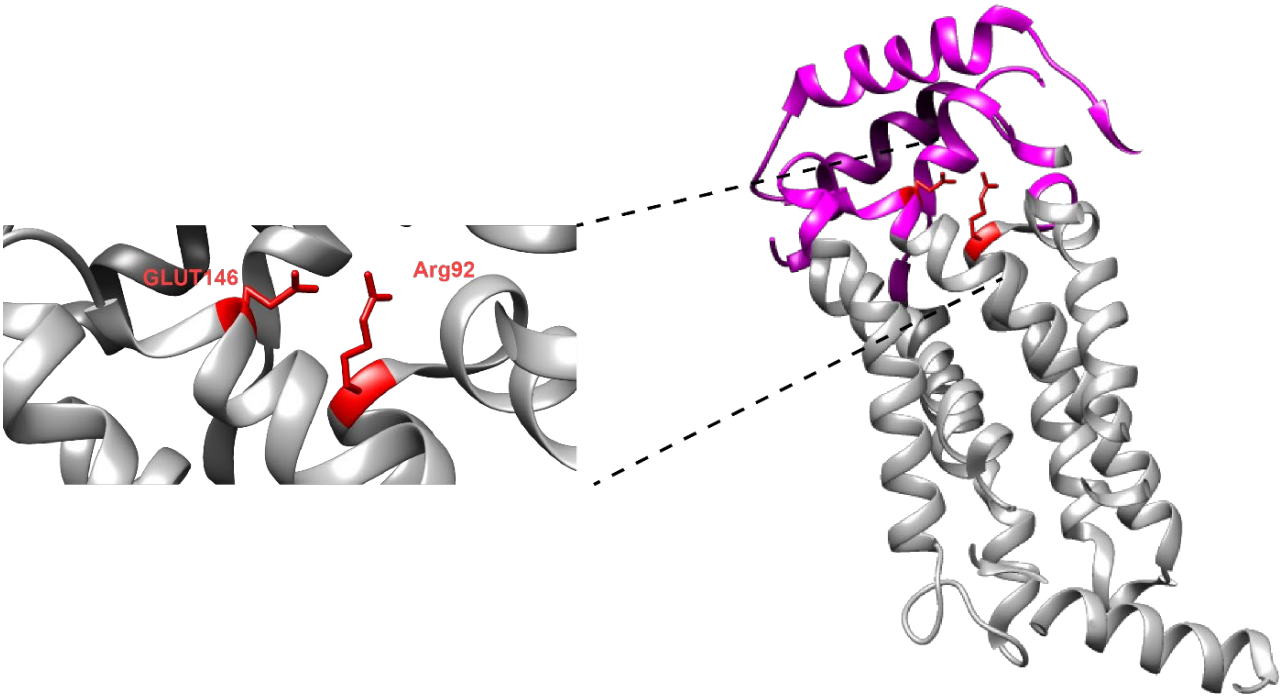

Figure 5.1: GLUT1 structure highlighting Arg92 and Glu146 residues (red). A Glu146Lys mutation has been reported in a GLUT1-DS patient. Cytoplasmic regions of GLUT1 are highlighted in magenta.

5.3.2 GLUT1 trafficking in cancer

GLUT1 is frequently overexpressed in cancer cells to increase glucose uptake (*126*) **(Table 5.2)**. There are several regulatory pathways that cancer cells use to increase GLUT1 at the PM. For instance, a mutation in the PDZ binding motif of phosphatase and negative regulator of retromer recycling, PTEN, abolishes the interaction of PTEN with the retromer recycling machinery and leads to increased recycling of GLUT1 back to the cell surface. This PDZ binding motif mutation has been identified in soft tissue sarcoma and was shown to increase glucose uptake (*167*). McDonald et. al. have shown that pancreatic ductal adenocarcinoma metastases have persistently suppressed TXNIP expression to stabilize GLUT1 at the PM, and therefore increase glucose uptake (*214*). There are several GLUT1 inhibitors being studied, that act by targeting mRNA and protein expression (*215*), directly inhibiting GLUT1 by blocking the transporter channel (*216*), or blocking aerobic glycolysis through inhibition of both GLUT1 and hypoxia-inducible factor-1 (HIF-1) (*217*). Knowing that adenosine monophosphate-activated kinase (AMPK) is activated in response to metabolic stress to induce apoptosis, researchers have been looking for AMPK activators to make cancer cells more susceptible to treatment in combination with GLUT1 inhibitors (*132, 218, 219*). It would also be interesting to test the affect that direct inhibitors of GLUT1 have on its trafficking and stability.

The findings in this dissertation provide new insights into the regulation of GLUT1, which may be useful for therapeutic development. For example, the observation that substrate transport alone triggers GLUT1 endocytosis and lysosomal trafficking **(Figure 3.11)** could be leveraged to find small molecules that target the removal of GLUT1 from the PM. Another finding that may prove useful for cancer therapeutics is the ubiquitylation of GLUT1. I have shown that the cytoplasmic lysine residues of GLUT1 are needed for proper lysosomal trafficking **(Figure 3.17-3.18)**, which suggests that ubiquitylation of the protein plays a part in trafficking of GLUT1 from the PM to lysosome. GLUT1, therefore, could potentially be targeted by proteolysis targeting chimeras (PROTACS), which are bivalent small molecules which interact with an E3 ligase moiety and a ligand to a target protein for ubiquitin modification (*220*). With the knowledge that GLUT1 trafficking is triggered by ubiquitylation, PROTACS may be an effective way to decrease GLUT1 levels at the cell surface and subsequently decrease

glucose uptake. Although one caveat to consider is that the ubiquitylation by PROTACS would not be targeted to cancer cells specifically. This could have potential side effects such as hyperglycemia or increased metabolic stress in healthy cells.

Cancer type	GLUT1 Alteration
Uterine serous carcinoma	Amplified or mutated in 9.17% of cases
Ovarian cancer	Amplified in 6.68% of cases
Soft-tissue cancer	Amplified in 6% of cases
Breast mucinous carcinoma	Mutated in 5.88% of cases
Uterine endometrioid carcinoma	Amplified or mutated in 5.01% of cases
Mucinous adenocarcinoma of the colon/rectum	Mutated in 4.92% of cases
Uterine mixed endometrial carcinoma	Amplified in 4.76% of cases
Bladder urothelial carcinoma	Amplified or mutated in 4.62% of cases
Mucinous stomach adenocarcinoma	4.55% of cases
Myxofibrosarcoma	Amplified in 4% of cases

Table 5.2: Prevalence of GLUT1 genomic alterations in human cancer. The top genetic alterations reported in GLUT1 that are found in human cancers. Data from the cBioPortal for Cancer Genomics database (www.cbioportal.org).

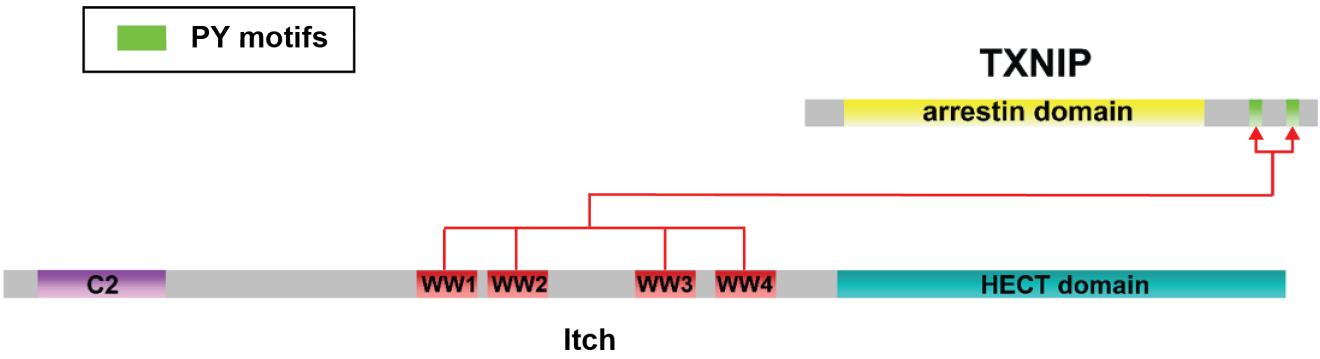

Figure 5.2: Interaction between the PY motifs of TXNIP and the WW domain of Nedd4 ligase Itch. Itch ubiquitylates Itch, promoting its degradation (*153*). Multivalent interaction between the 4 WW domains of Itch with both PY motifs of TXNIP results in strong binding avidity (*138*).

5.4 Future Directions

While this thesis dissertation helps to further our knowledge of GLUT1 regulation, many questions remain. Here I propose some future avenues of experimentation that could provide valuable insights into the regulation of GLUT1.

5.4.1 Looking for GLUT1 regulatory factors

A great deal could be learned by applying mass spectrometry analysis to GLUT1 isolated from cell lysates. First, a simple GLUT1 interaction profile generated using SILAC-MS would provide a wealth of information. The ligase(s) responsible for GLUT1 ubiquitylation *in vivo* remain unclear. An improved interaction profile for GLUT1 could uncover regulatory interactions with E3 ubiquitin ligases. GLUT1 does contain three PY motifs with a PXY sequence, rather than the typical PPXY. Looking at WT vs PY mutant GLUT1 could reveal any direct WW-domain interactions. And comparing GLUT1 interactions in WT versus KO TXNIP conditions would clarify what interactions (if any) TXNIP facilitates for GLUT1. This would also reveal any GLUT1 ubiquitylation events that are lost in the absence of TXNIP. While the data presented in **Figure 3.14** shows no change in GLUT1 ubiquitylation levels with TXNIP present, it is possible the coIP experiments are not sensitive enough to pick up the ubiquitin modifications important for GLUT1 trafficking regulation. Ubiquitylation signaling for the ESCRT pathway is frequently in the form of monoubiquitylation events and these ubiquitin modifications are removed during interaction with the ESCRT-III complex (*191*); therefore, it is possible that a monoubiquitylation event on GLUT1 facilitated by TXNIP is not significant enough to be detected by immunoblot, yet is vital for proper trafficking of GLUT1. As shown in **Chapter 3,** the trafficking defects of GLUT1 vary depending on which set of cytosol-facing lysine residues are mutated **(Figures 3.18, 3.20).** Performing a mass spectrometry experiment in which peptides with ubiquitin remnants (di-Gly) are enriched in TXNIP WT versus KO cells could reveal specific GLUT1 lysines that are ubiquitylated only in the presence of TXNIP. However, di-GLy experiments do not show polyubiquitylation events and additional experiment would be required to determine whether TXNIP was involved in polyubiquitylation of GLUT1. Performing a SILAC interactome with GLUT1 in WT TXNIP versus KO cells would reveal any changes in the overall amount of GLUT1 ubiquitylation in the presence of TXNIP. Comparing

interaction profiles of $6K_{loop}$→R GLUT1 versus $5K_{tails}$→R GLUT1 could also provide insight into the localized functions of ubiquitin modification on GLUT1.

While the GLUT1 lysine mutant phenotypes suggest a role for ubiquitylation in GLUT1 trafficking, it is possible these lysines are important for other regulatory modifications like acetylation. More experiments would be necessary to demonstrate ubiquitylation is playing a role in GLUT1 trafficking. One such experiment would be overexpression or loss of E3 ubiquitin ligases. While shRNA constructs for WWP1 have proven challenging, there is a WWP1 inhibitor, indole-3-carbinol (*221*), that could be utilized for GLUT1 trafficking assays. If WWP1 ubiquitylation of GLUT1 contributes to its trafficking, I would expect to see a phenotype similar to the 11K→R mutant. Also, the SGK inhibitor, GSK650394, activates Nedd4L by preventing the phosphorylation of Nedd4L that leads to 14-3-3 protein binding (*179, 222*). GSK650394 could be used to test the effect of increased ubiquitylation of GLUT1 in a trafficking assay. I would expect an increase in lysosomal trafficking of GLUT1 if Nedd4L ubiquitylation played a role in GLUT1 trafficking. As mentioned in **Chapter 4,** there is another E3 ubiquitin ligase that interacts with TXNIP, UBR4. UBR4 works in complex with Itch and other ligases to target TXNIP for degradation (*182*), but there is no established role for UBR4 in GLUT1 regulation. It may be informative to knockout UBR4 and observe how it affects both GLUT1 ubiquitylation and trafficking.

Another area of research that could be pursued is to characterize glucose transport using the GLUT1 variants described in this dissertation. This could be done with radio-labeled glucose analogues, using a fluorescent glucose analogue such as 2-[N-(7-nitrobenz-2-oxa-1,3-diazol-4-yl) amino]-2-deoxy-D-glucose (2NBDG) (*223*), or by measuring changes in the cell media glucose concentration (*214*). This would be a generally useful functional assay for disease-associated mutants as well as with the various TXNIP mutants and NEDD4 ligase overexpression conditions.

5.4.2 Further examination of TXNIP and the ARRDCs as Regulators of GLUT1

As discussed in the previous section, it is possible that other α-arrestin family members are involved in the regulation of GLUT1. To explore this possibility, GLUT1 trafficking assays in the context of overexpression and/or knockdown of various ARRDC family members should be performed. Multiple strategies to explore the role of ARRDCs

in the regulation of GLUT1 should be employed. Using GLUT1 trafficking as a readout, we can test (i) cell lines overexpressing each ARRDC family member, (ii) the ability of individual ARRDCs to rescue GLUT1 trafficking in the TXNIP knockout cell line, (iii) individual ARRDC knockout cell lines, and (iv) a complete ARRDC family knockout cell line. In addition to trafficking assays, these strategies could be used in the context of ubiquitylation assays (**Figure 3.14D - I).**

Additional TXNIP mass spectrometry would be a powerful tool to discover TXNIP's mechanism of action in GLUT1 regulation. Firstly, a comparison of the WT TXNIP and $TXNIP_{PY}$ interaction profiles will reveal any PY-dependent interactions. This would generate a list of candidates that could be involved in GLUT1 trafficking regulation. Also, analysis of TXNIP-dependent ubiquitylation events by quantitative ubiquitin remnant profiling would would be effective in revealing if TXNIP serves as a ubiquitin ligase adaptor for other targets. Finally, with so little known about the remaining ARRDCs, quantitative interaction profiling analysis would be a great place to start. A lot of information could be gained about the proteins and could lead to some interesting discoveries, whether GLUT1-related or not.

5.4.3 Testing the proposed models of GLUT1 lysosomal trafficking

In section **5.2,** I proposed various models for GLUT1 trafficking based on the findings in **Chapters 3** and **4.** There are several experiments that could be employed to test these models. In order to investigate the role of GLUT1 ubiquitylation in ESCRT pathway signaling **(5.2.1)**, I would start by comparing colocalization of WT GLUT1 and the 11K→R GLUT1 mutant with ESCRT complex components, such as the dominant negative VPS4A used in **Chapter 3** and ESCRT-0 subunits such Hrs. Observing colocalization with recycling components such as VPS35 and TfR would also be informative. I would also perform a SILAC experiment comparing WT GLUT1 and 11K→R GLUT1 in high glucose conditions. If this model were correct, I would expect to see an increase of recycling interactors with the lysine mutant and loss of ESCRT complex interactions in comparison to WT GLUT1.

Next, I proposed that the PY motifs of TXNIP were important for the lysosome versus recycling fate for GLUT1 **(5.2.2)**. To further interrogate this, the first step would be validating the TXNIP interaction with myoferlin by coIP and/or a second TXNIP

interactome in a different cell line. Also, looking at myoferlin ubiquitylation status with and without TXNIP present, similar to the experiments shown in **Figure 3.14,** would test the validity of this model. In order to test the involvement of myoferlin in GLUT1 recycling, I would perform a trafficking assay like the one shown in **Figure 3.3** with overexpression of myoferlin in high glucose conditions. If the protein plays a part in GLUT1 recycling, I would expect overexpression to result in a decrease of GLUT1 colocalization with the lysosome and increase of colocalization with the PM in comparison with wildtype conditions.

Finally, I suggested that GLUT1 ubiquitylation was dispensable for endocytosis but required for post-endocytic sorting onto the proper trafficking pathway. To investigate this possible model of GLUT1 trafficking, I would need to measure the kinetics of GLUT1 endocytosis. Using the exofacially FLAG-tagged GLUT1 (FLAG-GLUT1) shown in **Figure 3.3C** I would perform an experiment based on the HA-GLUT4 endocytosis assay described by Blot and McGraw (*224*). Live cells expressing either WT or 11K→R FLAG-GLUT1 would be fed αFLAG antibody at various time points post-glucose shift then fixed and labeled with a saturating concentration secondary antibody *prior* to permeabilization. Then the cells would be fixed again and permeabilized so the internal FLAG-GLUT1 can be detected with a different secondary antibody. After imaging, I could quantify the ratio of surface versus internal FLAG at each time point in both GLUT1 variants in order to obtain a rate of endocytosis. If ubiquitylation is important for GLUT1 endocytosis, I would expect the endocytosis rate to be drastically decreased with the 11K→R GLUT1 in comparison to wildtype.

The work presented in this thesis contribute to our understanding of how cells maintain glucose homeostasis. GLUT1 is a central component of this homeostasis as it is the ubiquitous transporter in humans and, therefore, affects glucose levels in virtually all cells. The further analysis of GLUT1 regulation will help us to understand not only how the protein functions in normal cells, but also GLUT1's contribution to disease.

Appendix A: List of acronyms used

GSVs: GLUT4 storage vesicles

TGN: *trans*-golgi network

GLUT1-DS: GLUT1 deficiency syndrome

GPCR: G protein-coupled receptor

PTM: post-translational modification

PM: Plasma membrane

GE: glucose-excited

GLUT: facilitative glucose transporter

SLC: solute carrier

TfR: transferrin receptor

ERK: extracellular signal regulated kinase

PI3K: phosphatidylinositol 3-kinase

IRS-1: insulin receptor substrate-1

PIP_3: phosphatidylinositol 3,4,5-triphosphate

GAP: GTPase-activating protein

SGK1 (serum- and glucocorticoid-inducible kinase 1)

coIP: co-immunoprecipitation

UBA: ubiquitin associated

ARRDC: arrestin domain-containing

TRX: thioredoxin

TXNIP: thioredoxin interacting protein

KD: knock down

KO: knock down

SNX27: sorting nexin 27

GSK3:glycogen synthase kinase-3

TSC: tuberous sclerosis complex

mTOR: mammalian target of rapamycin

2FDG: 2-[^{18}F]-2-deoxy-D-glucose

SILAC-MS: stable isotope labelling with amino acids in cell culture mass spectrometry

References

1. P. Mergenthaler, U. Lindauer, G. A. Dienel, A. Meisel, Sugar for the brain: the role of glucose in physiological and pathological brain function. *Trends Neurosci* **36**, 587-597 (2013).
2. G. D. Holman, Structure, function and regulation of mammalian glucose transporters of the SLC2 family. *Pflugers Arch* **472**, 1155-1175 (2020).
3. P. Van Damme *et al.*, N-terminal acetylome analyses and functional insights of the N-terminal acetyltransferase NatB. *Proc Natl Acad Sci U S A* **109**, 12449-12454 (2012).
4. L. B. Liu, W. Omata, I. Kojima, H. Shibata, The SUMO conjugating enzyme Ubc9 is a regulator of GLUT4 turnover and targeting to the insulin-responsive storage compartment in 3T3-L1 adipocytes. *Diabetes* **56**, 1977-1985 (2007).
5. H. Daub *et al.*, Kinase-selective enrichment enables quantitative phosphoproteomics of the kinome across the cell cycle. *Mol Cell* **31**, 438-448 (2008).
6. Y. Bian *et al.*, An enzyme assisted RP-RPLC approach for in-depth analysis of human liver phosphoproteome. *J Proteomics* **96**, 253-262 (2014).
7. J. V. Olsen *et al.*, Quantitative phosphoproteomics reveals widespread full phosphorylation site occupancy during mitosis. *Sci Signal* **3**, ra3 (2010).
8. C. Toda *et al.*, UCP2 Regulates Mitochondrial Fission and Ventromedial Nucleus Control of Glucose Responsiveness. *Cell* **164**, 872-883 (2016).
9. N. A. Yoon, S. Diano, Hypothalamic glucose-sensing mechanisms. *Diabetologia* **64**, 985-993 (2021).
10. M. Kouvari *et al.*, Metabolic Syndrome, Cognitive Impairment and the Role of Diet: A Narrative Review. *Nutrients* **14**, (2022).
11. M. Chomova, Toward the Decipherment of Molecular Interactions in the Diabetic Brain. *Biomedicines* **10**, (2022).
12. A. Tengholm, E. Gylfe, cAMP signalling in insulin and glucagon secretion. *Diabetes Obes Metab* **19 Suppl 1**, 42-53 (2017).
13. A. Klip, T. E. McGraw, D. E. James, Thirty sweet years of GLUT4. *J Biol Chem* **294**, 11369-11381 (2019).
14. A. M. Navale, A. N. Paranjape, Glucose transporters: physiological and pathological roles. *Biophys Rev* **8**, 5-9 (2016).
15. D. S. Hsia, O. Grove, W. T. Cefalu, An update on sodium-glucose co-transporter-2 inhibitors for the treatment of diabetes mellitus. *Curr Opin Endocrinol Diabetes Obes* **24**, 73-79 (2017).
16. M. Mueckler, B. Thorens, The SLC2 (GLUT) family of membrane transporters. *Mol Aspects Med* **34**, 121-138 (2013).
17. H. G. Joost *et al.*, Nomenclature of the GLUT/SLC2A family of sugar/polyol transport facilitators. *Am J Physiol Endocrinol Metab* **282**, E974-976 (2002).
18. D. Deng *et al.*, Crystal structure of the human glucose transporter GLUT1. *Nature* **510**, 121-125 (2014).
19. D. Deng *et al.*, Molecular basis of ligand recognition and transport by glucose transporters. *Nature* **526**, 391-396 (2015).
20. Y. Yuan *et al.*, Cryo-EM structure of human glucose transporter GLUT4. *Nat Commun* **13**, 2671 (2022).
21. L. J. McCulloch *et al.*, GLUT2 (SLC2A2) is not the principal glucose transporter in human pancreatic beta cells: implications for understanding genetic association signals at this locus. *Mol Genet Metab* **104**, 648-653 (2011).

22. M. T. Guillam, R. Burcelin, B. Thorens, Normal hepatic glucose production in the absence of GLUT2 reveals an alternative pathway for glucose release from hepatocytes. *Proc Natl Acad Sci U S A* **95**, 12317-12321 (1998).
23. M. Hosokawa, B. Thorens, Glucose release from GLUT2-null hepatocytes: characterization of a major and a minor pathway. *Am J Physiol Endocrinol Metab* **282**, E794-801 (2002).
24. I. A. Simpson *et al.*, The facilitative glucose transporter GLUT3: 20 years of distinction. *Am J Physiol Endocrinol Metab* **295**, E242-253 (2008).
25. X. Wu, H. H. Freeze, GLUT14, a duplicon of GLUT3, is specifically expressed in testis as alternative splice forms. *Genomics* **80**, 553-557 (2002).
26. S. C. Rumsey *et al.*, Dehydroascorbic acid transport by GLUT4 in Xenopus oocytes and isolated rat adipocytes. *J Biol Chem* **275**, 28246-28253 (2000).
27. L. P. Taylor, G. D. Holman, Symmetrical kinetic parameters for 3-O-methyl-D-glucose transport in adipocytes in the presence and in the absence of insulin. *Biochim Biophys Acta* **642**, 325-335 (1981).
28. V. Douard, R. P. Ferraris, Regulation of the fructose transporter GLUT5 in health and disease. *Am J Physiol Endocrinol Metab* **295**, E227-237 (2008).
29. H. S. Hundal *et al.*, Biochemical and immunocytochemical localization of the 'GLUT5 glucose transporter' in human skeletal muscle. *Biochem J* **286 (Pt 2)**, 339-343 (1992).
30. C. A. Stuart, M. E. Howell, D. Yin, Overexpression of GLUT5 in diabetic muscle is reversed by pioglitazone. *Diabetes Care* **30**, 925-931 (2007).
31. D. Shigemizu *et al.*, Exome Analyses of Long QT Syndrome Reveal Candidate Pathogenic Mutations in Calmodulin-Interacting Genes. *PLoS One* **10**, e0130329 (2015).
32. Q. Li *et al.*, Cloning and functional characterization of the human GLUT7 isoform SLC2A7 from the small intestine. *Am J Physiol Gastrointest Liver Physiol* **287**, G236-242 (2004).
33. K. Ebert *et al.*, Reassessment of GLUT7 and GLUT9 as Putative Fructose and Glucose Transporters. *J Membr Biol* **250**, 171-182 (2017).
34. V. Vitart *et al.*, SLC2A9 is a newly identified urate transporter influencing serum urate concentration, urate excretion and gout. *Nat Genet* **40**, 437-442 (2008).
35. N. Anzai *et al.*, Plasma urate level is directly regulated by a voltage-driven urate efflux transporter URATv1 (SLC2A9) in humans. *J Biol Chem* **283**, 26834-26838 (2008).
36. H. Doege *et al.*, Characterization of human glucose transporter (GLUT) 11 (encoded by SLC2A11), a novel sugar-transport facilitator specifically expressed in heart and skeletal muscle. *Biochem J* **359**, 443-449 (2001).
37. A. Scheepers *et al.*, Characterization of the human SLC2A11 (GLUT11) gene: alternative promoter usage, function, expression, and subcellular distribution of three isoforms, and lack of mouse orthologue. *Mol Membr Biol* **22**, 339-351 (2005).
38. H. Doege, A. Bocianski, H. G. Joost, A. Schürmann, Activity and genomic organization of human glucose transporter 9 (GLUT9), a novel member of the family of sugar-transport facilitators predominantly expressed in brain and leucocytes. *Biochem J* **350 Pt 3**, 771-776 (2000).
39. H. G. Joost, B. Thorens, The extended GLUT-family of sugar/polyol transport facilitators: nomenclature, sequence characteristics, and potential function of its novel members (review). *Mol Membr Biol* **18**, 247-256 (2001).
40. S. Maedera *et al.*, GLUT6 is a lysosomal transporter that is regulated by inflammatory stimuli and modulates glycolysis in macrophages. *FEBS Lett* **593**, 195-208 (2019).
41. R. Augustin, J. Riley, K. H. Moley, GLUT8 contains a [DE]XXXL[LI] sorting motif and localizes to a late endosomal/lysosomal compartment. *Traffic* **6**, 1196-1212 (2005).
42. B. J. DeBosch, M. Chi, K. H. Moley, Glucose transporter 8 (GLUT8) regulates enterocyte fructose transport and global mammalian fructose utilization. *Endocrinology* **153**, 4181-4191 (2012).
43. M. Villagrán *et al.*, GLUT1 and GLUT8 support lactose synthesis in Golgi of murine mammary epithelial cells. *J Physiol Biochem* **75**, 209-215 (2019).

44. P. A. Dawson *et al.*, Sequence and functional analysis of GLUT10: a glucose transporter in the Type 2 diabetes-linked region of chromosome 20q12-13.1. *Mol Genet Metab* **74**, 186-199 (2001).
45. A. Boel *et al.*, Arterial Tortuosity Syndrome: An Ascorbate Compartmentalization Disorder? *Antioxid Redox Signal* **34**, 875-889 (2021).
46. C. A. Stuart, M. E. Howell, Y. Zhang, D. Yin, Insulin-stimulated translocation of glucose transporter (GLUT) 12 parallels that of GLUT4 in normal muscle. *J Clin Endocrinol Metab* **94**, 3535-3542 (2009).
47. M. L. Macheda, E. D. Williams, J. D. Best, M. E. Wlodek, S. Rogers, Expression and localisation of GLUT1 and GLUT12 glucose transporters in the pregnant and lactating rat mammary gland. *Cell Tissue Res* **311**, 91-97 (2003).
48. M. Uldry *et al.*, Identification of a mammalian H(+)-myo-inositol symporter expressed predominantly in the brain. *EMBO J* **20**, 4467-4477 (2001).
49. S. W. Cushman, L. J. Wardzala, Potential mechanism of insulin action on glucose transport in the isolated rat adipose cell. Apparent translocation of intracellular transport systems to the plasma membrane. *J Biol Chem* **255**, 4758-4762 (1980).
50. K. Suzuki, T. Kono, Evidence that insulin causes translocation of glucose transport activity to the plasma membrane from an intracellular storage site. *Proc Natl Acad Sci U S A* **77**, 2542-2545 (1980).
51. L. J. Wardzala, B. Jeanrenaud, Potential mechanism of insulin action on glucose transport in the isolated rat diaphragm. Apparent translocation of intracellular transport units to the plasma membrane. *J Biol Chem* **256**, 7090-7093 (1981).
52. A. Klip, T. Ramlal, D. A. Young, J. O. Holloszy, Insulin-induced translocation of glucose transporters in rat hindlimb muscles. *FEBS Lett* **224**, 224-230 (1987).
53. D. E. James, R. Brown, J. Navarro, P. F. Pilch, Insulin-regulatable tissues express a unique insulin-sensitive glucose transport protein. *Nature* **333**, 183-185 (1988).
54. M. J. Charron, F. C. Brosius, S. L. Alper, H. F. Lodish, A glucose transport protein expressed predominately in insulin-responsive tissues. *Proc Natl Acad Sci U S A* **86**, 2535-2539 (1989).
55. H. Fukumoto *et al.*, Cloning and characterization of the major insulin-responsive glucose transporter expressed in human skeletal muscle and other insulin-responsive tissues. *J Biol Chem* **264**, 7776-7779 (1989).
56. A. Garcia de Herreros, M. J. Birnbaum, The acquisition of increased insulin-responsive hexose transport in 3T3-L1 adipocytes correlates with expression of a novel transporter gene. *J Biol Chem* **264**, 19994-19999 (1989).
57. K. H. Kaestner *et al.*, Sequence, tissue distribution, and differential expression of mRNA for a putative insulin-responsive glucose transporter in mouse 3T3-L1 adipocytes. *Proc Natl Acad Sci U S A* **86**, 3150-3154 (1989).
58. H. Doege *et al.*, Serine-294 and threonine-295 in the exofacial loop domain between helices 7 and 8 of glucose transporters (GLUT) are involved in the conformational alterations during the transport process. *Biochem J* **329 (Pt 2)**, 289-293 (1998).
59. M. J. Seatter, S. A. De la Rue, L. M. Porter, G. W. Gould, QLS motif in transmembrane helix VII of the glucose transporter family interacts with the C-1 position of D-glucose and is involved in substrate selection at the exofacial binding site. *Biochemistry* **37**, 1322-1326 (1998).
60. K. Du, S. Murakami, Y. Sun, C. L. Kilpatrick, B. Luscher, DHHC7 Palmitoylates Glucose Transporter 4 (Glut4) and Regulates Glut4 Membrane Translocation. *J Biol Chem* **292**, 2979-2991 (2017).
61. S. Jeyaraj, C. Boehmer, F. Lang, M. Palmada, Role of SGK1 kinase in regulating glucose transport via glucose transporter GLUT4. *Biochem Biophys Res Commun* **356**, 629-635 (2007).
62. P. D. Brewer, E. N. Habtemichael, I. Romenskaia, C. C. Mastick, A. C. Coster, Glut4 Is Sorted from a Rab10 GTPase-independent Constitutive Recycling Pathway into a Highly Insulin-responsive

Rab10 GTPase-dependent Sequestration Pathway after Adipocyte Differentiation. *J Biol Chem* **291**, 773-789 (2016).
63. R. J. Garippa, T. W. Judge, D. E. James, T. E. McGraw, The amino terminus of GLUT4 functions as an internalization motif but not an intracellular retention signal when substituted for the transferrin receptor cytoplasmic domain. *J Cell Biol* **124**, 705-715 (1994).
64. P. De Meyts, in *Endotext,* K. R. Feingold *et al.*, Eds. (MDText.com, Inc.

Copyright © 2000-2023, MDText.com, Inc., South Dartmouth (MA), 2000).
65. H. Sano *et al.*, Insulin-stimulated phosphorylation of a Rab GTPase-activating protein regulates GLUT4 translocation. *J Biol Chem* **278**, 14599-14602 (2003).
66. G. Ramm, M. Larance, M. Guilhaus, D. E. James, A role for 14-3-3 in insulin-stimulated GLUT4 translocation through its interaction with the RabGAP AS160. *J Biol Chem* **281**, 29174-29180 (2006).
67. C. A. Lamb, R. K. McCann, J. Stöckli, D. E. James, N. J. Bryant, Insulin-regulated trafficking of GLUT4 requires ubiquitination. *Traffic* **11**, 1445-1454 (2010).
68. M. Funakoshi, T. Sasaki, T. Nishimoto, H. Kobayashi, Budding yeast Dsk2p is a polyubiquitin-binding protein that can interact with the proteasome. *Proc Natl Acad Sci U S A* **99**, 745-750 (2002).
69. L. Rui, M. Yuan, D. Frantz, S. Shoelson, M. F. White, SOCS-1 and SOCS-3 block insulin signaling by ubiquitin-mediated degradation of IRS1 and IRS2. *J Biol Chem* **277**, 42394-42398 (2002).
70. D. L. Rothman, R. G. Shulman, G. I. Shulman, 31P nuclear magnetic resonance measurements of muscle glucose-6-phosphate. Evidence for reduced insulin-dependent muscle glucose transport or phosphorylation activity in non-insulin-dependent diabetes mellitus. *J Clin Invest* **89**, 1069-1075 (1992).
71. J. R. Zierath *et al.*, Insulin action on glucose transport and plasma membrane GLUT4 content in skeletal muscle from patients with NIDDM. *Diabetologia* **39**, 1180-1189 (1996).
72. W. T. Garvey *et al.*, Evidence for defects in the trafficking and translocation of GLUT4 glucose transporters in skeletal muscle as a cause of human insulin resistance. *J Clin Invest* **101**, 2377-2386 (1998).
73. J. W. Ryder *et al.*, Use of a novel impermeable biotinylated photolabeling reagent to assess insulin- and hypoxia-stimulated cell surface GLUT4 content in skeletal muscle from type 2 diabetic patients. *Diabetes* **49**, 647-654 (2000).
74. E. M. Gibbs *et al.*, Glycemic improvement in diabetic db/db mice by overexpression of the human insulin-regulatable glucose transporter (GLUT4). *J Clin Invest* **95**, 1512-1518 (1995).
75. J. R. Daugaard *et al.*, Fiber type-specific expression of GLUT4 in human skeletal muscle: influence of exercise training. *Diabetes* **49**, 1092-1095 (2000).
76. S. L. McGee, M. Hargreaves, Exercise and myocyte enhancer factor 2 regulation in human skeletal muscle. *Diabetes* **53**, 1208-1214 (2004).
77. M. Kasahara, P. C. Hinkle, Reconstitution and purification of the D-glucose transporter from human erythrocytes. *J Biol Chem* **252**, 7384-7390 (1977).
78. M. Kasahara, P. C. Hinkle, Reconstitution of D-glucose transport catalyzed by a protein fraction from human erythrocytes in sonicated liposomes. *Proc Natl Acad Sci U S A* **73**, 396-400 (1976).
79. M. Mueckler *et al.*, Sequence and structure of a human glucose transporter. *Science* **229**, 941-945 (1985).
80. S. A. Baldwin, G. E. Lienhard, Purification and reconstitution of glucose transporter from human erythrocytes. *Methods Enzymol* **174**, 39-50 (1989).
81. M. J. Birnbaum, H. C. Haspel, O. M. Rosen, Cloning and characterization of a cDNA encoding the rat brain glucose-transporter protein. *Proc Natl Acad Sci U S A* **83**, 5784-5788 (1986).
82. A. Schürmann *et al.*, Role of conserved arginine and glutamate residues on the cytosolic surface of glucose transporters for transporter function. *Biochemistry* **36**, 12897-12902 (1997).

83. M. Mueckler, W. Weng, M. Kruse, Glutamine 161 of Glut1 glucose transporter is critical for transport activity and exofacial ligand binding. *J Biol Chem* **269**, 20533-20538 (1994).
84. J. Brahm, Kinetics of glucose transport in human erythrocytes. *J Physiol* **339**, 339-354 (1983).
85. S. S. Vollers, A. Carruthers, Sequence determinants of GLUT1-mediated accelerated-exchange transport: analysis by homology-scanning mutagenesis. *J Biol Chem* **287**, 42533-42544 (2012).
86. E. K. Cloherty, K. B. Levine, A. Carruthers, The red blood cell glucose transporter presents multiple, nucleotide-sensitive sugar exit sites. *Biochemistry* **40**, 15549-15561 (2001).
87. H. L. Wieman *et al.*, An essential role for the Glut1 PDZ-binding motif in growth factor regulation of Glut1 degradation and trafficking. *Biochem J* **418**, 345-367 (2009).
88. J. C. Rathmell *et al.*, Akt-directed glucose metabolism can prevent Bax conformation change and promote growth factor-independent survival. *Mol Cell Biol* **23**, 7315-7328 (2003).
89. F. Maher, L. C. Harrison, Stabilization of glucose transporter mRNA by insulin/IGF-1 and glucose deprivation. *Biochem Biophys Res Commun* **171**, 210-215 (1990).
90. A. Mogyorósi, F. N. Ziyadeh, GLUT1 and TGF-beta: the link between hyperglycaemia and diabetic nephropathy. *Nephrol Dial Transplant* **14**, 2827-2829 (1999).
91. M. Hayashi *et al.*, Induction of glucose transporter 1 expression through hypoxia-inducible factor 1alpha under hypoxic conditions in trophoblast-derived cells. *J Endocrinol* **183**, 145-154 (2004).
92. C. A. Grimes, R. S. Jope, The multifaceted roles of glycogen synthase kinase 3beta in cellular signaling. *Prog Neurobiol* **65**, 391-426 (2001).
93. H. Tong, K. Imahashi, C. Steenbergen, E. Murphy, Phosphorylation of glycogen synthase kinase-3beta during preconditioning through a phosphatidylinositol-3-kinase--dependent pathway is cardioprotective. *Circ Res* **90**, 377-379 (2002).
94. K. Inoki *et al.*, TSC2 integrates Wnt and energy signals via a coordinated phosphorylation by AMPK and GSK3 to regulate cell growth. *Cell* **126**, 955-968 (2006).
95. K. Inoki, Y. Li, T. Xu, K. L. Guan, Rheb GTPase is a direct target of TSC2 GAP activity and regulates mTOR signaling. *Genes Dev* **17**, 1829-1834 (2003).
96. C. L. Buller *et al.*, A GSK-3/TSC2/mTOR pathway regulates glucose uptake and GLUT1 glucose transporter expression. *Am J Physiol Cell Physiol* **295**, C836-843 (2008).
97. F. Steinberg *et al.*, A global analysis of SNX27-retromer assembly and cargo specificity reveals a function in glucose and metal ion transport. *Nat Cell Biol* **15**, 461-471 (2013).
98. B. E. Lauffer *et al.*, SNX27 mediates PDZ-directed sorting from endosomes to the plasma membrane. *J Cell Biol* **190**, 565-574 (2010).
99. P. Temkin *et al.*, SNX27 mediates retromer tubule entry and endosome-to-plasma membrane trafficking of signalling receptors. *Nat Cell Biol* **13**, 715-721 (2011).
100. S. Roy, A. M. Leidal, J. Ye, S. M. Ronen, J. Debnath, Autophagy-Dependent Shuttling of TBC1D5 Controls Plasma Membrane Translocation of GLUT1 and Glucose Uptake. *Mol Cell* **67**, 84-95.e85 (2017).
101. H. Parikh *et al.*, TXNIP regulates peripheral glucose metabolism in humans. *PLoS Med* **4**, e158 (2007).
102. N. Wu *et al.*, AMPK-dependent degradation of TXNIP upon energy stress leads to enhanced glucose uptake via GLUT1. *Mol Cell* **49**, 1167-1175 (2013).
103. T. Asano *et al.*, The role of N-glycosylation in the targeting and stability of GLUT1 glucose transporter. *FEBS Lett* **324**, 258-261 (1993).
104. L. A. Witters, C. A. Vater, G. E. Lienhard, Phosphorylation of the glucose transporter in vitro and in vivo by protein kinase C. *Nature* **315**, 777-778 (1985).
105. E. E. Lee *et al.*, A Protein Kinase C Phosphorylation Motif in GLUT1 Affects Glucose Transport and is Mutated in GLUT1 Deficiency Syndrome. *Mol Cell* **58**, 845-853 (2015).
106. P. E. Driedger, P. M. Blumberg, The effect of phorbol diesters on chicken embryo fibroblasts. *Cancer Res* **37**, 3257-3265 (1977).

107. M. Castagna *et al.*, Direct activation of calcium-activated, phospholipid-dependent protein kinase by tumor-promoting phorbol esters. *J Biol Chem* **257**, 7847-7851 (1982).
108. M. J. Birnbaum, H. C. Haspel, O. M. Rosen, Transformation of rat fibroblasts by FSV rapidly increases glucose transporter gene transcription. *Science* **235**, 1495-1498 (1987).
109. J. Klepper *et al.*, Glut1 Deficiency Syndrome (Glut1DS): State of the art in 2020 and recommendations of the international Glut1DS study group. *Epilepsia Open* **5**, 354-365 (2020).
110. J. Klepper, Absence of SLC2A1 mutations does not exclude Glut1 deficiency syndrome. *Neuropediatrics* **44**, 235-236 (2013).
111. K. Meyer *et al.*, Mutations in Disordered Regions Can Cause Disease by Creating Dileucine Motifs. *Cell* **175**, 239-253.e217 (2018).
112. J. K. De Zutter, K. B. Levine, D. Deng, A. Carruthers, Sequence determinants of GLUT1 oligomerization: analysis by homology-scanning mutagenesis. *J Biol Chem* **288**, 20734-20744 (2013).
113. M. Raja, R. K. H. Kinne, Mechanistic Insights into Protein Stability and Self-aggregation in GLUT1 Genetic Variants Causing GLUT1-Deficiency Syndrome. *J Membr Biol* **253**, 87-99 (2020).
114. D. C. De Vivo *et al.*, Defective glucose transport across the blood-brain barrier as a cause of persistent hypoglycorrhachia, seizures, and developmental delay. *N Engl J Med* **325**, 703-709 (1991).
115. K. N. Pandey, Functional roles of short sequence motifs in the endocytosis of membrane receptors. *Front Biosci (Landmark Ed)* **14**, 5339-5360 (2009).
116. L. Sun *et al.*, Crystal structure of a bacterial homologue of glucose transporters GLUT1-4. *Nature* **490**, 361-366 (2012).
117. M. G. Madej, L. Sun, N. Yan, H. R. Kaback, Functional architecture of MFS D-glucose transporters. *Proc Natl Acad Sci U S A* **111**, E719-727 (2014).
118. M. Tang, S. H. Park, D. C. De Vivo, U. R. Monani, Therapeutic strategies for glucose transporter 1 deficiency syndrome. *Ann Clin Transl Neurol* **6**, 1923-1932 (2019).
119. M. Tang *et al.*, Brain microvasculature defects and Glut1 deficiency syndrome averted by early repletion of the glucose transporter-1 protein. *Nat Commun* **8**, 14152 (2017).
120. S. Nakamura *et al.*, Gene therapy for Glut1-deficient mouse using an adeno-associated virus vector with the human intrinsic GLUT1 promoter. *J Gene Med* **20**, e3013 (2018).
121. T. Yamamoto *et al.*, Over-expression of facilitative glucose transporter genes in human cancer. *Biochem Biophys Res Commun* **170**, 223-230 (1990).
122. T. Nishioka *et al.*, Distribution of the glucose transporters in human brain tumors. *Cancer Res* **52**, 3972-3979 (1992).
123. R. S. Brown, R. L. Wahl, Overexpression of Glut-1 glucose transporter in human breast cancer. An immunohistochemical study. *Cancer* **72**, 2979-2985 (1993).
124. G. Cantuaria *et al.*, GLUT-1 expression in ovarian carcinoma: association with survival and response to chemotherapy. *Cancer* **92**, 1144-1150 (2001).
125. A. Zambrano, M. Molt, E. Uribe, M. Salas, Glut 1 in Cancer Cells and the Inhibitory Action of Resveratrol as A Potential Therapeutic Strategy. *Int J Mol Sci* **20**, (2019).
126. V. Ganapathy, M. Thangaraju, P. D. Prasad, Nutrient transporters in cancer: relevance to Warburg hypothesis and beyond. *Pharmacol Ther* **121**, 29-40 (2009).
127. P. Som *et al.*, A fluorinated glucose analog, 2-fluoro-2-deoxy-D-glucose (F-18): nontoxic tracer for rapid tumor detection. *J Nucl Med* **21**, 670-675 (1980).
128. J. Wang *et al.*, Glucose transporter GLUT1 expression and clinical outcome in solid tumors: a systematic review and meta-analysis. *Oncotarget* **8**, 16875-16886 (2017).
129. C. C. Barron, P. J. Bilan, T. Tsakiridis, E. Tsiani, Facilitative glucose transporters: Implications for cancer detection, prognosis and treatment. *Metabolism* **65**, 124-139 (2016).
130. P. B. Ancey, C. Contat, E. Meylan, Glucose transporters in cancer - from tumor cells to the tumor microenvironment. *FEBS J* **285**, 2926-2943 (2018).

131. K. Shibuya *et al.*, Targeting the facilitative glucose transporter GLUT1 inhibits the self-renewal and tumor-initiating capacity of cancer stem cells. *Oncotarget* **6**, 651-661 (2015).
132. Y. Liu *et al.*, A small-molecule inhibitor of glucose transporter 1 downregulates glycolysis, induces cell-cycle arrest, and inhibits cancer cell growth in vitro and in vivo. *Mol Cancer Ther* **11**, 1672-1682 (2012).
133. C. E. Alvarez, On the origins of arrestin and rhodopsin. *BMC Evol Biol* **8**, 222 (2008).
134. W. E. Miller, R. J. Lefkowitz, Expanding roles for beta-arrestins as scaffolds and adapters in GPCR signaling and trafficking. *Curr Opin Cell Biol* **13**, 139-145 (2001).
135. A. F. O'Donnell, M. C. Schmidt, AMPK-Mediated Regulation of Alpha-Arrestins and Protein Trafficking. *Int J Mol Sci* **20**, (2019).
136. G. Polekhina *et al.*, Structure of the N-terminal domain of human thioredoxin-interacting protein. *Acta Crystallogr D Biol Crystallogr* **69**, 333-344 (2013).
137. J. Hwang *et al.*, The structural basis for the negative regulation of thioredoxin by thioredoxin-interacting protein. *Nat Commun* **5**, 2958 (2014).
138. Y. Liu *et al.*, Structural basis for the regulatory role of the PPxY motifs in the thioredoxin-interacting protein TXNIP. *Biochem J* **473**, 179-187 (2016).
139. A. Nishiyama *et al.*, Identification of thioredoxin-binding protein-2/vitamin D(3) up-regulated protein 1 as a negative regulator of thioredoxin function and expression. *J Biol Chem* **274**, 21645-21650 (1999).
140. P. C. Schulze *et al.*, Hyperglycemia promotes oxidative stress through inhibition of thioredoxin function by thioredoxin-interacting protein. *J Biol Chem* **279**, 30369-30374 (2004).
141. A. H. Minn, C. Hafele, A. Shalev, Thioredoxin-interacting protein is stimulated by glucose through a carbohydrate response element and induces beta-cell apoptosis. *Endocrinology* **146**, 2397-2405 (2005).
142. P. Patwari *et al.*, Thioredoxin-independent regulation of metabolism by the alpha-arrestin proteins. *J Biol Chem* **284**, 24996-25003 (2009).
143. A. Shalev *et al.*, Oligonucleotide microarray analysis of intact human pancreatic islets: identification of glucose-responsive genes and a highly regulated TGFbeta signaling pathway. *Endocrinology* **143**, 3695-3698 (2002).
144. S. Khoo *et al.*, MAP kinases and their roles in pancreatic beta-cells. *Cell Biochem Biophys* **40**, 191-200 (2004).
145. M. C. Lawrence, K. McGlynn, B. H. Park, M. H. Cobb, ERK1/2-dependent activation of transcription factors required for acute and chronic effects of glucose on the insulin gene promoter. *J Biol Chem* **280**, 26751-26759 (2005).
146. J. Chen, G. Saxena, I. N. Mungrue, A. J. Lusis, A. Shalev, Thioredoxin-interacting protein: a critical link between glucose toxicity and beta-cell apoptosis. *Diabetes* **57**, 938-944 (2008).
147. G. Saxena, J. Chen, A. Shalev, Intracellular shuttling and mitochondrial function of thioredoxin-interacting protein. *J Biol Chem* **285**, 3997-4005 (2010).
148. J. Lu, A. Holmgren, Thioredoxin system in cell death progression. *Antioxid Redox Signal* **17**, 1738-1747 (2012).
149. A. M. Borowiec, A. Właszczuk, E. Olakowska, J. Lewin-Kowalik, TXNIP inhibition in the treatment of diabetes. Verapamil as a novel therapeutic modality in diabetic patients. *Med Pharm Rep* **95**, 243-250 (2022).
150. N. M. Alhawiti, S. Al Mahri, M. A. Aziz, S. S. Malik, S. Mohammad, TXNIP in Metabolic Regulation: Physiological Role and Therapeutic Outlook. *Curr Drug Targets* **18**, 1095-1103 (2017).
151. E. Yoshihara *et al.*, Disruption of TBP-2 ameliorates insulin sensitivity and secretion without affecting obesity. *Nat Commun* **1**, 127 (2010).
152. C. A. Stoltzman *et al.*, Glucose sensing by MondoA:Mlx complexes: a role for hexokinases and direct regulation of thioredoxin-interacting protein expression. *Proc Natl Acad Sci U S A* **105**, 6912-6917 (2008).

153. P. Zhang *et al.*, The ubiquitin ligase itch regulates apoptosis by targeting thioredoxin-interacting protein for ubiquitin-dependent degradation. *J Biol Chem* **285**, 8869-8879 (2010).
154. A. N. Waldhart *et al.*, Phosphorylation of TXNIP by AKT Mediates Acute Influx of Glucose in Response to Insulin. *Cell Rep* **19**, 2005-2013 (2017).
155. B. Singh *et al.*, Induction of lateral lumens through disruption of a monoleucine-based basolateral-sorting motif in betacellulin. *J Cell Sci* **128**, 3444-3455 (2015).
156. S. Lee *et al.*, Ubiquitin turnover and endocytic trafficking in yeast are regulated by Ser57 phosphorylation of ubiquitin. *Elife* **6**, (2017).
157. G. Gyimesi, J. Pujol-Giménez, Y. Kanai, M. A. Hediger, Sodium-coupled glucose transport, the SLC5 family, and therapeutically relevant inhibitors: from molecular discovery to clinical application. *Pflugers Arch* **472**, 1177-1206 (2020).
158. S. S. Pao, I. T. Paulsen, M. H. Saier, Major facilitator superfamily. *Microbiol Mol Biol Rev* **62**, 1-34 (1998).
159. C. M. Alexander *et al.*, Alternative splicing and cleavage of GLUT8. *Mol Cell Biol*, (2020).
160. A. Brumfield *et al.*, Insulin-promoted mobilization of GLUT4 from a perinuclear storage site requires RAB10. *Mol Biol Cell* **32**, 57-73 (2021).
161. A. De Vos *et al.*, Human and rat beta cells differ in glucose transporter but not in glucokinase gene expression. *J Clin Invest* **96**, 2489-2495 (1995).
162. K. T. Coppieters, A. Wiberg, N. Amirian, T. W. Kay, M. G. von Herrath, Persistent glucose transporter expression on pancreatic beta cells from longstanding type 1 diabetic individuals. *Diabetes Metab Res Rev* **27**, 746-754 (2011).
163. F. Maher, S. J. Vannucci, I. A. Simpson, Glucose transporter proteins in brain. *FASEB J* **8**, 1003-1011 (1994).
164. P. J. Siska, J. C. Rathmell, PKCs Sweeten Cell Metabolism by Phosphorylation of Glut1. *Mol Cell* **58**, 711-712 (2015).
165. A. J. Evans, J. L. Daly, A. N. K. Anuar, B. Simonetti, P. J. Cullen, Acute inactivation of retromer and ESCPE-1 leads to time-resolved defects in endosomal cargo sorting. *J Cell Sci* **133**, (2020).
166. A. Kvainickas *et al.*, Retromer- and WASH-dependent sorting of nutrient transporters requires a multivalent interaction network with ANKRD50. *J Cell Sci* **130**, 382-395 (2017).
167. S. R. Shinde, S. Maddika, PTEN Regulates Glucose Transporter Recycling by Impairing SNX27 Retromer Assembly. *Cell Rep* **21**, 1655-1666 (2017).
168. D. S. Richardson *et al.*, SRpHi ratiometric pH biosensors for super-resolution microscopy. *Nat Commun* **8**, 577 (2017).
169. J. Votteler *et al.*, Designed proteins induce the formation of nanocage-containing extracellular vesicles. *Nature* **540**, 292-295 (2016).
170. S. Rauch, J. Martin-Serrano, Multiple interactions between the ESCRT machinery and arrestin-related proteins: implications for PPXY-dependent budding. *J Virol* **85**, 3546-3556 (2011).
171. C. P. Nielsen, K. K. Jernigan, N. L. Diggins, D. J. Webb, J. A. MacGurn, USP9X Deubiquitylates DVL2 to Regulate WNT Pathway Specification. *Cell Rep* **28**, 1074-1089.e1075 (2019).
172. H. Dykstra *et al.*, TXNIP interaction with GLUT1 depends on PI(4,5)P. *Biochim Biophys Acta Biomembr* **1863**, 183757 (2021).
173. B. Wollscheid *et al.*, Mass-spectrometric identification and relative quantification of N-linked cell surface glycoproteins. *Nat Biotechnol* **27**, 378-386 (2009).
174. T. S. Devi *et al.*, TXNIP mediates high glucose-induced mitophagic flux and lysosome enlargement in human retinal pigment epithelial cells. *Biol Open* **8**, (2019).
175. J. A. MacGurn, P. C. Hsu, S. D. Emr, Ubiquitin and membrane protein turnover: from cradle to grave. *Annu Rev Biochem* **81**, 231-259 (2012).
176. E. Lauwers, Z. Erpapazoglou, R. Haguenauer-Tsapis, B. André, The ubiquitin code of yeast permease trafficking. *Trends Cell Biol* **20**, 196-204 (2010).

177. E. Nikko, H. R. Pelham, Arrestin-mediated endocytosis of yeast plasma membrane transporters. *Traffic* **10**, 1856-1867 (2009).
178. K. Nagaki *et al.*, 14-3-3 Mediates phosphorylation-dependent inhibition of the interaction between the ubiquitin E3 ligase Nedd4-2 and epithelial Na+ channels. *Biochemistry* **45**, 6733-6740 (2006).
179. T. Ichimura *et al.*, 14-3-3 proteins modulate the expression of epithelial Na+ channels by phosphorylation-dependent interaction with Nedd4-2 ubiquitin ligase. *J Biol Chem* **280**, 13187-13194 (2005).
180. D. Wang, P. Kranz-Eble, D. C. De Vivo, Mutational analysis of GLUT1 (SLC2A1) in Glut-1 deficiency syndrome. *Hum Mutat* **16**, 224-231 (2000).
181. H. Koch, Y. G. Weber, The glucose transporter type 1 (Glut1) syndromes. *Epilepsy Behav* **91**, 90-93 (2019).
182. F. Ohtake, H. Tsuchiya, Y. Saeki, K. Tanaka, K63 ubiquitylation triggers proteasomal degradation by seeding branched ubiquitin chains. *Proc Natl Acad Sci U S A* **115**, E1401-E1408 (2018).
183. J. G. Kim *et al.*, Signaling Pathways Regulated by UBR Box-Containing E3 Ligases. *Int J Mol Sci* **22**, (2021).
184. T. Tasaki *et al.*, A family of mammalian E3 ubiquitin ligases that contain the UBR box motif and recognize N-degrons. *Mol Cell Biol* **25**, 7120-7136 (2005).
185. A. M. González-Jamett *et al.*, Dynamin-2 function and dysfunction along the secretory pathway. *Front Endocrinol (Lausanne)* **4**, 126 (2013).
186. Y. Dong *et al.*, Myoferlin, a Membrane Protein with Emerging Oncogenic Roles. *Biomed Res Int* **2019**, 7365913 (2019).
187. B. A. Castilho *et al.*, Keeping the eIF2 alpha kinase Gcn2 in check. *Biochim Biophys Acta* **1843**, 1948-1968 (2014).
188. T. Asano *et al.*, The role of N-glycosylation of GLUT1 for glucose transport activity. *J Biol Chem* **266**, 24632-24636 (1991).
189. H. Katayama, A. Yamamoto, N. Mizushima, T. Yoshimori, A. Miyawaki, GFP-like proteins stably accumulate in lysosomes. *Cell Struct Funct* **33**, 1-12 (2008).
190. F. Huang, D. Kirkpatrick, X. Jiang, S. Gygi, A. Sorkin, Differential regulation of EGF receptor internalization and degradation by multiubiquitination within the kinase domain. *Mol Cell* **21**, 737-748 (2006).
191. P. J. Cullen, F. Steinberg, To degrade or not to degrade: mechanisms and significance of endocytic recycling. *Nat Rev Mol Cell Biol* **19**, 679-696 (2018).
192. S. S. Shah, S. Kumar, Adaptors as the regulators of HECT ubiquitin ligases. *Cell Death Differ* **28**, 455-472 (2021).
193. C. H. Lin, J. A. MacGurn, T. Chu, C. J. Stefan, S. D. Emr, Arrestin-related ubiquitin-ligase adaptors regulate endocytosis and protein turnover at the cell surface. *Cell* **135**, 714-725 (2008).
194. E. Nikko, J. A. Sullivan, H. R. B. Pelham, Arrestin-like proteins mediate ubiquitination and endocytosis of the yeast metal transporter Smf1. *EMBO Rep* **9**, 1216-1221 (2008).
195. J. F. Nabhan, H. Pan, Q. Lu, Arrestin domain-containing protein 3 recruits the NEDD4 E3 ligase to mediate ubiquitination of the beta2-adrenergic receptor. *EMBO Rep* **11**, 605-611 (2010).
196. K. R. Doherty *et al.*, The endocytic recycling protein EHD2 interacts with myoferlin to regulate myoblast fusion. *J Biol Chem* **283**, 20252-20260 (2008).
197. P. Patwari *et al.*, The arrestin domain-containing 3 protein regulates body mass and energy expenditure. *Cell Metab* **14**, 671-683 (2011).
198. P. Patwari, R. T. Lee, An expanded family of arrestins regulate metabolism. *Trends Endocrinol Metab* **23**, 216-222 (2012).
199. S. Oka *et al.*, Thioredoxin-binding protein-2-like inducible membrane protein is a novel vitamin D3 and peroxisome proliferator-activated receptor (PPAR)gamma ligand target protein that regulates PPARgamma signaling. *Endocrinology* **147**, 733-743 (2006).

200. J. M. Pascual, R. L. Van Heertum, D. Wang, K. Engelstad, D. C. De Vivo, Imaging the metabolic footprint of Glut1 deficiency on the brain. *Ann Neurol* **52**, 458-464 (2002).
201. D. Wang *et al.*, Glut-1 deficiency syndrome: clinical, genetic, and therapeutic aspects. *Ann Neurol* **57**, 111-118 (2005).
202. D. W. Yuan-Yuan Ho, Veronica Hinton, Hong Yang, Alexandra Vasilesca, Kristin Engelstad, Sarah Jhung, Kristine K. Hanson, Jon A. Wolff, and Darryl C. De Vivo Ann Neurol 2001, S. . (Annals of Neurology, 2001), vol. 50, pp. S125.
203. W. G. Leen *et al.*, Glucose transporter-1 deficiency syndrome: the expanding clinical and genetic spectrum of a treatable disorder. *Brain* **133**, 655-670 (2010).
204. J. Klepper *et al.*, Autosomal dominant transmission of GLUT1 deficiency. *Hum Mol Genet* **10**, 63-68 (2001).
205. J. Klepper *et al.*, Defective glucose transport across brain tissue barriers: a newly recognized neurological syndrome. *Neurochem Res* **24**, 587-594 (1999).
206. W. C. Overweg-Plandsoen *et al.*, GLUT-1 deficiency without epilepsy--an exceptional case. *J Inherit Metab Dis* **26**, 559-563 (2003).
207. Y. G. Weber *et al.*, GLUT1 mutations are a cause of paroxysmal exertion-induced dyskinesias and induce hemolytic anemia by a cation leak. *J Clin Invest* **118**, 2157-2168 (2008).
208. C. Joshi *et al.*, GLUT1 deficiency without epilepsy: yet another case. *J Child Neurol* **23**, 832-834 (2008).
209. A. Suls *et al.*, Paroxysmal exercise-induced dyskinesia and epilepsy is due to mutations in SLC2A1, encoding the glucose transporter GLUT1. *Brain* **131**, 1831-1844 (2008).
210. A. Mauri *et al.*, Molecular Genetics of GLUT1DS Italian Pediatric Cohort: 10 Novel Disease-Related Variants and Structural Analysis. *Int J Mol Sci* **23**, (2022).
211. A. Suls *et al.*, Early-onset absence epilepsy caused by mutations in the glucose transporter GLUT1. *Ann Neurol* **66**, 415-419 (2009).
212. M. Anheim *et al.*, Excellent response to acetazolamide in a case of paroxysmal dyskinesias due to GLUT1-deficiency. *J Neurol* **258**, 316-317 (2011).
213. J. Klepper *et al.*, Autosomal recessive inheritance of GLUT1 deficiency syndrome. *Neuropediatrics* **40**, 207-210 (2009).
214. M. E. Bechard *et al.*, Pancreatic cancers suppress negative feedback of glucose transport to reprogram chromatin for metastasis. *Nat Commun* **11**, 4055 (2020).
215. L. G. Melstrom *et al.*, Apigenin inhibits the GLUT-1 glucose transporter and the phosphoinositide 3-kinase/Akt pathway in human pancreatic cancer cells. *Pancreas* **37**, 426-431 (2008).
216. T. E. Wood *et al.*, A novel inhibitor of glucose uptake sensitizes cells to FAS-induced cell death. *Mol Cancer Ther* **7**, 3546-3555 (2008).
217. D. Zhang *et al.*, Therapeutic role of EF24 targeting glucose transporter 1-mediated metabolism and metastasis in ovarian cancer cells. *Cancer Sci* **104**, 1690-1696 (2013).
218. T. Sanli *et al.*, Ionizing radiation activates AMP-activated kinase (AMPK): a target for radiosensitization of human cancer cells. *Int J Radiat Oncol Biol Phys* **78**, 221-229 (2010).
219. H. Shim, Y. S. Chun, B. C. Lewis, C. V. Dang, A unique glucose-dependent apoptotic pathway induced by c-Myc. *Proc Natl Acad Sci U S A* **95**, 1511-1516 (1998).
220. M. Schapira, M. F. Calabrese, A. N. Bullock, C. M. Crews, Targeted protein degradation: expanding the toolbox. *Nat Rev Drug Discov* **18**, 949-963 (2019).
221. Y. R. Lee *et al.*, Reactivation of PTEN tumor suppressor for cancer treatment through inhibition of a MYC-WWP1 inhibitory pathway. *Science* **364**, (2019).
222. C. Debonneville *et al.*, Phosphorylation of Nedd4-2 by Sgk1 regulates epithelial Na(+) channel cell surface expression. *EMBO J* **20**, 7052-7059 (2001).
223. C. Zou, Y. Wang, Z. Shen, 2-NBDG as a fluorescent indicator for direct glucose uptake measurement. *J Biochem Biophys Methods* **64**, 207-215 (2005).

224. V. Blot, T. E. McGraw, Use of quantitative immunofluorescence microscopy to study intracellular trafficking: studies of the GLUT4 glucose transporter. *Methods Mol Biol* **457**, 347-366 (2008).